



Artificial Intelligence Based Android Assistant for Colorimetric Detection

Submitted to the Graduate School of Natural and Applied Sciences
in partial fulfillment of the requirements for the degree of

Master of Science

in Electrical and Electronics Engineering

by

Vakkas DOĞAN

ORCID 0000-0001-5934-4156

June, 2023

This is to certify that we have read the thesis **Artificial Intelligence Based Android Assistant for Colorimetric Detection** submitted by **Vakkas Dođan**, and it has been judged to be successful, in scope and in quality, at the defense exam and accepted by our jury as a MASTER'S THESIS.

APPROVED BY:

Advisor: **Assoc. Prof. Dr. Volkan Kılıç**
İzmir Kâtip Çelebi University

Co-advisor: **Assoc. Prof. Dr. Mustafa Şen**
İzmir Kâtip Çelebi University

Committee Members:

Assoc. Prof. Dr. İlker Polatođlu
Celal Bayar University

Date of Defense: June 16, 2023

Declaration of Authorship

I, **Vakkas Doğan**, declare that this thesis titled **Artificial Intelligence Based Android Assistant for Colorimetric Detection** and the work presented in it are my own. I confirm that:

- This work was done wholly or mainly while in candidature for the Master's / Doctoral degree at this university.
- Where any part of this thesis has previously been submitted for a degree or any other qualification at this university or any other institution, this has been clearly stated.
- Where I have consulted the published work of others, this is always clearly attributed.
- Where I have quoted from the work of others, the source is always given. This thesis is entirely my own work, with the exception of such quotations.
- I have acknowledged all major sources of assistance.
- Where the thesis is based on work done by myself jointly with others, I have made clear exactly what was done by others and what I have contributed myself.

Date: 16.06.2023

Artificial Intelligence Based Android Assistant for Colorimetric Detection

Abstract

A colorimetric analysis is a technique that measures the properties of the substance using color changes in chemical or biochemical analysis. It is vital in analysing biological, medical, and environmental samples in many fields, such as the food, medicine, cosmetics, and paint industries. Colorimetric analysis requires correct measurement and calibration techniques to obtain accurate results. Therefore, artificial intelligence (AI) and smartphone technology have been widely used in developing biological sensors in chemistry and biomedicine in recent years. Images obtained using a smartphone camera are processed with AI techniques, resulting in highly accurate results. This thesis discusses AI approaches and smartphone-based on-site colorimetric analyses in three different subjects: hydrogen peroxide (H_2O_2) detection, lactate detection in sweat, and food spoilage detection, respectively. First, the iodide-mediated 3,3',5,5'-tetramethylbenzidine (TMB)- H_2O_2 reaction system was applied to a microfluidic paper-based analytical device (μPAD) for the non-enzymatic colorimetric determination of H_2O_2 . The proposed system is portable and includes a μPAD and a machine learning (ML)-based smartphone app. The colorimetric change in detection was achieved without using any enzymes or nanoparticles with catalytic properties, resulting in a low-cost and stable system. A smartphone application named "*Hi-perox Sens*" with image capture, cropping, and processing features has been developed to make the system simple and user-friendly. Briefly, circular μPADs were designed and tested with varying concentrations of H_2O_2 . After the color change, images of the μPADs were taken with four smartphones under seven lighting

conditions. To make the system more robust and adaptable to lighting variations and camera optics, images were first processed for feature extraction and then used to train ML classifiers. According to TMB+KI, it showed the highest classification accuracy (97.8%) with inter-phone reproducibility at $t=30$ s under illumination and maintained its accuracy for 10 minutes. Second, a μ PAD was combined with a deep learning (DL) based smartphone app called “*DeepLactate*” and then applied for quantitative and selective determination of lactate concentration in sweat. Images of μ PADs taken with smartphones of various brands in different lighting conditions were used to train DL models to make the system more robust and adaptable to lighting changes. The highest-performing model, Inception-v3, was later built into a smartphone app, making it easy to use for non-expert users. Unlike ML classifiers, DL models can automatically extract features and are embedded in a smartphone app, allowing analysis without internet access. According to the results, the current system showed 99.9% classification accuracy with phone-independent repeatability and less than 1 second processing time. Finally, μ PAD was converted into a patch to determine sweat lactate levels in two volunteers after rest and 15 minutes of jogging. The system detected lactate in human sweat and confirmed that the lactate level in sweat increased after running. Third, real-time and on-site food spoilage monitoring is still challenging to prevent food poisoning. At the beginning of food spoilage, microbial and enzymatic activities lead to the formation of volatile amines. Monitoring these amines by conventional methods requires complex, costly, labor-intensive, and time-consuming analyses. An anthocyanin-rich red cabbage extract (ARCE)-based colorimetric detection system was developed by incorporating embedded ML into a smartphone app for real-time food spoilage monitoring. FG-UV-CD100 films were first produced by crosslinking ARCE-doped fish gelatin (FG) with carbon dots (CDs) under UV light. The colorimetric responses of FG-UV-CD100 films to ammonia vapor were captured in different light sources with smartphones of various brands. A comprehensive dataset was created to train ML classifiers that are robust and adaptable to environmental conditions with 98.8% classification accuracy. Meanwhile, the ML classifier was integrated into our specially designed Android application “*SmartFood++*”, allowing analysis in about 0.1 seconds without internet access, unlike its counterpart using cloud operation over the internet. The proposed system was also tested on a real fish sample

with 99.6% accuracy, demonstrating its great advantage as a powerful tool for on-site, real-time monitoring of food spoilage by non-specialized personnel.

Keywords: Artificial intelligence, colorimetric analysis, deep learning, machine learning, Android, smartphone.

Kolorimetrik Tespit için Yapay Zeka Tabanlı Android Asistanı

ÖZ

Kolorimetrik analiz, kimyasal veya biyokimyasal analizde maddenin özelliklerinin renk değişimleri kullanılarak ölçülmesini sağlayan bir tekniktir. Gıda, ilaç, kozmetik ve boya endüstrileri gibi birçok farklı alanda biyolojik, tıbbi ve çevresel numunelerin analizinde hayati önem taşımaktadır. Kolorimetrik analiz, doğru sonuçlar elde etmek için doğru ölçüm ve kalibrasyon teknikleri gerektirir. Bu nedenle son yıllarda kimya ve biyotıpta biyolojik sensörlerin geliştirilmesinde yapay zeka ve akıllı telefon teknolojisi yaygın olarak kullanılmaktadır. Akıllı telefon kamerası kullanılarak elde edilen görüntüler, yapay zeka teknikleriyle işlenerek yüksek doğrulukta sonuçlar elde ediliyor. Bu tezde yapay zeka yaklaşımları ve akıllı telefon tabanlı yerinde kolorimetrik analizler sırasıyla hidrojen peroksit (H_2O_2) tespiti, terde laktat tespiti ve gıda bozulma tespiti olmak üzere üç farklı konuda ele alınmaktadır. İlk olarak, iyodür aracılı 3,3',5,5'-tetrametilbenzidin (TMB)- H_2O_2 reaksiyon sistemi, enzimatik olmayan kolorimetrik H_2O_2 belirleme için bir mikroakışkan kağıt bazlı analitik cihaza (μ PAD) uygulanmıştır. Önerilen sistem taşınabilir ve bir μ PAD ve makine öğrenimi tabanlı bir akıllı telefon uygulaması içermektedir. Tespitteki kolorimetrik değişim, katalitik özelliklere sahip herhangi bir enzim veya nanoparçacık kullanılmadan elde edilmiştir, bu da düşük maliyetli ve kararlı bir sistemle sonuçlanmıştır. Sistemin basit ve kullanıcı dostu olması için "*Hi-perox Sens*" isimli görüntü yakalama, kırpma ve işleme özelliklerine sahip bir akıllı telefon uygulaması geliştirilmiştir. Kısaca, dairesel μ PAD'ler tasarlanmış ve değişen konsantrasyonlarda H_2O_2 ile test edilmiştir. Renk değişiminden sonra yedi aydınlatma koşulunda dört akıllı telefon ile μ PAD'lerin

görüntüleri alınmıştır. Sistemi daha sağlam ve aydınlatma varyasyonlarına ve kamera optiklerine uyarlanabilir hale getirmek için görüntüler önce özellik çıkarımı için işlendi ve ardından makine öğrenimi sınıflandırıcılarını eğitmek için kullanılmıştır. TMB+KI'ye göre aydınlatma altında t=30 s'de telefonlar arası tekrarlanabilirlik ile en yüksek sınıflandırma doğruluğunu (%97,8) göstermiş ve doğruluğunu 10 dakika korumuştur. İkinci olarak, bir μ PAD, “*DeepLactate*” adlı derin öğrenme tabanlı bir akıllı telefon uygulamasıyla birleştirilmekte ve ardından terdeki laktat konsantrasyonunun kantitatif ve seçici olarak belirlenmesi için uygulanmıştır. Farklı aydınlatma koşullarında çeşitli markaların akıllı telefonlarıyla çekilen μ PAD'lerin görüntüleri, sistemi daha sağlam ve aydınlatma değişikliklerine uyarlanabilir hale getirmek için derin öğrenme modellerini eğitmek için kullanıldı. En yüksek performanslı model olan Inception-v3, daha sonra bir akıllı telefon uygulamasına yerleştirildi ve uzman olmayan kullanıcılar için kullanımı kolaylaştırdı. Makine öğrenimi sınıflandırıcılarından farklı olarak, derin öğrenme modelleri özellikleri otomatik olarak çıkarılabilir ve bir akıllı telefon uygulamasına gömülü olarak internet erişimi olmadan analiz yapılmasına olanak tanımaktadır. Elde edilen sonuçlara göre, mevcut sistem telefonda bağımsız tekrarlanabilirlik ve 1 saniyeden kısa işlem süresi ile %99.9 sınıflandırma doğruluğu göstermiştir. Son olarak, iki gönüllüde dinlenme ve 15 dakikalık koşu sonrasında ter laktat düzeylerini belirlemek için μ PAD bir yamaya dönüştürülmektedir. Sistem insan terinde laktat tespit etti ve koşu sonrasında terdeki laktat seviyesinin arttığını doğruladı. Üçüncüsü, gıda zehirlenmesini önlemek için gerçek zamanlı ve yerinde gıda bozulma izlemesi hala zordur. Gıda bozulmalarının başında mikrobiyal ve enzimatik faaliyetler uçucu aminlerin oluşumuna yol açmaktadır. Bu aminlerin geleneksel yöntemlerle izlenmesi, karmaşık, maliyetli, emek yoğun ve zaman alıcı analizler gerektirir. Antosiyanin açısından zengin kırmızı lahana özü tabanlı bir kolorimetrik algılama sistemi, gerçek zamanlı gıda bozulma izlemesi için bir akıllı telefon uygulamasına gömülü makine öğrenimi dahil edilerek geliştirilmiştir. FG-UV-CD100 filmleri ilk olarak ARCE katkılı balık jelatininin karbon noktalarla UV ışığı altında çapraz bağlanmasıyla üretildi. FG-UV-CD100 filmlerinin amonyak buharına verdiği kolorimetrik tepkiler, çeşitli markaların akıllı telefonlarıyla farklı ışık kaynaklarında yakalanmaktadır. Sağlam ve çevre koşullarına %98.8 sınıflandırma doğruluğu ile uyarlanabilen makine öğrenimi sınıflandırıcılarını eğitmek için kapsamlı bir veri seti oluşturuldu. Bu arada, makine öğrenimi

sınıflandırıcısı, özel olarak tasarlanmış Android uygulamamız “*SmartFood++*” ile entegre edilerek, internet üzerinden bulut işletimi kullanan benzerinden farklı olarak, internet erişimi olmadan yaklaşık 0,1 saniyede analiz yapılmasına olanak sağlamaktadır. Önerilen sistem aynı zamanda gerçek bir balık numunesi üzerinde %99.6 doğrulukla test edildi ve uzman olmayan personel tarafından gıda bozulmalarının yerinde, gerçek zamanlı izlenmesi için güçlü bir araç olarak büyük avantajını göstermektedir.

Anahtar Kelimeler: Yapay zeka, kolorimetrik analiz, derin öğrenme, makine öğrenmesi, Android, akıllı telefon.

To my family.

Acknowledgment

I could probably have written a whole chapter comparable to the contribution parts of this thesis to acknowledge those who, in different ways, have helped me in my MSc life at the İzmir Katip Çelebi University.

First and foremost, Assoc. Prof. Dr Volkan KILIÇ, my advisor, whose highly experienced and very kind way of providing guidance has helped transform my research work into an enjoyable endeavor during the period of my MSc study. His ongoing encouragement has motivated me strongly. I also want to thank him for helping me improve my writing skills.

I want to thank Assoc. Prof. Dr Mustafa ŞEN, my co-advisor, significantly for his beneficial guidance and constructive comments, from which I gained great insights into my research.

I am most grateful to my close friend, Gizem Nur AKSOY, who is always lovely to me. Her continuous support and great interest let me feel that I am part of her. I am sure it will continue to be so.

In addition, I want to thank my colleague, Elif YÜZER. She has been very helpful in the publications produced in the thesis.

Finally, I would like to express my profound appreciation to my family.

Table of Contents

Declaration of Authorship	ii
Abstract	iii
Öz	iv
Acknowledgment	vi
List of Figures	x
List of Tables.....	xi
List of Abbreviations.....	xii
List of Symbols	xiii
1 Introduction.....	1
1.1 Colorimetric Analysis and Motivation.....	1
1.2 Contributions	8
1.3 Outline of the Thesis.....	10
2 Methods.....	11
2.1 Feature Extraction	11
2.1.1 Color Features.....	11
2.1.2 Textures Features.....	14
2.2 Feature Selection	16
2.2.1 Feature Selection with Chi-Squared	17
2.3 Artificial Intelligence.....	18
2.3.1 Machine Learning Algorithms.....	19
2.4 Software Programs.....	24
2.4.1 MATLAB	25
2.4.2 Python.....	26
2.4.3 Java	26
2.4.4 WEKA	27

2.4.5	Firebase.....	27
2.4.6	Android Studio: Smartphone Applications.....	28
2.5	Performance Metrics.....	29
2.5.1	Accuracy.....	29
2.5.2	Precision.....	29
2.5.3	Recall.....	29
2.5.4	F1 Score.....	30
2.5.5	AUC-ROC Curve.....	30
2.5.6	Matthews Correlation Coefficient.....	30
3	Non-enzymatic colorimetric detection of hydrogen peroxide using a μPAD coupled with a machine learning-based smartphone app.....	31
3.1	Introduction.....	32
3.2	μ PAD Fabrication and Colorimetric Detection of H ₂ O ₂	34
3.3	Data Acquisition and Processing.....	35
3.4	Feature Extraction and Machine Learning Analysis.....	36
3.5	Smartphone Applications: Hi-perox Sens.....	37
3.6	Results and Discussion.....	39
4	Smartphone embedded deep learning approach for highly accurate and automated colorimetric lactate analysis in sweat.....	46
4.1	Introduction.....	47
4.2	Materials and Methods.....	50
4.3	Image Capturing.....	51
4.4	Proposed Deep Learning Architecture.....	53
4.5	Smartphones Applications: DeepLactate.....	54
4.6	Experimental Evaluations and Discussion.....	56
5	On-site food spoilage monitoring with smartphone embedded machine learning and colorimetric gelatin films.....	61
5.1	Introduction.....	62

5.2	Materials and Methods.....	64
5.2.1	Fabrication of Colorimetric Films	64
5.3	Experimental Design and Image Acquisition	66
5.4	Machine Learning for Colorimetric Analysis.....	66
5.4.1	Feature Extraction in Machine Learning	67
5.4.2	Feature Selection in Machine Learning.....	68
5.4.3	Classification with Random Forest.....	69
5.5	Smartphone Application: SmartFood++	69
5.6	Real Samples.....	70
5.7	Result and Discussion.....	71
6	Conclusions and future research.....	76
6.1	Conclusions.....	76
6.1.1	Non-enzymatic Colorimetric Detection of hydrogen peroxide using a μ PAD coupled with a machine learning-based smartphone app.....	76
6.1.2	Smartphone embedded deep learning approach for highly accurate and automated colorimetric lactate analysis in sweat.....	77
6.1.3	On-site food spoilage monitoring with smartphone embedded machine learning and colorimetric gelatin films	78
6.2	Future Research.....	78
	References	80
	Appendices.....	101
	Appendix A.....	102
	Appendix B	112
	Appendix C	117
	Curriculum Vitae	118

List of Figures

Figure 2.1: There are five basic steps used to perform an ML task.	19
Figure 2.2: Machine Learning Algorithms.....	21
Figure 2.3: Schematic illustration of the software programs.	25
Figure 2.4: Firebase interface.....	28
Figure 3.1: Schematic illustration of the proposed system. The color change of chromogenic agents can be detected with a smartphone camera under ambient light conditions.	34
Figure 3.2: Color changes with respect to chromogenic agents, time, and concentrations.....	35
Figure 3.3: Colorimetric hydrogen peroxide quantification steps on the Hi-perox Sens. The homepage of the Hi-perox Sens is given in (a). The user can select an image from the gallery or capture a new image using the smartphone camera in (b) and display it on the screen as in (c). The image can be cropped using an adjustable crop box in (d). The cropped patch is given in (e) and uploading the cropped patch is shown in (f). The user selection of the uploading patch as TMB+KI or KI is shown in (g). The classification result of the image is given in (h).	38
Figure 3.4: Evaluation of EBC with error bars in terms of precision, recall, and F1 score at t=30 s for TMB+KI using low concentrations.....	41
Figure 3.5: Confusion matrices of TMB+KI for the EBC classifier at t=30 s is given in (a) and at t=10 min in (b), and confusion matrices of KI for the LDA classifier at t=30 s are shown in (c) and at t=10 min in (d).....	45

Figure 4.1: A schematic illustration showing the working principle of the system. Lactate is first converted to pyruvate by LOx, releasing H ₂ O ₂ which is then used by HRP for the oxidation of TMB. The color change is imaged using a smartphone camera and the lactate is determined by DeepLactate, an app running a DL classifier.....	50
Figure 4.2: Images of μ PADs showing visually observable color changes with varying concentrations of lactate in artificial sweat at t = 0 min and t = 5 min. ..	52
Figure 4.3: General structure of the CNN.....	53
Figure 4.4: The steps for colorimetric lactate analysis in DeepLactate are as follows. The home page of DeepLactate is given in (a). The user can select an image from the gallery in (b) or capture a new image using the smartphone camera. Then, after selecting the image from the gallery, the crop alert dialogue is asked of the user as in (c). If the user taps the “NO” action, the result is calculated directly (without cropping) as shown in (d). Otherwise, the user is directed to the crop screen in (e), and (g) when the “YES” action is tapped. The app tests the concentrations of 0 mM in (f) and 50 mM in (h).	55
Figure 4.5: ROC curves of Inception-v3 in varying concentrations of the test dataset.	58
Figure 4.6: Confusion matrix of Inception-v3 in varying concentrations of the test dataset.....	59
Figure 4.7: Model Accuracy of Inception-v3 is given in (a) and Model Loss of Inception-v3 is shown in (b).	59
Figure 4.8: An image (a) showing the application of a lactate patch for human sweat analysis. The patch was made by sandwiching a μ PAD between a sticking plaster and a transparent tape (bi–ii). Classification results of the smartphone app DeepLactate for lactate level in the sweat of two volunteers after resting and 15 min jogging.....	60

Figure 5.1: A schematic illustration showing the working principle of the food spoilage detection system.	64
Figure 5.2: Feature selection using Chi-Squared algorithm.....	68
Figure 5.3: The general structure of Random Forest.	69
Figure 5.4: The steps for colorimetric food spoilage monitoring in SmartFood++ are as follows. The homepage of SmartFood++ is given in (a). The user can select an image from the gallery in (b) or capture a new image using the smartphone camera and crop the image using an adjustable crop box as in (c), (d), (g), and (h). Cropped patches are given in (e) and (i). The application is tested with the consumable food (fish) in (f), and the inconsumable one in (j).....	71
Figure 5.5: Confusion matrix of RF in different concentrations.....	75

List of Tables

Table 3.1: The smartphones are used to create a dataset with images of μ PADs for machine learning.	36
Table 3.2: The classification results at t=30s and t=10 min. for KI.....	43
Table 3.3: The classification results at t=30s and t=10 min. for TMB+KI.....	44
Table 4.1: Camera properties of the smartphones used for imaging.....	51
Table 4.2: Experimental results of CNN models.	56
Table 4.3: Evaluation of the Inception-v3 for lactate in terms of precision, recall, F1-score, and ROC-AUC.....	57
Table 5.1: Camera properties of the smartphones used for imaging in food spoilage detection.	65
Table 5.2: The color change of FG-UV-CD100 film with varying concentrations of ammonia vapor.....	67
Table 5.3: Classification accuracy results for colorimetric food spoilage detection with different ML classifiers.	73
Table 5.4: Evaluation of the RF for colorimetric food spoilage detection in terms of Precision, Recall, F1-score, Accuracy, ROC Area, and MCC.....	74

List of Abbreviations

TMB	Tetramethylbenzidine
μPADs	Microfluidic Paper-based Analytical Devices
H ₂ O ₂	Hydrogen Peroxide
AI	Artificial Intelligence
ARCE	Anthocyanin-Rich Red Cabbage Extract
FG	Fish Gelatin
CDs	Carbon Dots
ML	Machine Learning
DL	Deep Learning
CNN	Convolutional Neural Network
RF	Random Forest
MCC	Matthews Correlation Coefficient
ELISA	Enzyme-linked Immunosorbent Assay
LFA	Lateral Flow Immunoassay
RGB	Red-Green-Blue
CMYK	Cyan-Magenta--Black
Lab	Lightness-Red-green-Blue-yellow
HSV	Hue-Saturation-Value
YUV	Luminance-Blue-luminance-Red-luminance
CIE	International Commission on Illumination
LIMS	Laboratory Information Management Systems
KI	Potassium Iodide

RL	Reinforcement Learning
OLSR	Ordinary Least Squares Regression
LOESS	Local Estimated Distribution Line Correction
MARS	Multivariate Adaptive Regression Curves
kNN	k-Nearest Neighbor
CART	Classification and Regression Tree
ID3	Recursive Binary Tree
PCA	Principal Component Analysis
PCR	Principal Component Regression
PLSR	Partial Least Squares Regression
LDA	Linear Discriminant Analysis
EBC	Ensemble Bagging Classifier
QDA	Quadratic Differential Analysis
FDA	Flexible Differential Analysis
DBM	Deep Boltzmann Machine
DBN	Deep Belief Networks
JRE	Java Runtime Environment
JDK	Java Development Kit
WEKA	Waikato Environment for Knowledge Analysis
APK	Android Package Kit
TP	True-Positive
TN	True-Negative
FP	False-Positive
FN	False-Negative
AUC	Area Under Curves
ROC	Receiver Operating Characteristic
HRP	Horseradish Peroxidase

LOx	Lactate Oxidase
H	Halogen
F	Fluorescent
S	Sunlight
LOD	Limit of Detection
RNN	Recurrent Neural Networks
DI	Digital Image
TfLite	TensorFlow-Lite
HDF	Hierarchical Data Format
ROI	Region of Interest

List of Symbols

μ	Mean
σ	Standard Deviation
χ^2	Chi-Squared

Chapter 1

Introduction

This introductory chapter first presents colorimetric analysis and motivation of this thesis in Section 1.1. Then, Section 1.2 specifies our contributions of the work. Finally, the outline of the thesis is given in Section 1.3.

1.1 Colorimetric Analysis and Motivation

Colorimetric analysis is a quantitative analytical method that measures the concentration of a substance in a sample based on its color change. It relies on the principle that a substance will interact with a specific reagent to produce a measurable color change [1]. The colorimetric analysis is commonly used in various fields, such as chemistry [2], biochemistry [3], environmental science [4], food science [5], and medical diagnostics [6]. In colorimetric analysis, a sample is mixed with a reagent, which causes a chemical reaction to occur, leading to a color change. The intensity of the color change is proportional to the concentration of the analyte in the sample. The color change is measured using a colorimeter or a spectrophotometer, which determines the intensity of light absorbed by the sample. Colorimetric analysis can detect various analytes, including proteins [7], enzymes [8], sugars [9], metals [10], and organic compounds [11]. It is a simple and relatively inexpensive method compared to other analytical techniques. Colorimetric analysis is widely used in various industries for quality control and to monitor contaminants in the environment, food, and water. It is also used in medical diagnostics to detect diseases and monitor treatment progress.

Colorimetric analysis detection methods are techniques used to detect the presence or concentration of a substance in a sample based on color changes [12]. These methods

rely on the ability of a substance to interact with a reagent and produce a detectable color change. Some common colorimetric detection methods include:

- **Enzyme-linked Immunosorbent Assay (ELISA):** This method is commonly used in medical and biological research to detect the presence of specific antigens or antibodies in a sample. ELISA uses a specific antibody linked to an enzyme, producing a detectable color change when interacting with the target antigen [13].
- **Lateral Flow Immunoassay (LFA):** This is a rapid and simple detection method commonly used in point-of-care testing. It relies on the movement of a fluid along a nitrocellulose membrane that contains a specific antibody. When the target analyte in the sample binds to the antibody, a visible color change is produced [14].
- **Colorimetric Paper-based Assay:** A colorimetric paper-based assay is a type of colorimetric analysis that uses paper as a substrate for detecting the presence or concentration of a target substance in a sample [15]. The paper is functionalized with specific ligands or receptors that bind to the target substance, causing a color change. The color change can then be visually observed or analyzed using colorimetric techniques, such as spectroscopy or image analysis. Colorimetric paper-based assays have several advantages over traditional assays. They are low-cost, portable, and require minimal sample preparation, making them ideal for use in resource-limited settings or the field. They also have the potential for high sensitivity and specificity, making them suitable for various applications, including medical diagnostics, environmental monitoring, and food safety. Colorimetric paper-based assays have been used in various applications, including the detection of infectious diseases, such as hydrogen peroxide [16], lactate in sweat [17], and environmental contaminants, such as heavy metals [18] and pesticides [19]. They are a promising avenue for developing low-cost, portable, and easy-to-use assays that can be used in various settings.
- **Colorimetric Films:** Colorimetric films are a type of film that can be used in colorimetric analysis as a substrate for colorimetric assays [20]. In colorimetric analysis, a color change is used to detect the presence or concentration of a target substance in a sample. The colorimetric film can be functionalized with

specific ligands or receptors that bind to the target substance, causing a color change in the film. The color change in the colorimetric film can then be analyzed using colorimetric analysis techniques, such as spectroscopy or image analysis, to determine the concentration of the target substance in the sample. The colorimetric film can be optimized to ensure maximum sensitivity and accuracy by adjusting the film thickness, porosity, and functionalization method [21]. Colorimetric films have several advantages in colorimetric analysis [22]. They can be fabricated into films of different shapes and sizes, making them suitable for various applications. They can also be made from various materials, including natural polymers like gelatin or chitosan or synthetic polymers such as polyethylene or polystyrene, allowing for a wide range of options regarding film properties, such as mechanical strength, chemical stability, and biocompatibility. Fish Gelatin-UV-Carbon Dots-100 (FG-UV-CD100) films are a type of fish gelatin-based film that has been modified to enhance its mechanical and thermal properties. They have been specifically designed for use in food packaging applications, where their high strength and barrier properties make them ideal for protecting food products from contamination and deterioration [23].

Colorimetric analysis is closely related to color spaces, mathematical models that describe colors based on their physical attributes. Color spaces provide a standardized way of representing colors, allowing accurate color reproduction and comparison across different devices and media [24].

In colorimetric analysis, the color of a substance or solution is typically measured using a colorimeter or spectrophotometer, which detects the intensity of light absorbed or transmitted by the sample at different wavelengths. These measurements are then used to determine the concentration of the substance in the sample based on the known relationship between the color and the concentration.

Color spaces are often used to define the colors that are measured in colorimetric analysis. Some commonly used color spaces include RGB (Red, Green, Blue), CMYK (Cyan, Magenta, Yellow, Black), and CIELAB (L^* , a^* , b^*), which is based on the perception of color by the human eye. These color spaces provide a standardized way

of describing and measuring colors, which allows for accurate color reproduction and comparison.

In colorimetric analysis, various color spaces are used to describe and quantify the colors produced by a sample. Some of the commonly used color spaces in colorimetric analysis include:

- **RGB:** RGB is an additive color space that describes colors produced by digital displays such as monitors and televisions. It defines colors based on the red, green, and blue light required to produce a given color [25].
- **CMYK (Cyan, Magenta, Yellow, Key or Black):** CMYK is a subtractive color space used in printing. It defines colors based on the cyan, magenta, yellow, and black ink required to produce a given color [26].
- **Lab (Lightness, a, b):** Lab is a device-independent color space used in colorimetric analysis to quantify color differences. It defines colors based on their lightness, or L value, as well as their red-green (a) and blue-yellow (b) color components [27].
- **CIE Lab*:** CIE Lab* is a color space defined by the International Commission on Illumination (CIE) that is widely used in colorimetric analysis. It is similar to the Lab color space but is based on a standard observer model designed to match the human visual system [28].

These color spaces are used in colorimetric analysis to quantify and compare colors, and to calculate color differences and colorimetric parameters such as hue, saturation, and brightness. The choice of color space depends on the specific application and the characteristics of the sample being analyzed. In summary, colorimetric analysis and color spaces are closely related, as color spaces are often used to define and measure the colors that are analyzed in colorimetric analysis. Using standardized color spaces allows for accurate and consistent color measurements across different devices and media, essential in many fields, including graphic design, printing, and photography.

A calibration curve is a graphical representation of the relationship between the concentration of a substance and the corresponding signal intensity produced by a colorimetric analysis method [29]. The calibration curve is constructed by analyzing a series of standards with known concentrations of the target substance and plotting the

resulting signal intensities against the known concentrations. This relationship can then be used to determine the concentration of the substance in an unknown sample by measuring its signal intensity and comparing it to the calibration curve. In colorimetric analysis, a calibration curve is often used to determine the concentration of a particular substance in a sample [30]. The advantage of a calibration curve is that it provides a quantitative measure of the concentration of the substance in the sample, which is essential for accurate and reliable analysis [31].

The calibration curve also allows for the determination of the limit of detection (LOD) and limit of quantification of the colorimetric analysis method. These limits represent the minimum concentration of the substance that can be reliably detected and quantified using the method. The calibration curve also allows for the determination of the accuracy and precision of the colorimetric analysis method, which is essential for ensuring the reliability and reproducibility of the results.

A few potential disadvantages of the calibration curve in colorimetric analysis should be considered [32]. One disadvantage is that the calibration curve is specific to the method used for the colorimetric analysis. Any changes in the experimental conditions, such as temperature, pH, or reaction time, may affect the shape and position of the calibration curve and, therefore, require constructing a new calibration curve. In addition, the accuracy and precision of the colorimetric analysis method may be affected by factors such as interference from other substances in the sample matrix or instrument variability [33]. These factors can lead to inaccuracies in the calibration curve and affect the accuracy of the results obtained. Finally, the construction of a calibration curve assumes that the relationship between the concentration of the target substance and the measured signal intensity is linear over the entire range of concentrations being analyzed. However, in some cases, this relationship may not be linear, which can affect the accuracy of the analysis.

Due to these limitations, unlike the calibration curve, AI remains an essential tool in colorimetric analysis as it allows accurate and reliable measurement of the concentration of a substance in a sample and provides information about the sensitivity, accuracy, and precision of the analysis method [34]. With AI, colorimetric analysis can be used for data analysis and processing. For example, AI algorithms can

be trained to recognize patterns in colorimetric data and use this information to identify or quantify the presence of a particular substance in a sample.

Furthermore, AI algorithms (ML & DL) can optimize and automate colorimetric analysis processes, increasing the speed and accuracy of data analysis, reducing the time and cost associated with manual data analysis, and enabling faster and more reliable results. AI has several advantages in colorimetric analysis [35]:

- **Increased Accuracy:** AI algorithms can analyze large amounts of colorimetric data with high accuracy, reducing the chance of human error and increasing the reliability of the results.
- **Speed:** AI algorithms can process colorimetric data much faster than humans, enabling faster analysis and decision-making.
- **Automation:** AI algorithms can automate many aspects of colorimetric analysis, reducing the need for manual labor and making the process more efficient.
- **Optimization:** AI algorithms can optimize colorimetric analysis processes by identifying patterns and trends in the data that may not be immediately apparent to humans, which can help improve the accuracy and efficiency of the analysis.
- **Detection of Complex Patterns:** AI algorithms can detect complex patterns in colorimetric data that may be difficult or impossible for humans to detect, which can help to identify subtle changes in colorimetric data that may indicate the presence of a particular substance or condition.
- **Integration:** AI algorithms can be integrated with other technologies, such as robotics or laboratory information management systems (LIMS), to create a fully automated and integrated colorimetric analysis system.

AI has the potential to significantly improve the accuracy, speed, and efficiency of colorimetric analysis, making it a valuable tool in a wide range of applications, including food spoilage detection [36], medical diagnostics [37], environmental monitoring [38], and materials science [39].

Smartphones have become increasingly popular in scientific research due to their portability, affordability, and high-quality imaging capabilities. Several recent studies have explored using Android-based smartphones for colorimetric analysis [16, 17].

One way to use an Android-based smartphone in colorimetric analysis is to use its camera as a colorimeter, which involves capturing an image of the sample and then analyzing the RGB values of the image to determine the color change caused by the reaction. There are several advantages of using an Android-based smartphone as a colorimeter [40]:

- **Low-cost:** Compared to traditional colorimeters, smartphones are much more affordable, making them accessible to a wider range of researchers and students.
- **Portability:** Smartphones are compact and portable, allowing for field-based colorimetric analysis.
- **High-quality imaging:** Smartphone cameras have advanced significantly in recent years, allowing for capturing high-quality images.
- **Easy to use:** Most people are familiar with smartphones, making them an intuitive and user-friendly tool for colorimetric analysis.
- **Integration with apps:** Several apps have been developed for Android-based smartphones that enable colorimetric analysis. These apps can simplify the process of capturing and analyzing images and can also provide data management and analysis tools.

Overall, using Android-based smartphones in the colorimetric analysis is a promising field, offering many advantages over traditional colorimeters. However, there are still some limitations to be addressed, such as the need for calibration and validation of the smartphone camera and the potential for variability in lighting conditions that may affect the accuracy of the analysis [40].

In addition, Android-based smartphones can be used for both online and offline colorimetric analysis. In online colorimetric analysis, the smartphone is connected to the internet, and data is transmitted in real-time to a server for analysis, which can be useful for applications that require immediate feedback or monitoring, such as environmental monitoring or medical diagnostics. The application transmits the data to a server for analysis and feedback. The server may perform additional analysis, such as pattern recognition or ML, to provide more detailed information about the sample [41]. On the other hand, offline colorimetric analysis involves analyzing colorimetric data directly on the smartphone without an internet connection, which can be helpful

when a network connection is unavailable, such as in remote locations or the field. The application stores the data locally on the smartphone and performs the analysis without an internet connection [17]. The results can be displayed on the smartphone screen or exported for further analysis. In summary, Android-based smartphones can be helpful for online and offline colorimetric analysis, providing a portable, affordable, and convenient solution for many applications.

In this thesis, it was first aimed to improve the accuracy of different AI models related to the determination of concentration values in colorimetric analysis studies. Then, Android-based smartphones were used so that the user could view the results quickly. Therefore, a colorimetric analysis study was carried out to determine concentration levels in three areas: hydrogen peroxide detection, lactate detection in sweat, and food spoilage detection, respectively. In the first study, after the concentration levels of hydrogen peroxide are determined using ML classifiers, the results are sent online to the Android-based Hi-perox Sens application with the help of a Firebase remote server. In the second study, colorimetric lactate analysis concentration levels in sweat were determined, and DL classifiers were embedded in the Android-based application DeepLactate after training. This application can work offline without a remote server and internet. Thus, results were obtained faster and on-site. In the third study, ML classifiers were trained while determining concentration levels in food spoilage detection. The Random Forest (RF), which had the highest accuracy among all classifiers, was embedded into our custom-designed Android application SmartFood++. Unlike other Android applications that require internet access for data transfer to the remote server running the ML classifier, SmartFood++ includes an embedded ML classifier that can complete analysis in around 0.06 seconds.

1.2 Contributions

(1) Firstly, non-enzymatic μ PADs coupled with a ML-based smartphone app were developed for high-sensitive and selective determination of H_2O_2 in transparent liquids such as water. First, circular patterns were printed on filter paper using a solid ink (wax) printer, and then the patterns were processed at high temperatures to obtain hydrophobic boundaries of the μ PADs. The use of single or multiple indicators has been reported for the colorimetric detection of H_2O_2 , such as 3,3'-diaminobenzidine,

3,3',5,5'-tetramethylbenzidine (TMB), and potassium iodide (KI). The μ PADs were prepared for testing by adding only two indicators, TMB and KI, to the detection zones for color change in the presence of different concentrations of H_2O_2 . No enzyme or nanoparticle with catalytic properties was used to detect, making the system cost-efficient and chemically/thermally stable. The performance of the system was compared with those of using KI only and TMB only. An ML-based smartphone app with a simple interface was developed to make the process more user-friendly, robust, and adaptive against illumination variation and camera optics. ML classifiers were trained using features extracted from images taken under seven different illumination conditions. The trained classifiers were then integrated into the *Hi-perox Sens* app to be presented to the user. The results clearly showed that the proposed system has a high potential for practical use.

(2) Secondly, a DL approach has been adopted to determine lactate concentration quantitatively and selectively in sweat. First, a μ PAD capable of fluid absorption was designed and printed on filter paper using a wax printer, and then the patterns were turned into hydrophobic barriers at high temperatures. The detection area of the μ PAD was modified with 3,3',5,5'-TMB, horse radish peroxidase (HRP), and lactate oxidase (LOx) for enzymatic colorimetric detection of lactate. The performance of the sensor was tested in artificial sweat containing lactate at different concentrations. To improve the robustness of the system and its adaptability to illumination variation and camera optics, images captured by smartphones of different brands in various lighting conditions were used to train several DL models. The top-performing model, Inception-v3, was embedded into an Android-based smartphone app (*DeepLactate*) with a user-friendly interface for offline detection of lactate in sweat. To the best of our knowledge, this is the first study to apply a DL model for colorimetric analysis of chemical species. The system was also tested on volunteers with a patch in which the μ PAD was sandwiched between a plaster and transparent tape. The results showed that the current approach has a high potential for practical use, especially in sports medicine.

(3) Thirdly, ML was embedded in a smartphone application for colorimetric analysis of food freshness with our developed colorimetric fish gelation films, FG-UV-CD100, based on red cabbage anthocyanins and the carbon dot. The color response of FG-UV-

CD100 against nine different volatile ammonia concentrations was collected with smartphone cameras to detect the concentration using an ML classifier. In this regard, the classifiers were trained separately for the color response of FG-UV-CD100 film to each ammonia concentration, with a relevant dataset containing color features extracted from the captured images. The dataset was collected with four smartphones in seven illumination conditions and three pose angles to ensure robustness against camera optics and ambient light conditions. The RF, which had the highest accuracy among all classifiers, was embedded into our custom-designed Android application *SmartFood++*. Unlike other Android applications that require internet access for data transfer to the remote server running the ML classifier, *SmartFood++* includes an embedded ML classifier that can complete analysis in around 0.06 seconds. To the best of our knowledge, this is the first study that embeds an ML classifier into a smartphone application and links with FG films, enabling colorimetric food freshness monitoring for rapid and portable on-site surveillance. The proposed system was also tested in a real sample (e.g., fish), in which the results prove that it has great potential for food spoilage monitoring in resource-limited settings.

1.3 Outline of the Thesis

The thesis is organized as follows: The methods used in the related work are introduced in Chapter 2. Feature extraction, feature selection, AI, software programs, and performance metrics used throughout the thesis are described in detail. Chapter 3 presents our proposed non-enzymatic colorimetric detection of hydrogen peroxide using a μ PAD coupled with an ML-based smartphone application algorithm. Chapter 4 introduces a smartphone-embedded DL approach for highly accurate and automated colorimetric lactate analysis in sweat. In Chapter 5, on-site food spoilage monitoring with smartphone embedded ML and colorimetric gelatin films is presented. Chapter 6 concludes the thesis with conclusions and recommendations for future work.

Chapter 2

Methods

This chapter first introduces the feature extraction and selection from datasets in Section 2.1 and Section 2.2. Then, Section 2.3 presents algorithms of AI, such as ML and DL. In Section 2.4, Software programs, including MATLAB, Python, Java, WEKA, Firebase, and Android Studio, used throughout this thesis, are discussed in detail. Finally, several performance metrics proposed in the literature to measure the performance of AI algorithms are discussed in Section 2.5.

2.1 Feature Extraction

Feature extraction is the process of extracting more minor processed data from raw data [42]. This process can be considered a data compression process that removes unnecessary information by hiding essential information from raw data. Feature extraction plays a vital role in the pattern recognition problem. Therefore, the performance of the classifier largely depends on the quality of the feature vectors. This thesis uses color and texture features for feature extraction from raw image data.

2.1.1 Color Features

The color feature in the low-level set of attributes is one of the most common attributes to describe an image [43]. The color map of the image can be obtained with the color histograms of the image. Color is a potent property, especially for reflecting the general characteristics of an image and identifying objects within it. Before using the color features, the number of colors in the image should be converted to the other color spaces. In image processing, many color space models exist, such as RGB, Lab, HSV, YUV, and HLS [44].

Many color spaces are used for many applications, such as image processing [45], computer vision [46], and computer graphics [47]. The virtual color space in the RGB is represented as a combination of three primary colors, R, G, and B. Each pixel in the image consists of three-color channels known as RGB components. It is possible to convert the RGB color space to different color spaces according to the needs of the application. The RGB color space is converted to the HSV color space to obtain the channel (V) containing the luminance information and the other two channels (H and S) containing the color information. The HSV color space describes colors like the tendency of the human eye to perceive color. HSV color space, like the mechanism of human vision and consists of hue, saturation, and brightness color channels, differs from RGB color space in that it separates image intensity from color information. This feature provides an advantage with its resistance to light changes. In the HSV color space, hue distinguishes colors, saturation refers to the percentage of white added to the pure color, and brightness refers to the perceived light intensity. The brightness of the image changes with illumination; however, hue and saturation, channels containing color information, are either insensitive or less sensitive to the change in illumination. These features use the HSV color space for color analysis, color-based detection, and segmentation [48].

To analyze the effect of color spaces in determining the concentration level, images in RGB color space were converted to HSV and L*a*b* color spaces. Unlike the RGB color space, L*a*b* color space is designed as a device-independent color model that will be close to the perception of the human eye. Defining all the colors the human eye perceives enables the measurement of color differences that can be expressed in terms of human visual perception. L*, a*, and b* are the three coordinates of this color space and represent lightness. The mean, standard deviation, skewness, and kurtosis, which are first, secondary, third, and fourth-order color moments, are explained below, respectively.

2.1.1.1 Mean

The mean, μ , the first color moment, gives the average color value of the image (Equation (2.1)) [49].

$$Mean (\mu) = \frac{1}{pq} \sum_{i=1}^p \sum_{j=1}^q pixel_{ij} \quad (2.1)$$

Here, p and q are the pixel values in the i^{th} row j^{th} column at image $pixel_{ij}$.

2.1.1.2 Standard Deviation

Standard deviation measures how spread out the values in a dataset are from the mean [50]. In image processing, the standard deviation can measure the amount of variation or noise in an image. To calculate the standard deviation of an image, you first need to calculate the mean value of the pixel intensities. This can be done by summing up all the pixel values in the image and dividing them by the total number of pixels.

Once you have the mean value, you can calculate the standard deviation by taking the square root of the average of the squared differences between each pixel intensity and the mean. This formula (Equation (2.2)) can be expressed mathematically as:

$$Standard\ Deviation\ (\sigma) = \sqrt{\frac{1}{pq} \sum_{i=1}^p \sum_{j=1}^q (pixel_{ij} - \mu)^2} \quad (2.2)$$

2.1.1.3 Skewness

Skewness is a measure of asymmetry in distribution [51]. The dataset is symmetrical if the left and right sides of the center point are the same. If the skewness is positive (skewed to the right), the data is spread to the left of the mean. If the skewness is negative (skewed to the left), the data will apply to the right of the mean. To extract information from the image, darker and brighter surfaces tend to have positive skewness compared to lighter and matte surfaces. Skewness gives information about the color distribution, which is defined in Equation (2.3),

$$Skewness = \sqrt[3]{\frac{1}{pq} \sum_{i=1}^p \sum_{j=1}^q (pixel_{ij} - \mu)^3} \quad (2.3)$$

2.1.1.4 Kurtosis

Kurtosis is the normalized form of the fourth central moment of distribution [52]. It is also defined as the measure of the sharpness of the peak of a distribution. A high kurtosis distribution usually has a sharper rise, while a low kurtosis distribution usually has a more rounded elevation. Kurtosis is defined in Equation (2.4),

$$Kurtosis = \sqrt[4]{\frac{1}{pq} \sum_{i=1}^p \sum_{j=1}^q (pixel_{ij} - \mu)^4} \quad (2.4)$$

2.1.2 Texture Features

The texture is one of the critical components in the perception of visual content. Like color, texture is one of the essential properties to consider when querying image databases [53]. Anyone can notice the texture of an image; however, the texture is tough to define. Unlike the color feature, texture occurs over a specific region rather than a spot.

Texture features are related to the distribution of luminosity on the visual object and are a natural attribute of all optical surfaces. It contains crucial information about the structural arrangements of surfaces and their relationship with the environment. Texture has been studied in image processing and pattern detection. It has been observed to be very important in distinguishing and defining different pictures. Therefore, the texture is one of the active features used in multimedia access. Textures are used not only for painting surfaces, however, also for perceiving movements. Although no formal structure describes the texture, the concepts of uniformity, coarseness, regularity, direction, frequency, and similarity are used as scales that reflect textural features. Different methods are suggested for defining the texture of any image in the field of image processing. The most common method of extracting the texture feature is to

obtain the texture spectrum that can characterize the texture image by designing various masks or filters [54]. Studies based on feature extraction from the Fourier power spectrum have also been made to capture the overall repetitions in an image by identifying the high energies of an image [55].

The texture is usually defined by bringing the image to a gray level. It has qualities such as texture, periodicity, and size. Homogeneity, correlation, and contrast are defined as features.

2.1.2.1 Contrast

Contrast measures the intensity or gray level variations between a reference pixel and its neighbor [56]. Significant contrast indicates large density differences. A still image has a contrast value of 0. The contrast is defined in Equation (2.5),

$$Contrast = \sum_i \sum_j (i - j)^2 r(i, j) \quad (2.5)$$

Here, $r(i, j)$ is the gray level value of the pixel in the (i, j) coordinate.

2.1.2.2 Correlation

Correlation is the measure of linear dependence of gray level values which returns a measure between a pixel and its neighbors [57]. The correlation was calculated in Equation (2.8) with means μ_i, μ_j (Equation (2.6)), standard deviations σ_i, σ_j (Equation (2.7)),

$$\mu_i = \sum_i \sum_j i r(i, j), \mu_j = \sum_i \sum_j j r(i, j) \quad (2.6)$$

$$\sigma_i^2 = \sum_i \sum_j (i - \mu_i)^2 r(i, j), \sigma_j^2 = \sum_i \sum_j (j - \mu_j)^2 r(i, j) \quad (2.7)$$

$$Correlation = \sum_i \sum_j \frac{(i - \mu_i)(j - \mu_j)r(i, j)}{\sigma_i \sigma_j} \quad (2.8)$$

2.1.2.3 Homogeneity

Homogeneity measures how close the distribution of elements in the gray-level co-occurrence matrix is to the diagonal of the matrix [58]. As homogeneity increases, contrast decreases. Homogeneity is defined in Equation (2.9),

$$\text{Homogeneity} = \sum_i \sum_j \frac{r(i,j)}{1 + |i - j|} \quad (2.9)$$

2.1.2.4 Energy

The energy property, also called the angular second-moment property, is a measure of image homogeneity [59]. It is expressed as the sum of the squares of the matrix elements (Equation (2.10)),

$$\text{Energy} = \sum_i \sum_j r(i,j)^2 \quad (2.10)$$

2.1.2.5 Entropy

The entropy value was calculated by converting the color input image to a gray-level image [60]. The entropy of the image is calculated in Equation (2.11),

$$\text{Entropy} = - \sum n \log_2 n \quad (2.11)$$

where n is the number of normalized histograms.

2.2 Feature Selection

Feature selection is a technique used in AI to identify and select the most relevant features (or variables) from a more extensive set of available features [61]. The goal of feature selection is to improve the accuracy and efficiency of an AI model by reducing the number of input features while maintaining or even improving the

quality of the results. There are several methods for feature selection, including [62]:

- **Filter methods:** These methods use statistical measures to rank the importance of each feature and select the top-ranked features. Examples include correlation-based feature selection, Chi-Squared feature selection, and mutual information-based feature selection [62].
- **Embedded methods:** These methods incorporate feature selection into the AI model's training process, selecting the most relevant features during the model training. Examples include Lasso and Ridge regression [62].

The benefits of feature selection include reducing the dimensionality of the input data, which can improve the efficiency and accuracy of an AI model. Additionally, feature selection can help to avoid overfitting and improve the interpretability of the model's results. However, it is essential to note that feature selection is not always necessary or beneficial. In some cases, using all available features may be the best approach, especially when dealing with complex datasets or when the potential benefits of feature selection are not clear.

The number of features and samples can be pretty high in databases such as image processing, customer relationship management, and gene analysis. Working with such large databases can create a problem for ML algorithms [63]. One of these problems is the prolongation of classification times. Another problem is that many unnecessary and unimportant features degrade the performance of ML algorithms. For these reasons, feature selection methods have become crucial and essential for ML algorithms working with high-dimensional datasets. Feature selection algorithms offer higher generalization ability in classifying large datasets and better results in solving recognition problems. In this thesis, the Chi-Squared was used for feature selection.

2.2.1 Feature Selection with Chi-Squared

The Chi-Squared (χ^2) test is a statistical method used to determine the dependence or independence of two categorical variables [64]. In feature selection, it is often used as a filter method to rank the relevance of features based on their association with the

target variable. The Chi-Squared test would measure the difference between the observed frequencies of two categorical variables and the expected frequencies if the variables were independent. The test produces a Chi-Squared statistic, which measures how much the observed frequencies differ from the expected frequencies.

In the Chi-Squared (χ^2) algorithm (Equation (2.12)), a t_i feature set is selected based on its correlation with a C_j class, and the discrimination ability (χ^2) of the t_i feature set with respect to the C_j class is calculated as:

$$\text{Chi - Squared } (\chi^2) = \frac{S \times (a_{ij} \times d_{ij} - b_{ij} \times c_{ij})^2}{(a_{ij} \times (b_{ij} + c_{ij})) \times (c_{ij} \times (b_{ij} + d_{ij}))} \quad (2.12)$$

where S is the total number of samples, the a_{ij} is the number of instances in the category C_j containing the attribute t_i , and the b_{ij} is the number of instances in the category C_j that does not contain the attribute t_i . The c_{ij} is the number of samples that contain the t_i attribute; however, it does not belong to the C_j category. The d_{ij} is the number of samples that do not belong to the C_j category and do not contain the t_i attribute [64].

2.3 Artificial Intelligence

The idea that AI was first introduced in 1956 is that machines can think like humans. It started to be developed with the idea that machines act like humans. The famous English mathematician and computer scientist Alan Turing developed a test to measure whether machines are intelligent in this context [65]. According to the test, another human asks a human and machine questions. It is a test based on distinguishing between humans and machines according to the answers received by the person asking the question.

AI is shaped by the joint work of many branches of science, including philosophy, mathematics, economics, neurology, psychology, and engineering [66]. There are many algorithms developed under AI, such as ML and DL. When a machine encounters a problem, separate algorithms can be used for each stage of analyzing, navigating, solving, and learning the solution. The definition of machine learning and its algorithms used in the thesis are explained in this context.

2.3.1 Machine Learning Algorithms

ML is the ability of the computer to make decisions about similar events that may occur in the future and to produce solutions to the problems that will occur by learning the information and experience gained by the computer about an event [67]. ML uses some methods to take advantage of past data and finds the most suitable model for new data. It is not easy to manually process and analyze vast amounts of data. The aim here is to make predictions for future situations using past data. Regardless of the application area, the importance of ML methods is increasing daily, with the analysis of large amounts of data, making predictions, and helping us make decisions (Figure 2.1).

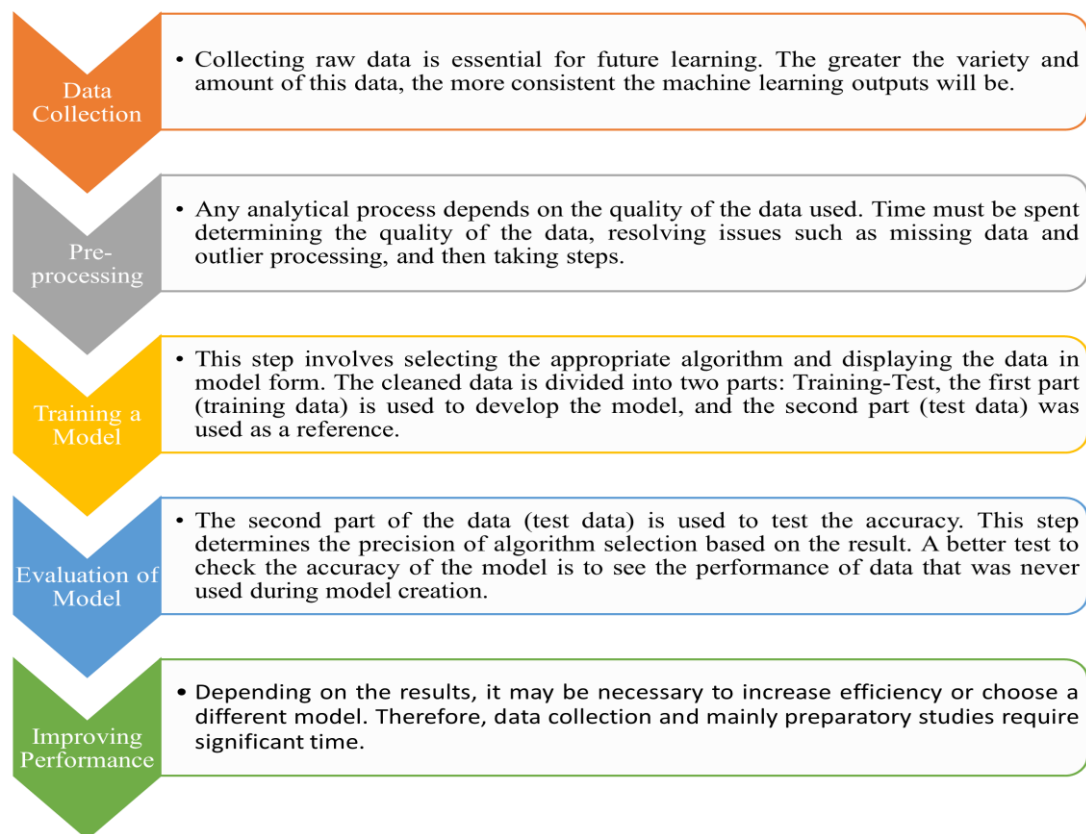


Figure 2.1: There are five basic steps used to perform an ML task.

ML, a branch of the field of AI, deals with developing algorithms and techniques to perform the “learning” task of computers [68]. ML is used in many areas, such as Natural Language Processing [69], Speech and Handwriting Recognition [70], Object Recognition [71], Robot Gestures [72], and Medical Diagnostics [73]. In addition, ML algorithms are shown in Figure 2.2.

ML is classified under three categories based on learning styles, including Supervised Learning [74], Unsupervised Learning [75], and Reinforcement Learning (RL) [76].

- **Supervised Learning:** The system compares the target results produced with the evaluated dataset and the model created by combining different inputs. It is essential to catch the optimum by minimizing the errors by the system. In supervised learning, also called predictive models used to predict future outcomes based on historical data, clear instructions are usually given on what to learn and how to learn from the beginning [74]. Some examples of algorithms used: Nearest neighbor, Naive Bayes, Decision Trees, Regression, etc.
- **Unsupervised Learning:** Without specifying a target in the dataset that makes up the system, the model is expected to create a template by evaluating the inputs of the given parameters within itself. It is used to train explanatory models where no goals are set, and no feature is more important than another [75]. Some examples of algorithms can be given as K-Means / Clustering Algorithms.
- **RL:** Based on supervised learning, this system is based on a new target parameter creation logic that shows how accurate the target parameter outputs are in the model. It is an example of ML, where the machine makes certain decisions based on business needs to maximize performance. The idea of RL is that the machine constantly trains itself depending on the environment. This continuous learning process is time-saving with less involvement of human expertise. An example of an algorithm used in RL is the Markov Decision Process. There is a subtle difference between Supervised Learning and RL. RL involves learning in interaction with an environment. An RL representative learns from experience rather than a continuous trial-and-error learning process against supervised learning, for which an external supervisor provides examples [76].

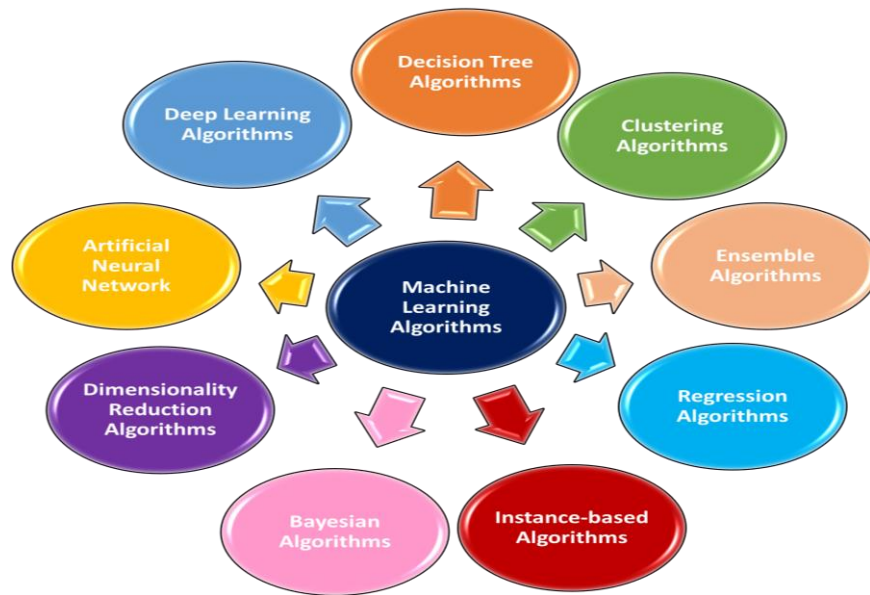


Figure 2.2: Machine Learning Algorithms.

2.3.1.1 Regression Algorithms

Regression is about modeling the relationship between variables using a measure of the error in the predictions made by the model [77]. Regression algorithms study statistics and have been incorporated into statistical ML. This can be confusing because regression can be used to refer to problem class and algorithm class. Popular regression algorithms:

- Ordinary Least Squares Regression (OLSR)
- Linear Regression
- Logistic Regression
- Local Estimated Distribution Line Correction (LOESS)
- Multivariate Adaptive Regression Curves (MARS)

2.3.1.2 Instance-based Algorithms

An instance-based algorithm is a decision problem about the sample or training data required for the model [78]. These algorithms typically create a sample database and compare new data to the database using a similarity measure to find the best match and make an estimate. For this reason, instance-based

algorithms are also called memory-based learning with practice and acquisition methods. The focus is on the representation of stored samples and the similarity measures used between samples. The popular instance-based algorithm is:

- k-Nearest Neighbor (kNN)

2.3.1.3 Decision Tree Algorithms

Decision tree algorithms create a decision model based on the actual values of the attributes in the data [79]. Decisions made in tree structures are valid until an estimation decision is made for a particular record. Decision trees are trained on data for classification and regression problems. Decision trees are generally fast and precise, also a favorite in ML. Popular decision tree algorithms:

- Classification and Regression Tree (CART)
- Recursive Binary Tree (ID3)
- C4.5 and C5.0 (different versions of a strong approach))
- Decision Root
- M5
- J48

2.3.1.4 Bayesian Algorithms

Bayesian is algorithms that explicitly apply Bayes' Theorem for problems such as classification and regression [80]. Popular Bayesian algorithms:

- Naive Bayes
- Gauss Naive Bayes
- Multinomial Naive Bayes

2.3.1.5 Clustering Algorithms

Clustering, like regression, defines the problem and method classes [81]. Clustering methods are typically organized by modeling approaches such as center-based and hierarchy. All methods are about using natural structures in

the data best to organize the data into groups with the best commonality. Popular clustering algorithms are:

- K-Average
- K-Medians
- Hierarchical clustering

2.3.1.6 Ensemble Algorithms

Ensemble algorithms are models of weaker models that have been independently trained and whose predictions are somehow combined to make an overall prediction [82]. Much effort goes into combining the factors that undermine learning and how to combine them. These are a potent class of techniques.

Popular ensemble algorithms:

- Boosting
- Bootstrapped Collection (Bagging)
- AdaBoost
- Stacked Generalization (Stacking)
- RF

2.3.1.7 Dimensionality Reduction Algorithms

Like clustering algorithms, dimensionality reduction looks for natural structure in the data; however, in this case, to summarize or explain the data using less information in an unsupervised or sequential manner [83]. This can be useful for visualizing dimensional data or simplifying data that can later be used in supervised learning. Many of these algorithms can be adapted for use in classification and regression. Popular dimensionality reduction algorithms:

- Principal Component Analysis (PCA)
- Principal Component Regression (PCR)
- Partial Least Squares Regression (PLSR)
- Linear Discriminant Analysis (LDA)

- Quadratic Differential Analysis (QDA)
- Flexible Differential Analysis (FDA)

2.3.1.8 Artificial Neural Network Algorithms

Artificial Neural Networks are models inspired by the structure and function of biological neural networks. It is a model-matching class often used for regression and classification problems; however, it is an enormous subfield of hundreds of algorithms and variations for all kinds of problems [84]. Due to the enormous growth and popularity in the field, more classical methods are discussed here, keeping DL separate from neural networks. Popular neural network algorithms:

- Perceptron
- Backpropagation

2.3.1.9 Deep Learning Algorithms

DL algorithms are a modern update to Neural Networks that use copious amounts of shoddy computation. They deal with building much larger and more complex neural networks, and as mentioned above, many methods deal with semi-supervised learning problems where large datasets contain very few labeled data [85]. Popular DL algorithms:

- Deep Boltzmann Machine (DBM)
- Deep Belief Networks (DBN)
- Convolutional Neural Network (CNN)

2.4 Software Programs

The software programs used in the thesis, MATLAB, Python, Java, WEKA, Firebase, and Android Studio are mentioned here (Figure 2.3).

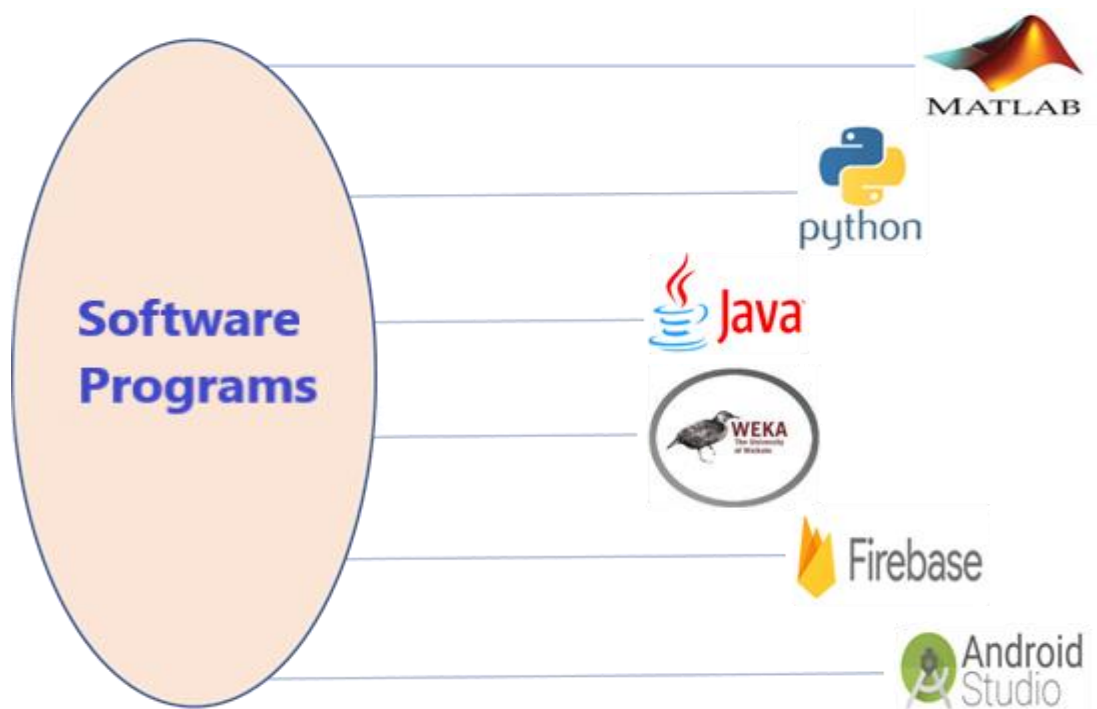


Figure 2.3: Schematic illustration of the software programs.

2.4.1 MATLAB

MATLAB is a computer program used for positive science and engineering calculations. Developed by the MathWorks company, MATLAB is also a programming language [86]. MATLAB, which is formed by combining the words “Matrix Laboratory” in English, has a matrix-based working system, as the name suggests. The MATLAB program enables many mathematical calculations such as linear algebra, statistics, optimization, numerical analysis, optimization, and Fourier analysis to be performed effectively and quickly; it is also used for 2D and 3D graphic drawing. Users can create their programs with MATLAB, which allows programming with matrices and the functions they interact with, and even very complex mathematical calculations are completed in a few seconds. Effective and practical programs can be prepared with MATLAB, where basic programming and similar functions can be used. It is possible to work with matrices in one, two, or more dimensions in the MATLAB program, where matrices are used with the same logic as arrays in programming languages such as C and Java [86].

2.4.2 Python

Python is a programming language that can do scientific calculations quickly, is very useful, advanced, and open source, can run smoothly on different platforms such as Windows / macOS / Linux, and is highly flexible and straightforward to learn [87]. The most important feature is that, unlike other programming languages, it does not need any compiler.

Advanced data analytics has become a crucial topic for IT today. Python has been the most suitable programming language for these situations. Most of the libraries in the Python interface are suitable for ML and data science. Its high-quality commands in libraries in these areas have greatly aided the continued development of ML libraries and other numerical algorithm libraries.

2.4.3 Java

Developed by Sun Microsystems, Java was first released in 1995. Java: is a class- based, object-oriented programming language with many uses. Java is also a computing platform for application development and execution. Java is also an application run software that the end user can download for free [88]. Since Java is a programming language that has been used for many years, it has received many different updates and versions. Finally, Java SE 15 version was released in September 2020. The software users will download to run applications is the Java 8 version [89].

The Java software that users will use to run applications is called the Java Runtime Environment, or JRE for short, and the computing platform used by application developers is called JRM for short. A Java Development Kit (JDK) tool is also available to application developers [88]. Java owes its popularity to its ease of use. Here are some reasons why developers continue to choose Java over other programming languages:

- High-quality learning resources
- Integrated functions and libraries
- Active community support

- High-quality development tools
- Security

2.4.4 WEKA

WEKA is the name of one of the packages used in ML, one of the crucial subjects of computer science. It was developed as an open source in the Java language at the University of Waikato and distributed under the GPL license. Waikato is an acronym for Environment for Knowledge Analysis [90]. WEKA reads data from a simple file and assumes that stochastic variables on the data are numeric or nominal values. It can also pull data from the database; however, it is expected to be file data in this case. Many libraries about ML and statistics are available at WEKA [90]. For example, data pre-processing, regression, classification, clustering, feature selection, or feature extraction are some. In addition, there are visualization tools that allow the results of these operations to be displayed visually.

2.4.5 Firebase

Developed with new features added by Google, Firebase is a platform that claims to meet all these needs and offers free use. There is a need for application development on any platform for any reason, followed by a control panel and, in any case, a user data store [91]. Applications today want to access the same data from every device regardless of platform. Developers whose applications are installed by many users also need a management panel to easily manage operations such as saving and keeping session information, analyzing the usage data of applications, sending notifications to the user to make new announcements, and testing the application. Firebase, which is constantly evolving with new features added by Google, is a platform that offers free use to application developers to meet all these needs.

Firebase, which performs applications such as application management, usage tracking, data storage, and sending notifications without needing to write a different server and server-side code, provides access to every application

equipped with features such as Real-Time Database and Notification [91]. Remote Config in its new developer-friendly interface (Figure 2.4).

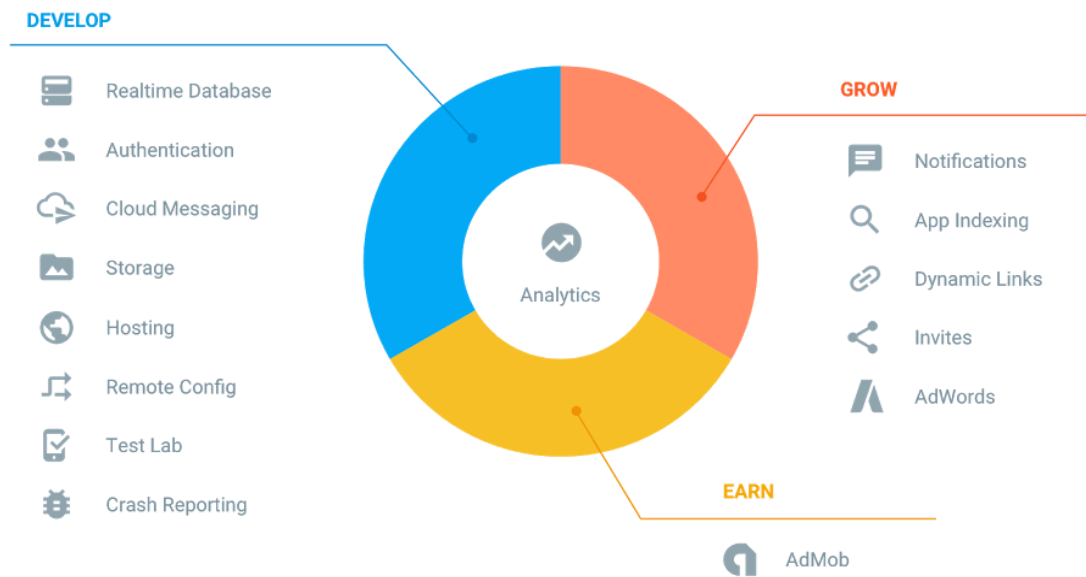


Figure 2.4: Firebase interface.

2.4.6 Android Studio: Smartphone Applications

Electronic devices such as mobile phones or tablets must have an operating system. A device cannot work without an operating system. Android is a communication system developed by Google and billions of people [92]. It uses the Linux operating system kernel. It also supports APK extension. It is beneficial for such reasons. When this project is completed, it will be available on Android operating systems. Android Studio is a programming tool for developing Android applications. Some essential features of Android Studio are mentioned below:

- Gradle-based, flexible project-building system
- Fast project generation with the help of basic templates
- The editor that facilitates screen designs
- Easily add Google services to the app
- Easy and secure APK signing

2.5 Performance Metrics

During the performance evaluations of the proposed classifiers, accuracy (Equation (2.13)), precision (Equation (2.14)), recall (Equation (2.15)), F1 score (Equation (2.16)), AUC-ROC Curve (Equation (2.17)) and Matthews Correlation Coefficient (MCC) (Equation (2.18)) were calculated.

2.5.1 Accuracy

Accuracy is the most used metric in the classification comparison. It is the ratio of correctly classified samples to total samples [16].

$$Accuracy = \frac{TP + TN}{TP + TN + FP + FN} \quad (2.13)$$

where TP (True-Positive) and TN (True-Negative) describe the number of correctly identified positive and negative samples, while FP (False-Positive) and FN (False-Negative) define the incorrectly predicted samples.

2.5.2 Precision

Precision is a performance metric used in AI and ML to evaluate the accuracy of a model's predictions. Precision measures how often the model correctly identifies true positive cases, meaning the instances where the model predicted a positive outcome and it was true. In other words, precision is the ratio of true positives to the total number of positive predictions made by the model [16].

$$Precision = \frac{TP}{TP + FP} \quad (2.14)$$

2.5.3 Recall

The recall is the ratio of positively labeled samples to the total number of truly positive samples [16].

$$Recall = \frac{TP}{TP + FN} \quad (2.15)$$

2.5.4 F1 Score

The F1 score is calculated using precision and recall metrics. It optimises the system towards precision or recall [16].

$$F1\ score = 2 \times \frac{Precision \times Recall}{Precision + Recall} \quad (2.16)$$

2.5.5 AUC-ROC Curve

ROC curves are one of the methods used to measure the success of the models in distinguishing each class. The area under these curves (AUC) approaches shows that the CNN model has successfully classified the concentrations [17].

$$ROC\ area = \frac{1}{2} \times \left(\frac{TP}{TP + FN} + \frac{TN}{TN + FP} \right) \quad (2.17)$$

2.5.6 Matthews Correlation Coefficient

MCC measures the quality of binary (two-class) classification models [93]. It considers TP, TN, FP, and FN predictions of the model. MCC is calculated as follows:

$$MCC = \frac{(TP \times TN) - (FP \times FN)}{\sqrt{(TP + TN)(TP \times FN)(FP \times TN)(FN \times TN)}} \quad (2.18)$$

Chapter 3

Non-enzymatic colorimetric detection of hydrogen peroxide using a μ PAD coupled with a machine learning-based smartphone app

In this chapter, iodide-mediated 3,3',5,5'-TMB- H_2O_2 reaction system was applied to a μ PAD for non-enzymatic colorimetric determination of H_2O_2 . The proposed system is portable, incorporating a μ PAD and an ML-based smartphone app. The colorimetric change in detection was obtained without using any enzymes or nanoparticles with catalytic properties, resulting in a low-cost and stable system. A smartphone app called “Hi-perox Sens” capable of image capture, cropping and processing was developed to make the system simple and user-friendly. Briefly, circular μ PADs were designed with three different detection mixtures containing: (i) TMB, (ii) KI, and (iii) TMB+KI, respectively. The μ PADs were then tested with varying concentrations of H_2O_2 . Following the color change, the images of the μ PADs were taken with four different smartphones under seven different illumination conditions at $t=30$ s and $t=10$ min. Visual inspection showed that H_2O_2 induced color change only in the case of KI and TMB+KI. Unlike KI, the mixture of TMB+KI performed best at lower concentrations of H_2O_2 . To make the system more robust and adaptive against illumination variation and camera optics, the images were first processed for feature extraction and then used to train ML classifiers. Twenty-three ML classifiers were tested to determine the best-performing ML classifier

for KI and TMB+KI, respectively. A cloud system was used in the application to communicate with a remote server running ML classifiers. According to the results, TMB+KI showed the highest classification accuracy with inter-phone repeatability at $t=30$ s under versatile illumination and maintained its accuracy for 10 minutes. In addition, the performance of the system was also comparable to two different commercially available H_2O_2 kits in real samples.

3.1 Introduction

Hydrogen peroxide (H_2O_2) is a reactive oxygen species produced by mammalian cells to mediate several physiological processes, including cell proliferation, migration, differentiation, and even apoptosis [94]. Even though H_2O_2 is not so reactive, it can generate hydroxyl radicals that can attack specific cell components such as DNA and membrane lipids. Changes in its concentration have been associated with the development of various diseases, including cancer, Alzheimer, and diabetes mellitus [95]. It is widely used as a disinfectant due to its antibacterial and virus activity. It is also a by-product of oxidases, and therefore its high-sensitive detection is of great importance in developing biosensors for fields ranging from medical diagnostics to environmental monitoring [96]. Several methods, including chemiluminescence, fluorescence, electrochemical and colorimetric, have been proposed to detect H_2O_2 for qualitative and quantitative analysis. Among these methods, colorimetry is promising due to its cost-efficiency and easy operation. HRP is frequently used in colorimetric sensors where it catalyzes the conversion of a chromogenic agent [40, 97]. Even though H_2O_2 sensors with HRP offer high sensitivity and selectivity, they suffer from a narrow pH working range, poor reproducibility, high cost, and low thermal/chemical stability of the enzyme. To overcome these limitations, researchers are actively studying the catalytic properties of nanomaterials, particularly noble metals, and their alloys, to replace enzymes in sensor applications. However, these nanomaterials still suffer from high cost, aggregation, and poor stability, and their toxic effects on living things have not been thoroughly investigated [98, 99]. Apart from enzymes or nanomaterials, the use of biopolymers with peroxidase-like activity or antioxidative activity,

such as chitosan and gelatin, have also been reported for the detection of H₂O₂ [98].

In addition to being sensitive, selective, and affordable, H₂O₂ sensors need to be portable, reliable, fast, and environmentally friendly to operate in remote locations or resource-limited settings [100]. In that sense, μ PADs are found to be adequate to meet the requirements, resulting in the development of various types of sensors. Although different methods are used in the fabrication of μ PADs, the most preferred method is the one that was first introduced by Whitesides et al. [101]. The method is based on printing wax patterns that define the microfluidic channels and the boundaries of the detection zone with a solid ink (wax) printer. In μ PADs, the concentration of many different analytes can be quantified simultaneously based on the intensity variation due to the concentration-dependent color change [40].

In colorimetric analysis, intensity information can be utilized with several color spaces, including RGB, HSV, and L*a*b* [102]. The conventional approach derives a calibration curve based on single or multiple channels, leading to the highest correlation between intensity and concentration (magnitude) [103]. For example, the average of R, V, and L* was used to obtain the calibration in the quantification of glucose in artificial saliva [103]. Even though the calibration curve performs well in a controlled environment, it tends to deviate in the case of ambient light conditions as the intensity values are sensitive to the illumination sources. This problem is handled with sophisticated methodologies like ML, which has emerged as a powerful tool for classification problems due to its flexibility and adaptability to dynamic conditions based on the features extracted from colorimetric information [104, 105]. The alcohol level in saliva was detected using features of four-color spaces (RGB, HSV, YUV, and L*a*b*) under three ML classifiers [104]. ML classifiers quantified The peroxide concentration with colour features [105]. Molgaard et al. [106] also employed an ML approach to detect H₂O₂ using colorimetric sensor technology for air sampling. One benefit of ML is to be compatible with smartphone apps that perform colorimetric analysis in the field without extensive training [107]. The SPAQ2 app was developed to test the alcohol level in saliva [104]. The ChemTrainer app detected

peroxide according to the color changes in the colorimetric test strips [105]. All these apps provide user-friendly interfaces to perform colorimetric analysis with ML (Figure 3.1).

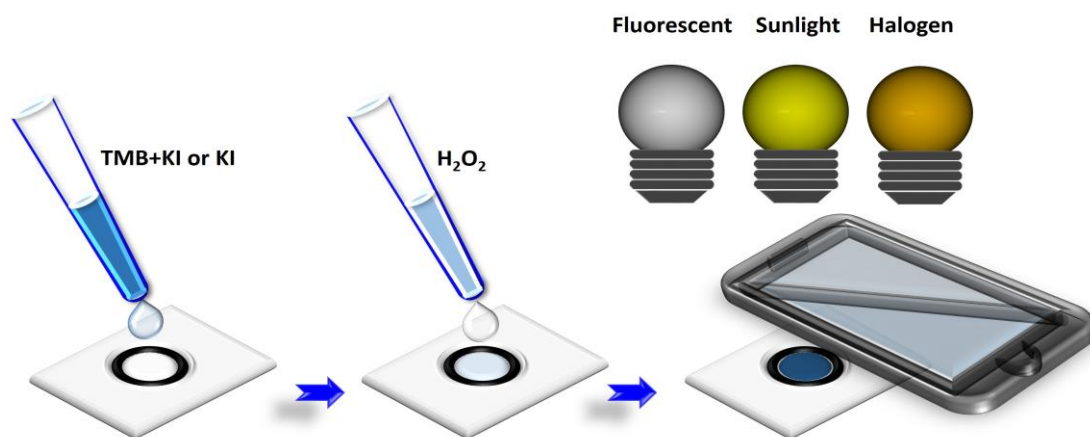


Figure 3.1: Schematic illustration of the proposed system. The color change of chromogenic agents can be detected with a smartphone camera under ambient light conditions.

3.2 μ PAD fabrication and colorimetric detection of H_2O_2

First, a circular design to be used as a reaction/detection zone of μ PADs was drawn in Microsoft PowerPoint. This design was then printed on a Whatman filter paper with a solid ink (wax printer) printer. Solid ink is a mixture of hydrocarbons and hydrophobic carbamates with a melting point of about 120 °C. After printing, the solid ink was kept on a heater at approximately +150 °C for 3 minutes. An aluminum foil and a planar weight (1–2 kg) were placed on top of the paper to ensure uniform heat transfer from the hot plate to the paper and penetration of the melted solid ink into the pores of the chromatography paper. Hence, solid ink boundaries that define the reaction/detection zone were obtained. Next, three different μ PADs were prepared by introducing 0.8 μ l KI (6 M), TMB (10 mM) +KI (6 M), and TMB (10 mM) into μ PADs, respectively. The μ PADs were left to dry for about 5 minutes for the liquids to dry. Next, the μ PADs were tested for the colorimetric detection of H_2O_2 at varying

concentrations (0.01, 0.05, 0.1, 0.2, 0.5, 1, 5, 10, 25, 50 mM), in which case 2 μL aliquots of test solutions were introduced into the reaction/detection zones of μPADs . The image of each μPAD was captured using a smartphone camera at $t=30\text{ s}$ and $t=10\text{ min}$, respectively.

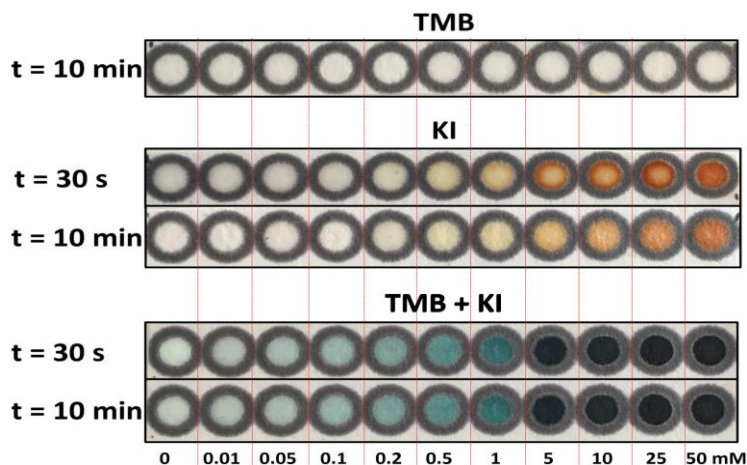


Figure 3.2: Color changes with respect to chromogenic agents, time, and concentrations.

3.3 Data Acquisition and Processing

ML classifiers must be trained with a dataset with a strong representation of all possible conditions to get a significant classification performance [108]. The robustness and adaptability of the system, therefore, are highly dependent on the dataset, which needs to be enlarged considering illumination conditions and camera optics. To address these issues, the images of the μPAD were captured with multiple smartphones under halogen (H), fluorescent (F), and sunlight (S) light bulb sources to imitate the conditions. The H bulb emits 2700 K warm colors, while the F and S bulbs give 4000 K neutral and 6500 K cool colors, respectively. Three light sources were used to get seven light conditions including H, F, S, HF, HS, FS, and HFS, running single or multiple light sources together. The bulb sources were located 50, 53, and 57 cm away from H, F, and S, respectively. In addition, the capturing was performed at an incidence angle of 30° under a homogeneously illuminated area with a constant distance of 8 cm between the smartphone and the μPAD .

To maintain inter-phone operability, four different smartphones with different brands (Oppo A5 2020, Reeder P10, iPhone 5SE, and iPhone 6S) and operating systems (Android and iOS) were used for capturing. The specifics of the cameras for each smartphone are shown in Table 3.1. Images were captured in automatic mode at $t=30$ s and $t=10$ min as shown in Figure 3.2.

Table 3.1: The smartphones are used to create a dataset with images of μ PADs for machine learning.

Smartphone Brand	Image Resolution	Optics	Camera Resolution
iPhone 5SE	4032 x 3024	f/2.2	7 MP
iPhone 6S	4032 x 3024	f/2.2	12 MP
Oppo A5 2020	4000 x 3000	f/1.8	12 MP
Reeder P10	4160 x 3120	f/2	13 MP

Twenty-eight images were taken with each smartphone separately under seven different illumination conditions at two-time steps, resulting in fifty-six images. Since the group of eleven concentrations was captured at a single frame, 616 images of each concentration were collected for TMB+KI and KI, respectively. These images were then transferred to a computer to process in MATLAB (MathWorks, MA, USA) environment for feature extraction.

3.4 Feature Extraction and Machine Learning Analysis

Feature extraction is identifying an object based on properties such as size, shape, composition, and location of the object [109]. In mathematical terms, it is the process of inferring from raw data information to increase the variability of the class pattern while minimizing the in-class pattern variability, which facilitates quantitative measurements, classification, and object identification [110]. Feature extraction is a crucial step in visual inspection as it has an observable effect on the efficiency of the ML classifiers. Before training the

classifiers, image features were extracted based on color and texture information. The region of interest (ROI) for each concentration was cropped to convert the RGB image into HSV and L*a*b*, resulting in a total of nine color channels (R, G, B, H, S, V, L*, a*, b*) information. Then, the mean, skewness, and kurtosis values were calculated for each color channel, leading to twenty-seven features. As texture features, contrast, correlation, homogeneity, and energy were also extracted [111]. In addition to the color and texture features, the entropy and intensity values were also added to have a total of thirty-three features.

To determine the H₂O₂ based on color changes, twenty-three ML classifiers were trained with the extracted features, and their performances were compared regarding classification accuracy. Among these classifiers, LDA and Ensemble Bagging Classifier (EBC) outperformed the others for KI and TMB+KI, respectively. The LDA is a supervised classifier that applies Bayesian and maximum likelihood rules to estimate the highest likelihood between input and pre-defined classes using a discriminant function [112]. EBC is an ensemble technique used to improve the performance of ML classifiers in terms of stability and accuracy. It combines the classifications of randomly generated training sets to estimate the final prediction [113] based on the bagging algorithm.

As the LDA and EBC showed the best classification performance, they were integrated into our smartphone application called Hi-perox Sens.

3.5 Smartphone Applications: Hi-perox Sens

Our custom-designed Android app, Hi-perox Sens, was developed for quantitative evaluation of H₂O₂ in μ PADs with ML, enabling colorimetric analysis operable whenever or wherever needed. The LDA and EBC ML classifiers, running in the remote server, were integrated into the Hi-perox Sens due to their outstanding performances. The Hi-perox Sens uses a Firebase cloud system to transfer the image to the remote server and receive the classification result back to the app.

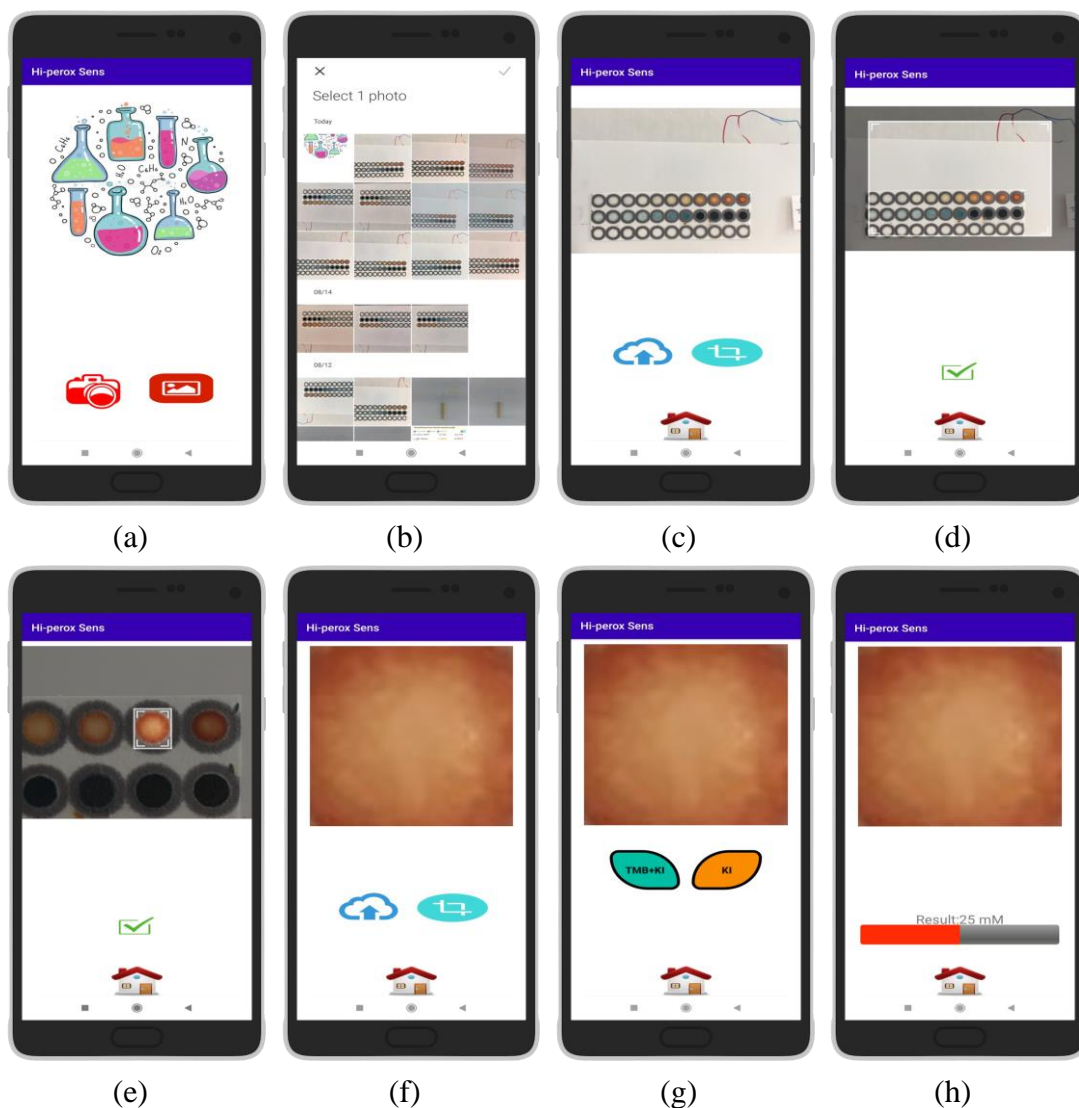


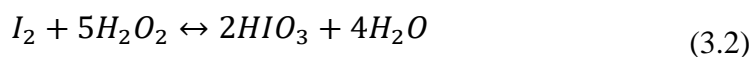
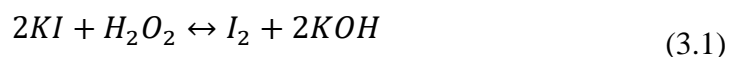
Figure 3.3: Colorimetric hydrogen peroxide quantification steps on the Hi-perox Sens. The homepage of the Hi-perox Sens is given in (a). The user can select an image from the gallery or capture a new image using the smartphone camera in (b) and display it on the screen as in (c). The image can be cropped using an adjustable crop box in (d). The cropped patch is given in (e) and uploading the cropped patch is shown in (f). The user selection of the uploading patch as TMB+KI or KI is shown in (g). The classification result of the image is given in (h).

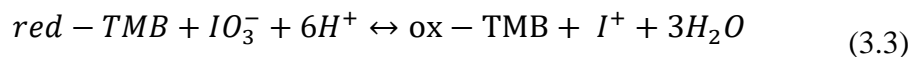
With a simple and user-friendly interface, Hi-perox Sens is demonstrated in Fig. 3.3. The home page is given in Figure 3.3(a) where an image can be taken from the gallery of the smartphone (Figure 3.3(b)) or a new image can be captured using the smartphone camera. Once the image is selected or captured, it is

displayed on the app, as shown in Figure 3.3(c). Next, the ROI on the image needs to be drawn using an adjustable crop box, as shown in Figure 3.3(d-e). Then, the ROI is cropped and displayed on the app (Figure 3.3(f)) to double-check the ROI and whether the selected area is suitable for the analysis. If not, the ROI can be re-drawn before the cropped patch is transferred to the remote server via a Firebase by tapping the upload icon. ML classifiers running in the remote server quantify the concentration level. As shown in Figure 3.3(g), the colorimetric reagent information (TMB+KI or KI) must also be sent to the remote server to choose the best classifier for the colorimetric analysis. Last, the result is returned to Hi-perox Sens via a Firebase to display on the app (Figure 3.3(h)).

3.6 Results and Discussion

Here, the iodide-mediated TMB-H₂O₂ reaction system was used instead of an enzyme or a nanomaterial with catalytic properties to detect H₂O₂. Briefly, three different chromogenic agent mixtures were tested with varying concentrations of H₂O₂; i) only TMB, ii) only KI, and iii) TMB+KI. As shown in Figure 3.2, no color change was observed in the case of only TMB, which clearly demonstrates that TMB alone cannot catalyze the oxidation of H₂O₂. However, in the case of only KI, H₂O₂ catalyzes the conversion of KI to iodine and produces a visual brownish color. Although the changing color intensity was not proportional to the low concentration of H₂O₂, a linear correlation was observed when the H₂O₂ concentration exceeded the 1 mM level (Figure 3.2). When TMB+KI was used as the detection mixture, a blue color appeared in the presence of H₂O₂. The oxidation of TMB caused the color change. A possible chemical reaction equation involving three steps is presented below.





In the first step (Equation (3.1)), KI gets into a reaction with H₂O₂ and produces I₂, which then once again reacts with H₂O₂ to produce iodic acid (HIO₃) (Equation (3.2)). As HIO₃ ionizes, iodate (IO⁻³) is formed. In the final stage (Equation (3.3)), the oxidation of TMB is induced by the reduction of IO⁻³ to I⁻, resulting in the formation of blue color. According to this reaction, iodide catalyzes the rapid oxidation of TMB. Unlike the chromogenic agent KI, TMB+KI performed best in the low concentration range of H₂O₂, and the color intensity became saturated when the H₂O₂ concentration level exceeded 5 mM (Figure 3.2). In addition, the effect of pH and ionic strength on the signal response of μPADs were tested in the presence of 1 mM H₂O₂. No significant change in colour formation was observed in the pH range of 5 to 11. However, the intensity of the color formed at pH 3 was lower than the rest. As for the ionic strength, the color intensity slightly increased with NaCl concentration. The adopted strategy has the potential to provide an essential basis for simple, rapid, cost-effective, sensitive, and selective colorimetric assay for the detection of H₂O₂.

In this study, H₂O₂ concentration was detected using ML classifiers based on the color change that occurred in the μPADs. ML classifiers need to be trained in advance with a dataset that contains similar images that the user might use in testing. Therefore, the dataset was created with four different smartphones (iPhone 5SE, iPhone 6S, Oppo A5 2020, and Reeder P10) under seven illumination conditions (H, F, S, HF, HS, FS, HFS). This dataset was transferred to a computer for pre-processing in MATLAB 2021b. The ROI for each concentration was cropped to extract features for training ML classifiers. First, twenty-three classifiers were trained for TMB+KI and KI with eleven concentrations ranging from 0 to 50 mM at t=30 s. The best classification results were 81.3% and 91.9% for KI and TMB+KI, respectively. After careful analysis of confusion matrices of the classifiers, it was observed that KI and TMB+KI failed to classify H₂O₂ in lower and higher concentration ranges, respectively. Therefore, classifiers were trained again with low concentration values (0, 0.01, 0.05, 0.1, 0.2, 0.5, 1, 5 mM) for TMB+KI, and high concentration values (0, 0.2,

0.5, 1, 5, 10, 25, 50 mM) for KI. As a result, the classification accuracies were improved to 97.3% and 92.4% for TMB+KI and KI, respectively. These results were summarized in Table 3.2. The same process was repeated with images taken at $t=10$ min., and the results were given in

Table 3.3. The system shows similar classification accuracy even after 10 min., which proves the robustness of the system.

In classification, the EBC gave the highest accuracy for TMB+KI while the LDA outperformed for KI. Besides the classification accuracy (Equation (2.13)), the performance of these classifiers was also tested in terms of precision (Equation (2.14)), recall (Equation (2.15)), and F1 score (Equation (2.16)).

As can be seen from the performance metrics (Figure 3.4), TMB+KI had the highest accuracy value, with 97.8% using EBC. The detailed classification reports and confusion matrices with respect to the type of chromogenic agents, timing, and concentration range can be found in Appendix A Tables A1-8 and Appendix A Figures A1-11.

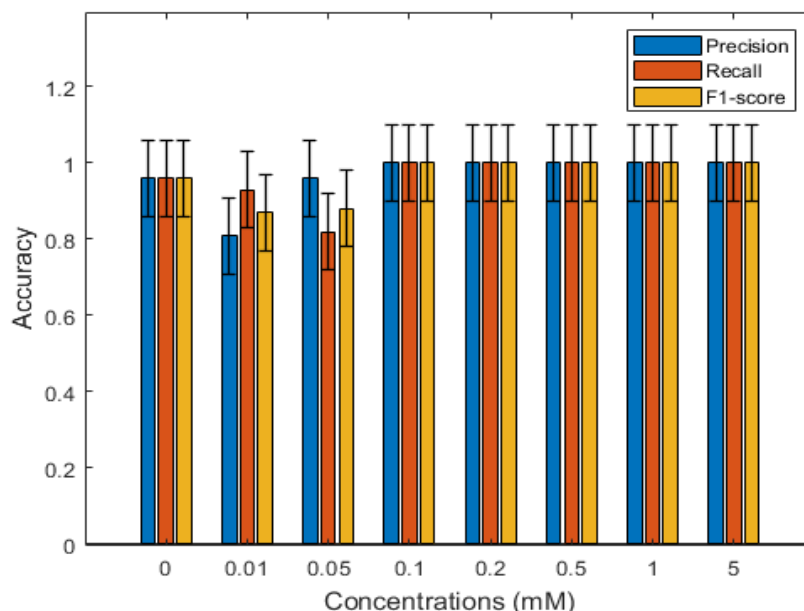


Figure 3.4: Evaluation of EBC with error bars in terms of precision, recall, and F1 score at $t=30$ s for TMB+KI using low concentrations.

It should be noted that the performance metric results were lower than the average values in the cases of 0.01 and 0.05 mM H_2O_2 . This can also be observed

in the confusion matrix shown in Figure 3.5(a), visualizing the performance metrics. A confusion matrix is mainly used to illustrate the relation between the true and predicted outputs of the classifier concerning each class. The robustness of the system can be quickly and visually observed when the confusion matrices of TMB+KI at 30 s (Figure 3.5(a)) and 10 min (Figure 3.5(b)) were compared. Figure 3.5(c) and (d) show performance analysis of LDA for KI at 30 s and 10 min, respectively. According to the matrices, much better prediction accuracy and robustness were achieved in the high concentration range of H₂O₂, as in TMB+KI.

Finally, our study integrated LDA and EBC classifiers with Hi-perox Sens, a simple and user-friendly mobile app for H₂O₂ detection. Images of this app are shown in Figure 3.3. The photo is selected from the gallery or captured using the camera; then, the ROI is cropped and sent via Firebase to the remote server running the ML classifier to measure the concentration level. The result is then returned and displayed in Hi-perox Sens. For example, the processes performed on an uploaded image are shown step by step in Figure 3.3. At last, Hi-perox Sens correctly classified the H₂O₂ concentration as 25 mM. The smartphone-based system successfully worked and quantified H₂O₂ levels in water with ML classifiers. The LOD of the sensor with TMB+KI was calculated to be 5.4 μM based on the RGB data of images taken under HFS with iPhone 6S (LOD = $3.3 \cdot \sigma / \text{Slope}$). Although the system works without a calibration curve, the calculated LOD value demonstrates its potential to be trained for lower concentrations of H₂O₂.

The most relevant studies include [105, 106, 114, 115], which, however, still substantially differ from the present study. First of all, either enzymes or catalytic nanoparticles were used in these papers to induce color change in the presence of H₂O₂. On the contrary, an iodide-mediated TMB-H₂O₂ reaction system was applied to μPADs for non-enzymatic H₂O₂ quantification, making the system low-cost. Solmaz et al. [105] and Molgaard et al. [106] also employed machine learning classifiers and reported that H₂O₂ was detected with 95 % accuracy in both studies. In addition, unlike Cheng et al. [115] and Bandi et al. [114], where a calibration curve-based colorimetric H₂O₂

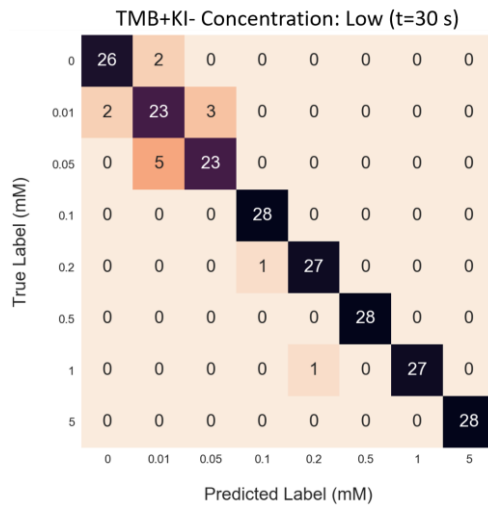
detection was performed, our proposed system is based on ML, offering more robustness and adaptability against ambient illumination conditions and camera optics. Therefore, the proposed system is state-of-the-art in robustness, adaptability, and classification accuracy.

Table 3.2: The classification results at t=30s and t=10 min. for KI.

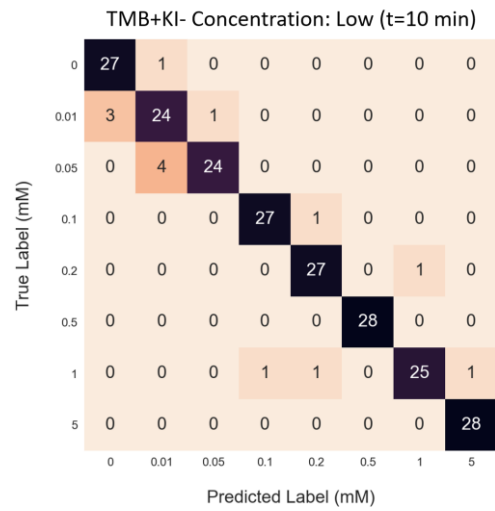
ML Classifiers	Classification Accuracy (%)					
	t=30 s			t=10 min		
	0-50 mM	High	Low	0-50 mM	High	Low
Decision Tree	40.8	44.8	-	40.84	44.9	-
Bagging Classifier	42.68	45.48	-	42.01	45.58	-
QDA	52.24	54.4	-	43.35	54.68	-
Ensemble Subspace Discriminant	50.22	57.02	-	46.13	58.12	-
Extra Tree Classifier	54.58	57.46	-	47.45	57.89	-
Naive Bayes	55.17	58.77	-	49.53	59.18	-
AdaBoost	55.94	58.97	-	50.02	59.63	-
PCA	58.24	59.64	-	51.18	59.98	-
RBF SVM	60.24	61.83	-	53.63	61.71	-
Ensemble RUS Boosted Tree	60.82	62.02	-	55.73	63.17	-
Gradient Boosting Classifier	60.82	62.74	-	56.12	62.77	-
Weighted KNN	62.86	64.56	-	57.06	64.96	-
Gaussian Process	64.44	65.04	-	62.31	66.16	-
Bernoulli Naive Bayes	67.84	72.34	-	65.79	73.14	-
EBC	71.78	72.98	-	67.16	73.88	-
Logistic Regression	74.89	76.43	-	69.54	76.93	-
Random Forest	79.78	81.8	-	72.34	81.9	-
kNN	80.85	82.69	-	75.08	83.29	-
Linear SVM	77.52	85.95	-	76.21	84.81	-
Coarse Tree	77.74	88.69	-	76.94	89.12	-
SVM	76.4	89.5	-	79.4	89.6	-
Bagging	78.74	90.93	-	80.09	90.98	-
LDA	81.3	92.3	-	89.1	92.4	-

Table 3.3: The classification results at t=30s and t=10 min. for TMB+KI.

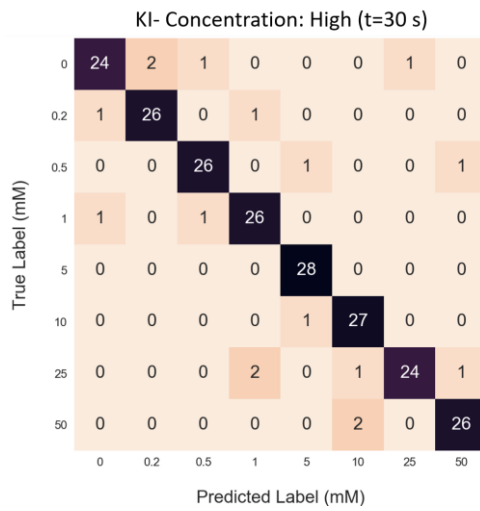
ML Classifiers	Classification Accuracy (%)					
	t=30 s			t=10 min		
	0-50 mM	High	Low	0-50 mM	High	Low
AdaBoost	26.15	-	32.12	29.2	-	34.36
Ensemble Subspace Discriminant	32.06	-	35.12	30.36	-	39.17
Naive Bayes	33.85	-	41.28	30.51	-	43.26
QDA	36.54	-	43.57	33.07	-	43.81
SVM	40.31	-	47.39	33.95	-	47.22
PCA	42.19	-	47.66	34.06	-	47.59
RBF SVM	46.03	-	52.93	35.57	-	49.23
LDA	49.68	-	53.82	38.67	-	54.46
Gaussian Process	51.68	-	54.3	41.17	-	54.84
Bagging Classifier	53.14	-	55.23	43.2	-	60.31
Extra Tree Classifier	57.02	-	64.32	45.32	-	61.92
Linear SVM	58.1	-	65.33	48.58	-	65.29
Ensemble RUS Boosted Tree	58.23	-	66.28	49.2	-	65.55
Gradient Boosting Classifier	61.32	-	68.3	51.14	-	71.36
Weighted KNN	65.32	-	71.23	52.41	-	74.47
Decision Tree	65.64	-	73.42	57.2	-	80.42
Bernoulli Naive Bayes	70.65	-	75.32	62.24	-	81.41
Coarse Tree	76.04	-	80.05	63.61	-	85.86
Bagging	80.47	-	81.19	63.82	-	88.08
Random Forest	80.54	-	83.29	66.84	-	89.43
Logistic Regression	81.89	-	87.73	69.93	-	94.12
kNN	86.37	-	93.3	75.36	-	96.43
EBC	91.9	-	97.8	85.1	-	97.3



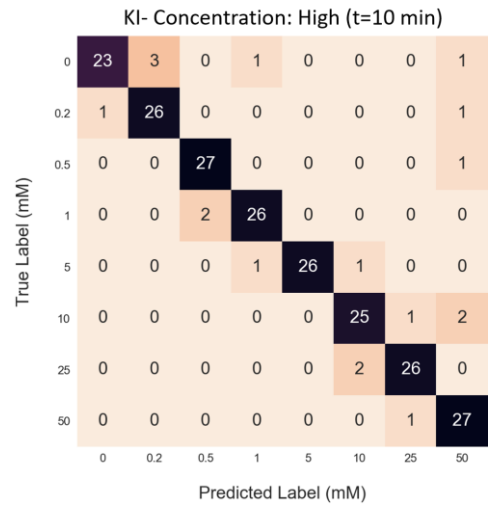
(a)



(b)



(c)



(d)

Figure 3.5: Confusion matrices of TMB+KI for the EBC classifier at t=30 s is given in (a) and at t=10 min in (b), and confusion matrices of KI for the LDA classifier at t=30 s are shown in (c) and at t=10 min in (d).

Chapter 4

Smartphone embedded deep learning approach for highly accurate and automated colorimetric lactate analysis in sweat

Here, a μ PAD was combined with a DL-based smartphone app called “*DeepLactate*” and then applied for quantitative and selective determination of lactate concentration in sweat. The μ PAD was made using wax printing protocol, and the detection area was modified with HRP, LOx, and the chromogenic agent 3,3',5,5'-TMB for enzymatic detection. The images of μ PADs taken by smartphones of several brands in different lighting conditions were used to train various DL models to make the system more robust and adaptable to lighting changes. The top-performing model, Inception-v3, was then embedded into a smartphone app, offering easy operation for non-expert users. Unlike ML classifiers, DL models can automatically extract features and be embedded in a smartphone app, enabling analysis without internet access. According to the results, the current system showed a classification accuracy with phone-independent repeatability and a processing time of less than 1 sec. It also showed excellent selectivity towards lactate over different interfering species. Finally, μ PAD was turned into a patch to determine the level of sweat lactate in two volunteers after resting and 15 min of jogging. The system successfully detected lactate in human sweat and confirmed that the lactate level in sweat increased after jogging. Since the μ PAD was designed first to

absorb a sample and then transfer it to the detection area, avoiding direct contact with the skin, the system reduces the possibility of skin irritation and has great potential for practical use in various fields, including self-health monitoring and sports medicine.

4.1 Introduction

Wearable sensors have attracted considerable attention lately with their applications in various fields, such as sports medicine and self-monitoring for health [116]. Although blood biomarkers are still considered reliable indicators of health status, wearable sensors based on non-invasive measurement protocols are gaining more attention as they do not cause blood vessel or skin injuries [117]. Various body fluids, such as sweat, saliva, and tear, can be used for non-invasive measurement protocols. However, a well-established correlation of analyte concentrations between body fluids and blood is required to use them as a reliable source in clinical applications [118]. A vital part of human thermoregulation, sweat is a slightly acidic biological fluid produced by sweat glands. It contains a variety of biomarkers for continuous and non-invasive measurements, including ions, metabolites (e.g., lactate, glucose), small molecules, and proteins [119, 120].

Recent reports have shown that blood and sweat lactate levels correlate [121, 122]. Lactate, the second low molecular weight metabolite after glucose, can be used as a biomarker to evaluate an individual's physical training and performance in sports medicine since it is a product of anaerobic metabolism [123]. During intense exercise, aerobic metabolism cannot meet the energy need, which initiates anaerobic metabolism and, thus, lactate accumulation in muscles. This phenomenon, known as lactic acidosis, is usually temporary and results in discomfort, pain, muscle cramps, soreness, and fatigue [124]. The amount of lactate production depends on the biological characteristics of a person, gender, frequency of exercise, and living conditions [125]. Lactate monitoring is essential, especially for people exposed to oxygen-deficient conditions, including athletes and military personnel. If lactate concentration reaches a critical level, it could change the pH of body fluids (blood, sweat, etc.) and

cause severe damage to various organs, including kidneys and blood vessels [126]. Furthermore, sweat lactate can be used to diagnose cystic fibrosis and monitor hypoxia, drug effects, and disease progression.

The enzyme lactate oxidase is commonly used to detect lactate, where it catalyzes the conversion of lactate to pyruvate and releases H_2O_2 as a by-product. H_2O_2 and, thus, lactate detection has been performed with various detection protocols such as electrochemical, chemiluminescence, and colorimetric [127-129]. Colorimetric detection is particularly interesting among them due to its simplicity, practicality, rapidity, low-cost, and high universality [23, 111].

Colorimetric analysis with complex instruments requires extensive prior training and high maintenance costs [130-132]. There are several commercially available electro-chemical and optical sensors used for lactate analysis, such as Lactate Scout 4 (EKF Diagnostics, UK), BM-Lactate (Roche, Switzerland), and Lactel (Marwan Technologies, Italy), all in a strip form. Lactate Scout 4 and Lactel are electrochemical devices that require a portable electrochemical reader, while BM-Lactate is a colorimetric sensor that requires a reflection photometer for an accurate quantitative analysis. Lactel is known to be the first sensor commercialized for lactate analysis in sweat, whereas the other two are primarily used for blood analysis. Although they are sensitive enough to detect lactate in real samples, their cost and dependence on a reader device may limit their widespread use, especially in remote locations. Alternatively, statistical analysis or AI-based smartphone applications offer a low-cost solution for non-expert users [40, 41, 105]. A representative method in statistical analysis is to employ the calibration curve derived from channel information of color spaces like RGB, HSV, and $L^*a^*b^*$ [23, 103]. The calibration curve has advantages such as computational cost and simplicity, making it easily applicable for colorimetric analysis. Kılıç et al. employed kurtosis of the a^* channel to derive a calibration curve and applied it for the colorimetric detection of food spoilage [23]. Similarly, Golcez et al. used average R, V and L^* channels to obtain a calibration curve for glucose detection in artificial saliva [103]. However, the performance of a calibration curve-based analysis is adversely affected by factors such as

ambient light, camera optics, and illumination variance [16, 40]. ML, a subset of AI, is not restricted by these limitations due to its robustness, adaptability, and compatibility, as reported by various groups. For instance, Doğan et al. detected H₂O₂ concentration in different water samples using an ML classifier trained with paper-based test images [16], while Mercan et al. developed a portable ML-based system to determine glucose concentration in artificial saliva [40]. ML also has some limitations application-wise. The first problem stems from manual feature extraction, which does not always guarantee to obtain distinctive features. The second problem is the requirement of internet access for quantitative and qualitative analysis, which makes such systems inoperable in resource-limited settings. All reported systems were built on a cloud system to transfer the data between a smartphone and a server, running the ML classifiers. Depending on the internet speed, this could cause a delay in the analysis due to data transfer. In addition, the server needs to be always running, which increases operational costs.

To address these problems, DL has emerged as a useful tool that automatically detects important features without human supervision. DL-based CNNs offer tremendous advantages for feature extraction due to their high learning capacity from many images. However, creating a CNN architecture from scratch is highly complicated, and slight modification to the structure or parameters significantly impacts model performance [133]. Therefore, there is a tendency to employ well-known CNN architectures, including MobileNet [134], Xception [135], VGG16 [136], VGG19 [137], ResNet50 [138], and Inception-v3 [139]. These architectures are compatible with Android, allowing them to be embedded in smartphones. Therefore, no internet connection (offline), cloud, or server is needed, contrary to the existing ML-based systems. The working principle of the proposed system is shown in Figure 4.1.

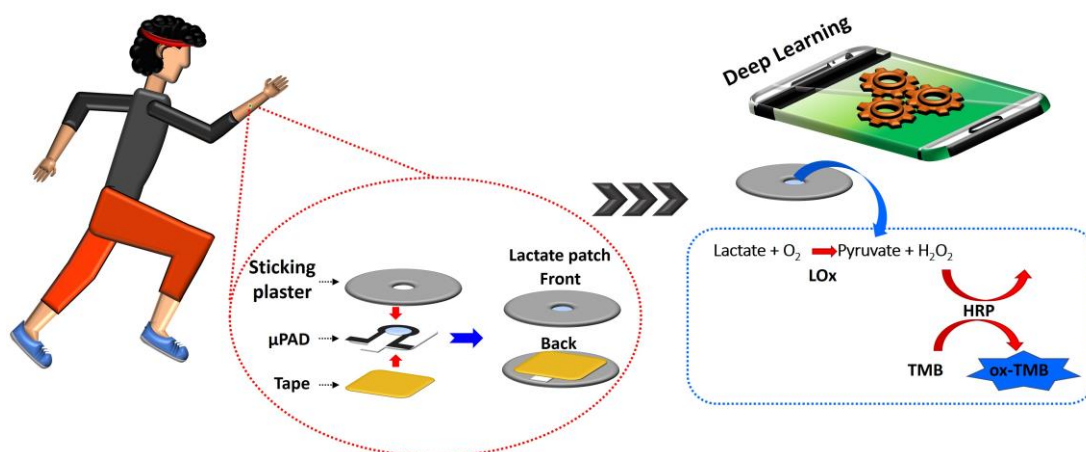


Figure 4.1: A schematic illustration showing the working principle of the system. Lactate is first converted to pyruvate by LOx, releasing H₂O₂ which is then used by HRP for the oxidation of TMB. The color change is imaged using a smartphone camera and the lactate is determined by DeepLactate, an app running a DL classifier.

4.2 Materials and Methods

The µPAD for lactate detection was made using a wax printing protocol. Briefly, the µPAD was designed on Microsoft PowerPoint 2013 Software, and then the patterns were transferred onto a Whatman filter paper using a wax printer (Xerox ColorQube 8900, Xerox Corporation, USA). Subsequently, the microfluidic paper-based analytical device (µPAD) was placed on a hot plate at 180 °C for 120 seconds, where the wax melted and diffused into the pores of the filter paper, forming hydrophobic channels that allowed controlled fluid flow. The detection areas of the µPADs were modified by first adding 0.8 µL TMB and then an enzyme mixture containing 0.2 µL LOx and 0.8 µL HRP. After each solution addition, the µPADs were left to dry for about 10 min at +4 °C. The colorimetric behavior of µPADs was evaluated using artificial sweat. Briefly, µPADs were immersed in artificial sweat solutions containing lactate at different concentrations (0, 1, 5, 10, 20, and 50 mM), allowing these solutions to reach the detection areas under lateral flow. Color changes in the detection areas were imaged at time points of 0, 5, 10, and 15 min. To turn the µPAD into a lactate patch, a sticking plaster purchased from a local pharmacy was used.

The plaster was cut with a CNC laser-cutting machine (Genmitsu 3018-PRO CNC, SainSmart, China) so that only the detection area of the μ PAD was visible. The lactate detecting μ PAD was sandwiched between the plaster and a transparent tape to avoid direct contact between the detection area and the skin. As shown in Figure 4.8, a sample pad was used to absorb a sweat sample for analysis.

4.3 Image Capturing

For the DL models to interpret a given image data accurately under various conditions, the training dataset needs to be fed into the models first, and then validation and testing datasets are used to optimize the parameters of these models. The dataset used for training, validation, and testing should contain enough high-quality images captured under various conditions such as rotation, illumination conditions, and camera optics. Therefore, image acquisition is a crucial step as it increases the adequacy of the dataset and leads to better performance for DL models.

Table 4.1: Camera properties of the smartphones used for imaging.

Smartphone Brand	Image Resolution	Optics	Camera Resolution
Huawei Mate 20 Lite	4000 × 3000	<i>f</i> /1.8	12 MP
Lenovo P2a42	4032 × 3024	<i>f</i> /2.2	12 MP
Oppo A5 2020	4000 × 3000	<i>f</i> /1.8	12 MP
Xiaomi Note 8 Pro	4160 × 3120	<i>f</i> /2	13 MP

As a proof of concept, the images here were captured under different combinations of three light sources, four smartphone camera optics, and five shooting angles to mimic as many varying conditions as possible. H, F, and S bulbs were used as light sources in this context. The color temperature of the halogen (Osram 60 W) is 2700 K (warm), the fluorescent (Klite 6 W) color temperature is 4000 K (neutral), and the sunlight (Philips 5.5 W) bulb has a 6500

K (cold). Switching on these light sources in different sequences created seven lighting conditions (H, F, S, HF, HS, FS, HFS).

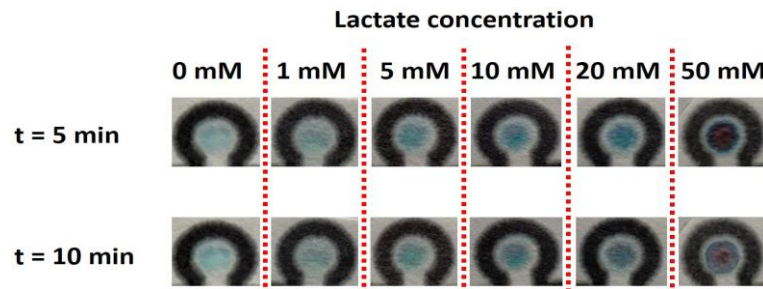


Figure 4.2: Images of μ PADs showing visually observable color changes with varying concentrations of lactate in artificial sweat at $t = 0$ min and $t = 5$ min.

In addition, images were captured at five angles (30° , 60° , 90° , 120° , and 150°) concerning the vertical axis between the μ PAD and the smartphone camera. The bulb sources were placed 40 cm away from the smartphones, and the distance between each lamp source was 9 cm. The images were captured at an incidence angle of 35° between the sources and μ PAD. Android smartphones of four different brands (Huawei Mate 20 lite, Lenovo P2a42, Oppo A5 2020, and Xiaomi Note 8 Pro) with unique camera properties (Table 4.1) were used for image capturing to ensure interoperability and compatibility. A total of 840 images were captured using the camera settings of the smartphones in automatic mode.

Since the number of images in the dataset affects the performance in DL, the number of images was increased with additional methods such as data augmentation. The benefits of data augmentation are two-fold. First, it helps prevent overfitting, which causes the training data to be memorized, making it unable to interpret new data. Second, new images are created based on altering the existing ones, which offers an artificially expanded dataset. Seven methods were employed for augmentation, including a rotation at 90° angles on the horizontal, vertical, and horizontal-vertical axes and square cropping with 180, 240, 300, and 400 pixels. As a result, the total number of images in the dataset reached 10080. The images were then resized to 400×400 so that the size of the images in the dataset was the same as before being fed into the neural networks.

4.4 Proposed Deep Learning Architecture

DL is the branch of ML-based on neural network architectures, including CNNs [140], recurrent neural networks (RNN) [141], autoencoders [142], and deep belief nets [143]. CNNs perform outstandingly in processing grid-like topology data such as a digital image (DI) among these architectures. DI represents visual data in the form of two-dimensional matrices driven by applications such as classification [144], clustering [145], and object recognition [146].

Considering their multi-layered structure, CNNs are very powerful and computationally efficient in image classification as they employ convolution and pooling operations and perform parameter sharing. Therefore, this study tested several CNN-based DL models for quantitative and qualitative analysis of lactate on μ PAD images captured by a smartphone camera. CNN models follow similar architecture, consisting of convolution and pooling operations and several fully connected layers, as demonstrated in Figure 4.3.

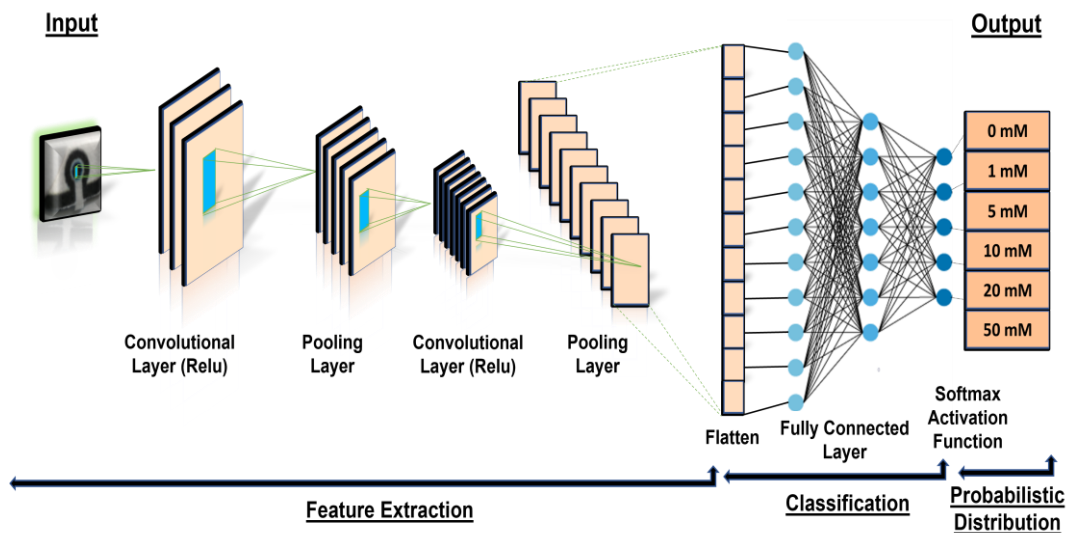


Figure 4.3: General structure of the CNN.

The convolutional layer is the main block of CNN which applies a convolution filter on the input data to generate a feature map. The output of the convolution layer then passes through pooling operations to reduce the

dimensionality, leading to a smaller number of parameters and shortened training time. The convolution and pooling operations may be repeated several times depending on the structure of the architecture. Before the fully connected layer, the output of the final pooling layer is converted to a vector by flattening. It is the last and most crucial layer of CNN, which takes the data from the flattened layer and performs the learning process through the neural network.

Here, six CNN models were trained, and it was observed that Inception-v3 outperforms the others in terms of validation and test accuracy. The dataset used in training CNN models has a crucial role in performance, as described in the next section.

4.5 Smartphones Application: DeepLactate

A smartphone app has been developed for susceptible colorimetric lactate analysis in sweat with a DL approach. To embed the trained CNN model into Android smartphones, the TensorFlow-Lite (.tflite) library is used to make the model compatible with smartphones. Here, the Inception-v3 model was saved as a data file in the Hierarchical Data Format (HDF - .h5 file) due to its superior performance among the tested CNN models. Then, the .h5 file was converted to the .tflite file using Python and embedded in our custom-designed DeepLactate app.

DeepLactate having a simple and user-friendly interface is demonstrated in Figure 4.4. The home page is given in Figure 4.4(a), where an image can be selected from the gallery of the smartphone (Figure 4.4(b)), or a new image can be captured using the smartphone camera. Then, after selecting or capturing the image from the gallery or camera, the crop alert dialogue is displayed to the user in Figure 4.4(c). If the user taps the “NO” action, the result is calculated directly (without cropping), as shown in Figure 4.4(d). Otherwise, the user is directed to the crop screen when tapping the “YES” action. Next, the ROI on the image is cropped using an adjustable crop box (Figure 4.4(e)) and displayed on the app as shown in Figure 4.4(g). Then, the cropped image is loaded into the model using the

“UPLOAD” icon to perform the colorimetric lactate analysis. The results are displayed in Figure 4.4(f) and (h) on the app screen for two different solutions with 0 and 50 mM concentrations.

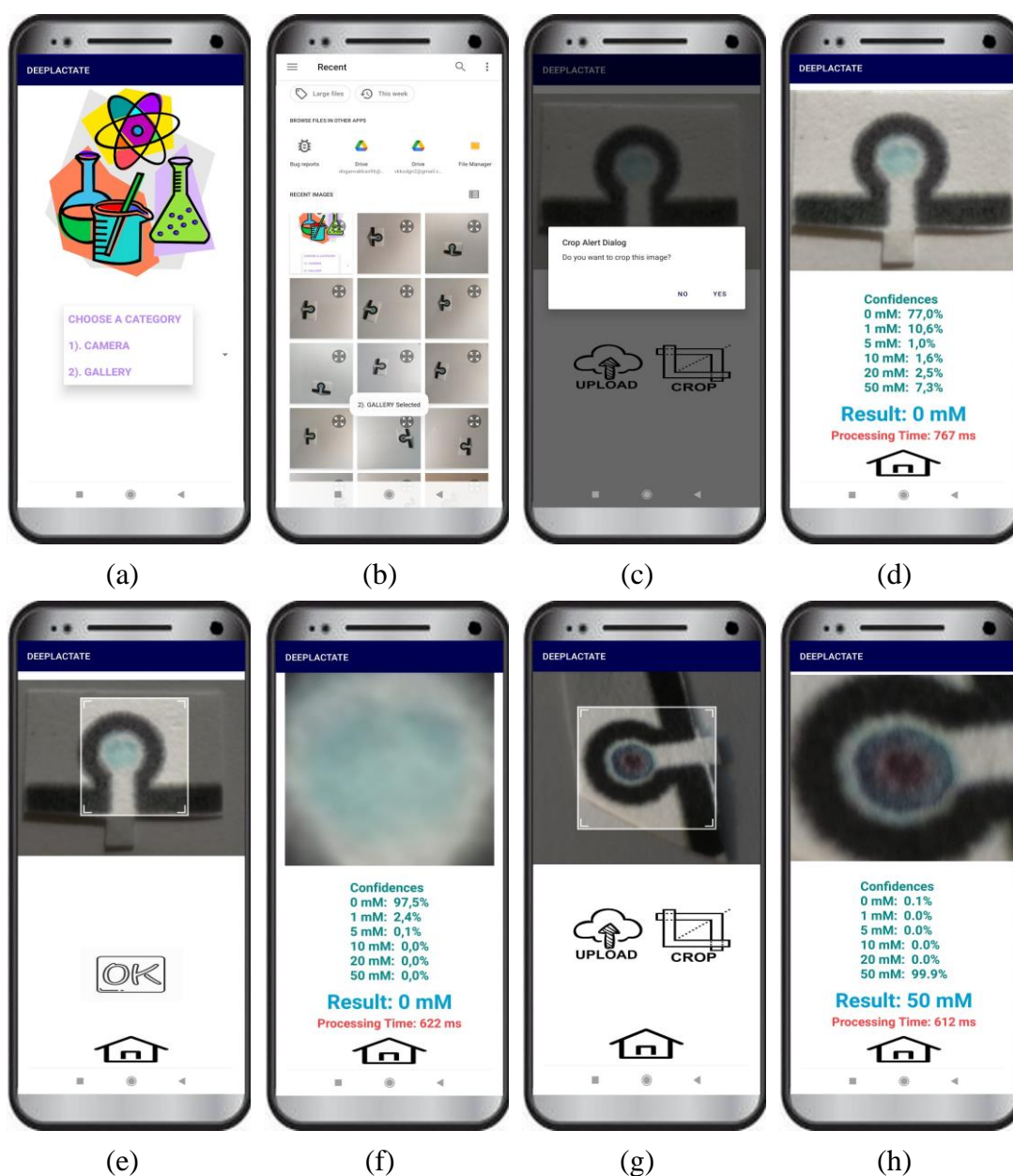


Figure 4.4: The steps for colorimetric lactate analysis in DeepLactate are as follows. The home page of DeepLactate is given in (a). The user can select an image from the gallery in (b) or capture a new image using the smartphone camera. Then, after selecting the image from the gallery, the crop alert dialogue is asked of the user as in (c). If the user taps the “NO” action, the result is calculated directly (without cropping) as shown in (d). Otherwise, the user is directed to the crop screen in (e),

and (g) when the “YES” action is tapped. The app tests the concentrations of 0 mM in (f) and 50 mM in (h).

4.6 Experimental Evaluations and Discussion

A DL model embedded into a smartphone app was used with a μ PAD for offline colorimetric lactate determination in artificial and/or human sweat. The μ PAD with a single detection area was designed first to absorb a sample and then transfer it to the detection area for colorimetric analysis. The two enzymes LOx and HRP and TMB were used for lactate determination. Briefly, LOx catalyzes the oxidation of L-lactate to pyruvate and produces H_2O_2 as a by-product [147]. The second enzyme HRP uses the by-product H_2O_2 to oxidize the chromogenic substrate TMB, forming a blueish color change. μ PADs were initially tested with artificial saliva containing lactate at various concentrations. As can be visually observed in Figure 4.2, a bluish color formed, and color intensity increased with increasing lactate concentration at both 5 and 10 min time points. A detection limit (LOD) of 0.67 mM was calculated based on color intensity (RGB data) of images taken by Oppo A5 2020 at 5 min (LOD = $3.3 \cdot \sigma / \text{Slope}$). The μ PAD requires less than 5 μ L of sample to complete the analysis. The images of μ PADs were captured via four different Android smartphones (Huawei Mate 20 lite, Lenovo P2a42, Oppo A5 2020, and Xiaomi Note 8 Pro) with unique camera properties (Table 4.1) under various conditions such as rotation and illumination. A total of 840 images were captured and augmented to 10080 images to train various DL models.

Table 4.2: Experimental results of CNN models.

Models	Validation Accuracy	Test Accuracy
MobileNet	0.9986	0.9869
Xception	0.9990	0.9365
VGG16	0.9926	0.9582
VGG19	0.9665	0.9463
ResNet50	0.9989	0.9767
Inception-v3	0.9992	0.9906

In this study, six popular CNN models were trained using the created dataset (Section 4.3). Hyper-parameters of CNN models such as epochs, learning rate, batch size, and optimizer significantly impact performance. The number of epochs was set to 30, and the learning rate was chosen as 0.001 with a batch size of 64 under the optimizer of Adam, which was found to be adequate based on extensive experimental studies. Regarding validation accuracy, the Inception-v3 model showed the highest performance with 0.9992 compared to other models (Table 4.2). Furthermore, the accuracy and loss results for each epoch in the training and testing of Inception-v3 are graphically shown in Figure 4.7. Besides validation accuracy (Equation (2.13)), precision (Equation (2.14)), recall (Equation (2.15)), F1-score (Equation (2.16)), and ROC curve (Equation (2.17)) values were also used in the comparison (Table 4.3). The confusion matrix (Figure 4.6) is also used to represent the true and predicted labels, which consist of four indices, including TP, TN, FP, and FN.

ROC curves are one of the methods used to measure the success of the models in distinguishing each class. The AUC approaches show that the CNN model has successfully classified the concentrations. The threshold value was used to classify probability values of colorimetric lactate analysis in artificial sweat and was chosen as 0.5 to obtain the ROC curve. The ROC curve and AUC value of the proposed CNN model (Inception-v3) to detect lactate in artificial sweat were shown in Figure 4.5. The y-axis and x-axis in the ROC curve represent the TP and FP rates, respectively.

Table 4.3: Evaluation of the Inception-v3 for lactate in terms of precision, recall, F1-score, and ROC-AUC.

Moles (mM)	Precision	Recall	F1-score	ROC-AUC
0	0.990	1.000	0.990	1.000
1	0.990	1.000	0.990	1.000
5	0.990	0.970	0.980	0.980
10	1.000	0.990	1.000	1.000
20	0.970	0.990	0.980	0.990
50	1.000	1.000	1.000	1.000
Average	0.990	0.992	0.990	0.995

The Inception-v3 model was tested with 1008 new sample data for each concentration value. In Table 4.3 and Figure 4.4, these performance metrics and

the robustness of the system for six different concentration values were illustrated for Inception-v3. Figure 4.4 shows that the 5 and 20 mM concentrations deviated from the predicted labels slightly more than the other concentrations. However, the test accuracy was close to the validation accuracy and outperformed the other models (Table 4.2). Next, the Inception-v3 model was integrated into a user-friendly and simple smartphone app, DeepLactate, for colorimetric lactate determination in sweat.

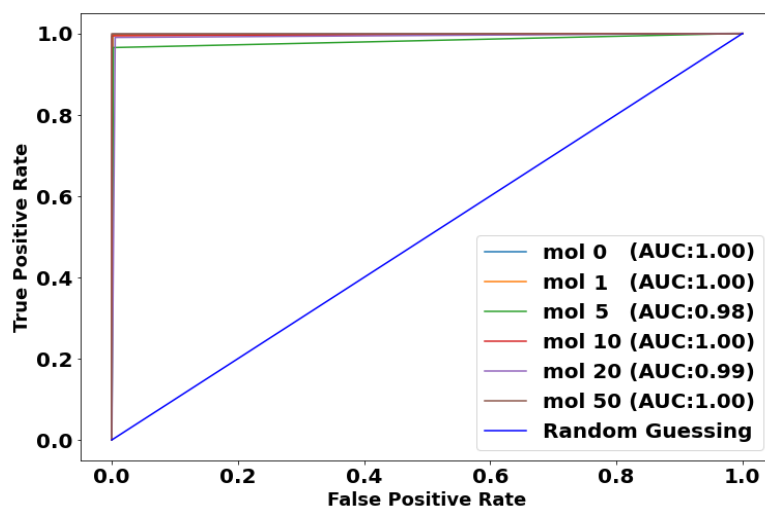


Figure 4.5: ROC curves of Inception-v3 in varying concentrations of the test dataset.

The screenshots of the app were demonstrated step by step in Figure 4.4, where the selected image from the gallery was classified for lactate detection. After the concentration classification, the results were displayed in DeepLactate for two different samples, as in Figure 4.4(g) and (i), where the samples were correctly classified as 0 and 50 mM, respectively. In addition, confidence and processing time were given for each concentration value, as shown in Figure 4.4(d), to highlight the impact of cropping. The comparison results in Figure 4.4(d) and (g) proved that both confidence (77% - 97.5%) and processing times (767 ms - 622 ms) were improved for the same sample as cropping operation reduces the size of the image by removing redundant areas. In addition, the proposed model was robust against rotated images and showed a reliable performance (Figure 4.4(h) and (i)).

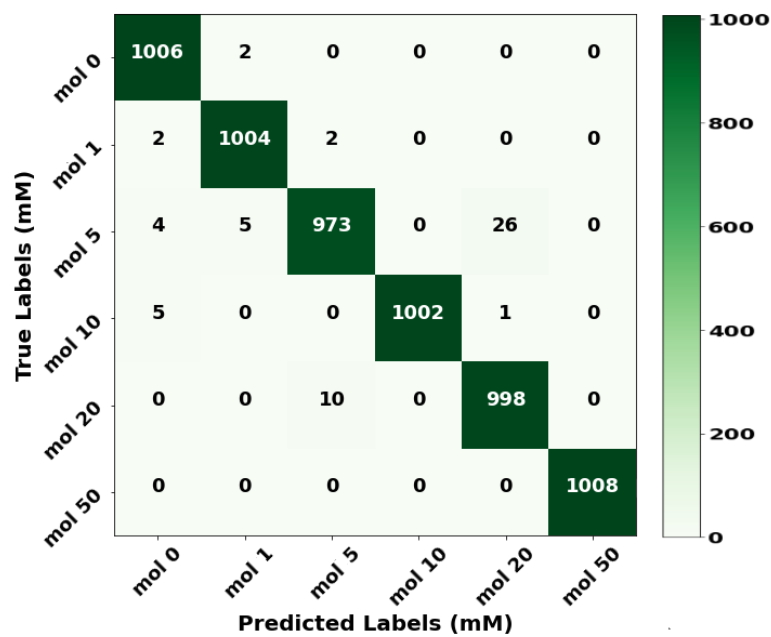


Figure 4.6: Confusion matrix of Inception-v3 in varying concentrations of the test dataset.

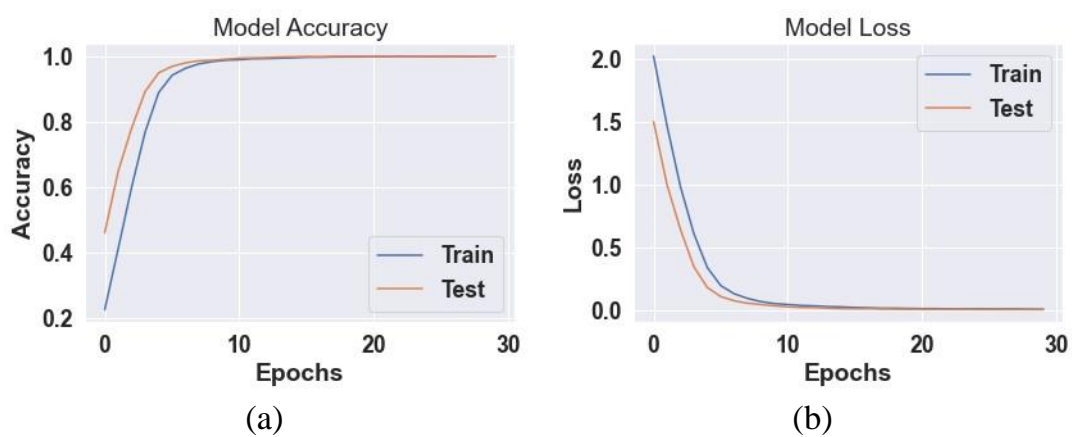


Figure 4.7: Model Accuracy of Inception-v3 is given in (a) and Model Loss of Inception-v3 is shown in (b).

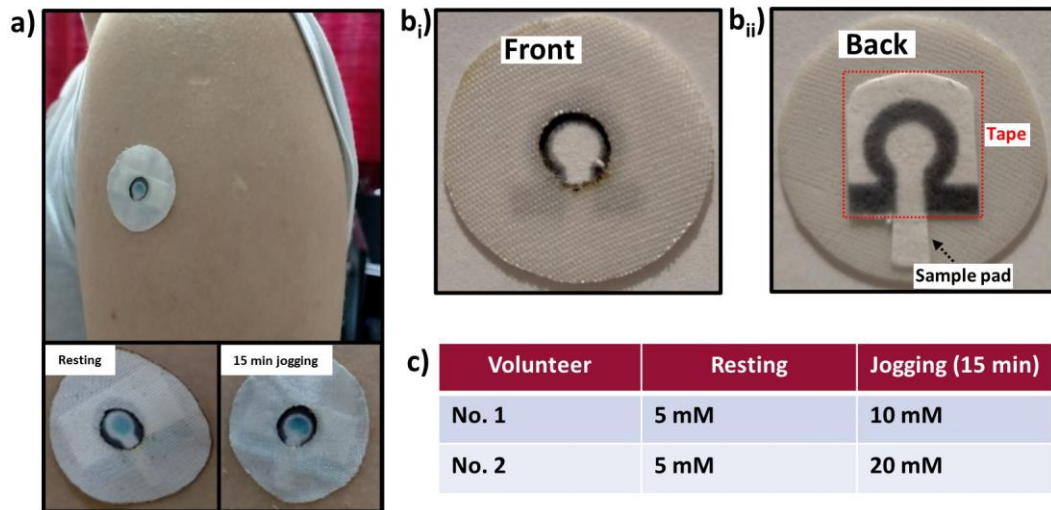


Figure 4.8: An image (a) showing the application of a lactate patch for human sweat analysis. The patch was made by sandwiching a μ PAD between a sticking plaster and a transparent tape (bi–ii). Classification results of the smartphone app DeepLactate for lactate level in the sweat of two volunteers after resting and 15 min jogging.

Chapter 5

On-site food spoilage monitoring with smartphone embedded machine learning and colorimetric gelatin films

Real-time and on-site food spoilage monitoring is still challenging to prevent food poisoning. At the onset of food spoilage, microbial and enzymatic activities lead to the formation of volatile amines. Monitoring these amines with conventional methods requires sophisticated, costly, labor-intensive, and time-consuming analysis. Here, ARCE based colorimetric sensing system was developed with the incorporation of embedded ML in a smartphone application for real-time food spoilage monitoring. FG-UV-CD100 films were first fabricated by crosslinking ARCE-doped FG with CDs under UV light. The colorimetric responses of FG-UV-CD100 films to ammonia vapor were captured in different light sources with smartphones of various brands, and a comprehensive dataset was created to train ML classifiers to be robust and adaptable to ambient conditions. Meanwhile, the ML classifier was integrated into our custom-designed Android application, SmartFood++, enabling analysis in about 0.1 sec without internet access, unlike its counterpart using cloud operation via the internet. The proposed system was also tested on a real fish sample, demonstrating that it has a significant advantage as a potent tool for on-site, real-time monitoring of food spoilage by non-specialized personnel.

5.1 Introduction

Food waste is a globally growing concern due to its potential impacts on ecological, social, and economic consequences, including greenhouse gas emissions, nutritional insecurity, unsustainable production, and distribution chain [148].

According to the Food and Agriculture Organization of the United Nations, annual food waste reaches 1.3 billion tons [149]. On the other hand, the world population is expected to increase by almost 25% and reach nearly 10 billion by 2050 [150]. This drastic population growth means increased consumption of highly perishable protein-rich food and an expected increase in food waste [151]. Concern about ensuring the sustainability and safety of food production for the rapidly growing world population has led to the development of new strategies, including innovative packaging applications. Smart packaging systems offer sustainable approaches to reducing food waste by incorporating active and intelligent compounds into biodegradable and biocompatible polymers [152]. Normally, conventional packaging aims only to maintain food safety and quality by serving as a physical barrier, while smart packaging presents beyond the role of the physical barrier by adding specific functionality to conventional packaging [153]. Thanks to their antioxidant and halochromic properties, anthocyanins, natural color pigments, have been widely used in smart packaging applications [154].

Recent studies have demonstrated the advantage of anthocyanins as colorimetric freshness indicators in intelligent food packaging labels [23, 155]. The freshness of food is often monitored by manual observation of the color change of anthocyanins, which is time-consuming and sensitive to human perception [156]. Therefore, there is a need for an automated system that can detect a color change to assess the freshness of the food to improve monitoring performance. The color analysis is mainly based on the intensity values in various color spaces consisting of three or four channels such as RGB (Red-Green-Blue), HSV (Hue-Saturation-Value), L*a*b* (Lightness, Green-Red, Blue-Yellow), YUV (Luminance, Blue-

Luminance, Red-Luminance) and CMYK which have been employed in many applications including analyte detection [157] and freshness monitoring [23].

The traditional approach in colorimetric analysis is to use single or multiple channels to derive the calibration curve that establishes a relationship between intensity and output [130]. The calibration curve offers simplicity and ease of use, making it widely used for colorimetric analysis in a controlled environment [23]. However, intensity values are easily affected by the camera optics, brightness, and source of the lights, causing the curve to be recalibrated for specific conditions [16]. To overcome this problem and increase robustness, advanced algorithms such as ML have been used, which learn how to classify inputs based on features extracted from color information. In [158], a food freshness detection prototype was developed by ML-based colorimetric analysis obtained from a glycerol-based sensory film. A colorimetric sensor was used to detect H₂O₂ with ML classifiers for air sampling [106]. The alcohol level in saliva was determined using three ML classifiers with features extracted from four color channels [104].

In addition to its robustness, ML is highly preferred due to its adaptability and easy integration into smartphone-based imaging systems for quantitative and qualitative colorimetric analysis. SPAQ [159] application was developed to detect the alcohol level in saliva. GlucoSensing [40] application was developed to determine glucose concentration. A low-cost paper-based microfluidic device for nitrite concentration measurement and pH determination was integrated with a custom Android application [160]. A custom-designed smart-phone application, GlucoQuantifier, was developed to communicate with the remote server running ML classifiers to determine the glucose concentration of the assay [128]. One drawback of the mentioned studies is the necessity of cloud operations to transfer the data to the remote server for colorimetric analysis with ML classifiers. Internet access is required due to cloud operations, causing inoperable analysis in resource-limited environments. The speed of the Internet is also critical to complete the data transfer, which affects the response time for analysis. Moreover, remote servers need to be kept up and running, resulting in higher

operating and maintenance costs. The working principle of the proposed system for food spoilage detection is shown in Figure 5.1.

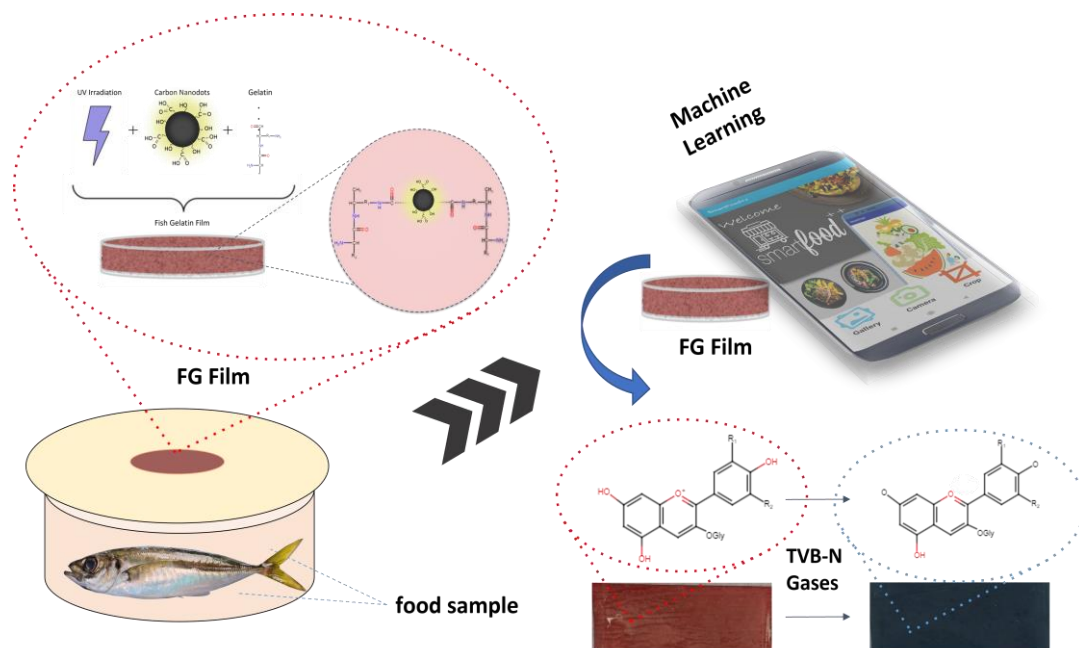


Figure 5.1: A schematic illustration showing the working principle of the food spoilage detection system.

5.2 Materials and methods

FG (200 bloom) was supplied by SG Chemicals. Magnesium oxide, boric acid, sodium monobasic, potassium dibasic phosphates, and bromocresol green-methyl red mixed indicator solution, were acquired from Sigma-Aldrich (St. Louis, MO). Fuming hydrochloric acid (37%), ammonium chloride, and citric acid were acquired from ISOLAB (Wertheim, Germany). Merck supplied ammonium hydroxide solution (32%) (Darmstadt, Germany).

5.2.1 Fabrication of colorimetric films

The method used in this study was adapted from methods described in [23]. First, red cabbage extract was prepared following the method [161] where chopped red cabbage was put in a beaker with distilled water at a 1: 2 cabbages: water (w/v) ratio and left stirring overnight. The extract was then

filtered and stored in the dark at 4 °C until further use. The concentration of the extract was determined by a modified pH differential method [162]. Next, carbon nanodots were synthesized based on microwave-assisted carbonization of citric acid [163]. Briefly, a 10% w/v citric acid monohydrate solution was prepared with distilled water. After it was completely dissolved, the mixture was heated at 550 W for 7 min in a microwave lab station (Ethos D Microwave Labstation, Milestone Inc., USA). The obtained residue was dissolved in distilled water and dialyzed against ultrapure water with a dialysis tubing (1200 Da cutoff, Sigma, D7884–10 FT) for 48 h. The resulting solution was then freeze-dried (Christ Alpha 2–4 LD Plus, Martin Christ, Germany) and used to prepare a 100 mg/ml stock solution in a sodium phosphate buffer at pH 8. The films were prepared using the solvent casting method. FG, red cabbage extract, glycerol, and carbon nanodot were mixed at a final concentration of 10% w/v, 0.5 mg/l, 1% w/v, and 100 mg/l, respectively while the pH of the final mixture was adjusted to 8. The solution was then ultrasonicated for 90 min until the gelatin was completely dissolved. 20 ml of the solution was poured into a (10 cm X 10 cm) square petri dish and treated with 365 nm UV light for 45 min (1.5 mW/cm, 365 nm, Vilber ECX-F20.L-V1) and placed into a desiccator (0% relative humidity) to dry at 23 °C for 48 h. Next, films were placed inside a climate chamber with 50% RH at 20 °C and conditioned for at least 24 h before further use.

Table 5.1: Camera properties of the smartphones used for imaging in food spoilage detection.

Smartphone Brand	Image Resolution	Optics	Camera Resolution
iPhone 6	1024×768	f/1.8	8 MP
iPhone 11	4032 × 3024	f/2.4	12 MP
LG 6	4160 × 3120	f/1.8	13 MP
Samsung Galaxy A23	4080 × 1836	f /2	13 MP

5.3 Experimental Design and Image Acquisition

ML models can achieve a high classification accuracy after training on an appropriate dataset with quantitative and qualitative representations of all possible conditions [16, 34]. In addition, the dataset needs to be a collection of data that ensures the robustness and adaptability of the system to new environments, regardless of illumination conditions and camera optics. Therefore, in this study, images were captured using smartphones (iPhone 6, iPhone 11, LG 6, and Samsung Galaxy A23) from Android and iOS operating systems with different camera properties (Table 5.1) under the combination of LED (L), F, and S to ensure inter-phone repeatability and robustness against ambient illumination conditions. Besides, imaging was repeated for three angles (60° , 90° , and 120°) to consider rotation and direction effects. The L (Osram 9 W), F (Klite 6 W), and S (Philips 5.5 W) light sources were deliberately chosen to ensure imaging under different light characteristics, including warm (2700 K), neutral (4000 K), and cold (6500 K) colors, respectively. The light sources and imaging angles can be increased to expand the dataset. However, it is found to be sufficient based on the experiments. The distances of the light sources to the smartphones during imaging were kept constant at 20, 24 and 28 cm for L, F and S, respectively. In addition, the capturing was taken at a 30° angle of incidence with 10 cm between the smartphone and the film. The film response (Table 5.2) was captured with nine different ammonia gas concentration values under seven lighting conditions (L, F, S, LF, LS, FS, LFS) in auto mode with four smartphones and three angles, resulting in 756 images for the dataset. Before training the ML classifiers, the dataset was transferred to a computer for pre-processing, as discussed in the next.

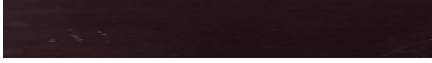
5.4 Machine Learning for Colorimetric Analysis

Here, ML processes, including feature extraction, selection, and classification with RF, are introduced for colorimetric analysis of spoilage monitoring.

5.4.1 Feature Extraction in Machine Learning

Feature extraction, a crucial step in ML training, is a size reduction process through efficiently representing an image with information such as color, texture, size, shape, and location [40]. Removing redundant or irrelevant information from the image increases the accuracy of the classifiers as the learning relies on relevant features and reduced dimensionality. In that sense, the number and type of the features are critical for the image representation and thus directly linked to the classifier performance. Here, color information is used to extract the image features, as it is found to be promising in image representation [41]. The ROI, namely film response, was cropped to convert the captured RGB images to HSV, L*a*b*, YUV, and CMYK, so that single channels (R, G, B, H, S, V, L*, a*, b*, Y, U, V, C, M, Y, and K) were obtained to determine the color features. Then, the mean, standard deviation, and kurtosis values for channels were calculated, leading to forty-eight features. To further reduce the computational complexity and improve the performance, feature selection was employed as discussed next.

Table 5.2: The color change of FG-UV-CD100 film with varying concentrations of ammonia vapor.

Ammonia (mg N/100 g)	Film Response Images
0 (ref)	
10	
20	
30	
40	
50	
60	
90	
120	

5.4.2 Feature Selection in Machine Learning

Feature selection is the process of identifying the most relevant subset features, providing robust and improved classification with reduced computational burden [164]. Eliminating irrelevant features contributes to computational efficiency, leading to a rapid response in colorimetric analysis [165]. In that sense, various feature selection algorithms were employed, including ReliefF [166], Mutual Information [167], Gain Ratio [168], Information Gain [169], Fisher's [170], Correlation Coefficient [171], and Chi-Squared [64]. These algorithms were used to select the most relevant subset among the forty-eight features, and their contribution to the overall performance was observed to select the most appropriate one. Based on extensive comparative studies, Chi-Squared was found to be adequate as a feature selection algorithm in this study. After the Chi-Squared feature selection, eighteen irrelevant features were eliminated, and the number of features was narrowed down to thirty (Figure 5.2).

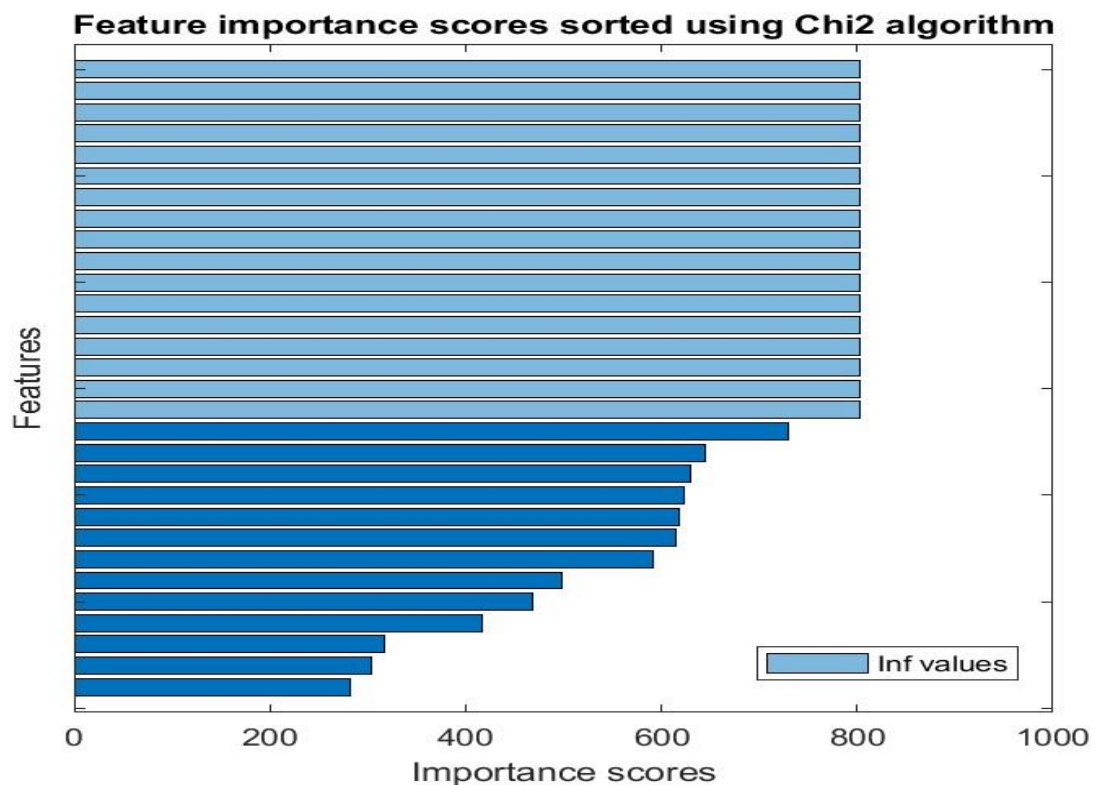


Figure 5.2: Feature selection using Chi-Squared algorithm.

5.4.3 Classification with Random Forest

Twenty-three ML classifiers were tested using the finalized feature set to monitor food spoilage based on color variation in film response images. After comparison in terms of accuracy, precision, recall, F1-score, ROC Area, and MCC, the RF was chosen due to its superior performance compared to its counterparts.

The RF consists of multiple decision trees and nodes to utilize ensemble learning combining many classifiers to solve classification and regression problems [172]. In the RF, each node is split using the best of a subset of randomly selected estimators at that node, whereas, in other standard trees, each node is split using the best distribution among all variables. Therefore, the RF is more robust against overfitting, an undesirable ML problem. It uses only two variables, including the number of variables in the random subset and the number of trees in the forest [173]. The structure of the RF classifier is shown in Figure 5.3.

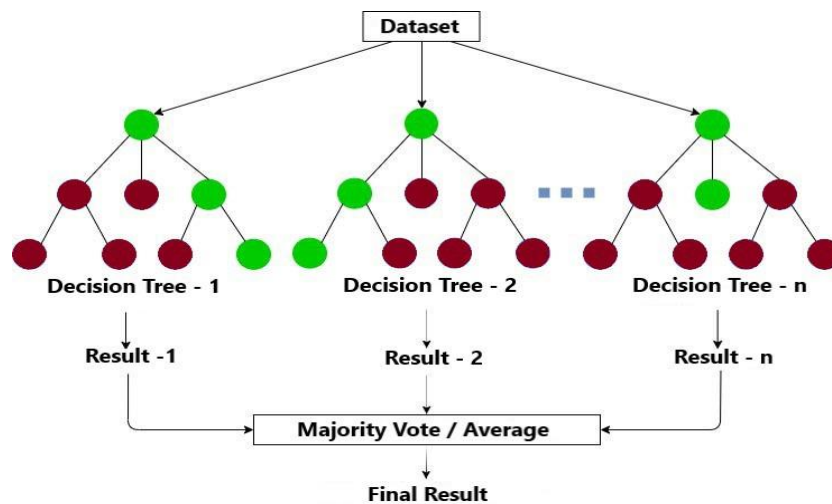


Figure 5.3: The general structure of Random Forest.

5.5 Smartphone Application: SmartFood++

SmartFood++, our ML-based Android application for food spoilage monitoring, was improved to perform colorimetric analysis without a remote server and an internet connection (offline). In the SmartFood++ application, the classification was run in Android with an embedded RF, resulting in more

robustness than SmartFood [23], the previous version running with the calibration curve. In addition, the interface of the application has been improved to be simple and user-friendly with designs and icons.

To run an embedded ML classifier in the application, the feature extraction and the ML model must be Java-compatible as the application was developed in Android Studio with Java language. To test an ML classifier in the application, the input must be represented with the same feature types used in training the classifier. Therefore, the feature extraction script was first coded in the Eclipse IDE for Java Developers (2022-06) before being integrated into the application in Android Studio. The same script was also used to create a “.CSV” file, containing the feature set to train the RF classifier. To ensure the compatibility of the trained model with Android, the WEKA 3.9.6 environment was used as it was also developed in Java. The CSV file was then converted to ARFF (“.arff”) file extension for the training of the RF in the WEKA. After the training, it was saved with the model extension file (“.model”) to embed into the Android application.

With the improved interface, even non-expert users can easily perform operations such as uploading, viewing, and cropping images. The image can be uploaded to the application in two ways: an image can be selected by the user from the gallery, as in Figure 5.4(b), or a new image can be captured using the built-in camera. Then, using the adjustable crop box, the ROI can be determined from the image as in Figure 5.4(c), (d), (g) and (h). When the “CALCULATE” button is tapped in Figure 5.4(e) and (i), the concentration value can be calculated based on the RF classifier and displayed on the screen (Figure 5.4f and j).

5.6 Real samples

Freshly caught horse mackerels were purchased from a local market (Ankara, Turkey) and transported immediately to the laboratory in an ice bucket. Horse mackerel samples (25-30 g) were put into square petri plates (10 cm × 10 cm). A film piece of 1 cm × 1 cm was attached to the cellophane and then placed 1

cm above the fish sample. The plates were kept at 4°C during 8 days of storage. The color of the films was monitored daily by taking images of the films with a smartphone.

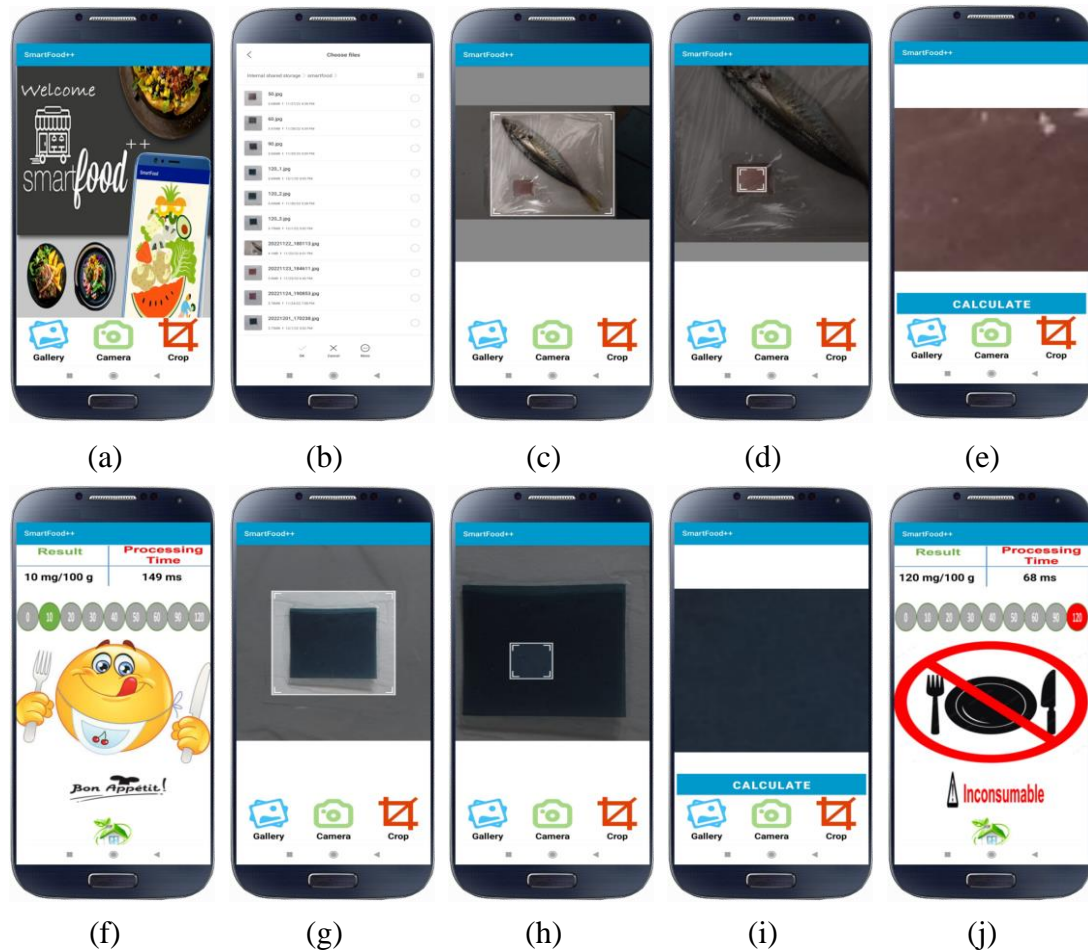


Figure 5.4: The steps for colorimetric food spoilage monitoring in SmartFood++ as follows. The homepage of SmartFood++ is given in (a). The user can select an image from the gallery in (b) or capture a new image using the smartphone camera and crop the image using an adjustable crop box as in (c), (d), (g), and (h). Cropped patches are given in (e) and (i). The application is tested with the consumable food (fish) in (f), and the inconsumable one in (j).

5.7 Result and Discussion

Gases such as ammonia, trimethylamine, and dimethylamine, also known as TVB-N compounds, are produced during the spoilage of protein-rich foods due to microbial and enzymatic activities. Ammonia among these volatile

nitrogenous with the lowest boiling point is released rapidly at the onset of spoilage of fish and meat products and thereby can be used as a model TVB-N compound to develop food freshness labels [174]. In response to ammonia and other TVB-N compounds, a visible color change of anthocyanins is expected because of their structural conversion. Therefore, we collected images of the developed films for different ammonia concentrations. As illustrated in Table 5.2, the color of the films changed drastically from bright red to dark green when films were exposed to ammonia concentration above 20 mg N/ 100 g. The alkaline environment on the surface of the films is created due to the formation of ammonium ions by hydration and hydrolysis of ammonia vapor [175]. Under primary conditions, deprotonation of the phenolic hydroxyl groups of anthocyanins leads to color change [176]. Altogether, these results indicated that ARCE-loaded films were sensitive enough to detect changes in fish freshness.

Here, we report ML-based colorimetric monitoring of food spoilage using the color change in FG-UV-CD100 films resulting from the interaction of TVB-N compounds with anthocyanins. To ensure the robustness of the classifier, a comprehensive dataset was created by capturing the color response of FG-UV-CD100 films to nine different ammonia gas concentrations with four different brands of smartphones under seven different lighting conditions. The images were then processed to extract forty-eight features from the ROI on films. Next, the Chi-Squared algorithm was used to select a new subset with thirty features. Twenty-three ML classifiers were trained with selected features and RF outperformed other classifiers, as shown in Table 5.3. The performance of the classifiers was compared with classification accuracy (Equation (2.13)), precision (Equation (2.14)), recall (Equation (2.15)), F1-score (Equation (2.16)), ROC (Equation (2.17)), and MCC (Equation (2.18)).

The performance metrics results of ML classifiers in (Table 5.3) showed that RF had the highest accuracy for colorimetric food spoilage detection. The ROC AUC has also proved that the RF has successfully classified the concentrations (in Appendix B Figures B1-9). Classification metric results and confusion matrix are available in Table 5.4 and Figure 5.5(a) and (b), respectively. The

confusion matrices visualize the relationship between the true and predicted classes of the classifier. In Table 5.3, the metric results are below the average values for 40 and 50 mg N/100 g concentrations which can be seen in the confusion matrix (Figure 5.5(a) and (b)) where the true and predicted classes of RF for each concentration value of FG-UV-CD100 films are illustrated. Next, the RF classifier was embedded into a user-friendly and simple smartphone application, SmartFood++, for colorimetric food spoilage detection.

Table 5.3: Classification accuracy results for colorimetric food spoilage detection with different ML classifiers.

ML Classifiers	Classification Accuracy (%)
Random Forest	98.8
SVM	96.5
Nearest Neighbors (KNN)	94.69
Coarse Tree	94.69
Ensemble Bagged Tree	93.93
Linear SVM	85.95
LDA	79.52
Logistic Regression	76.43
EBC	72.98
Bernoulli Naive Bayes	72.34
Gaussian Process	65.04
Weighted KNN	64.56
Gradient Boosting Classifier	62.74
Ensemble RUS Boosted Tree	62.02
RBF SVM	61.83
PCA	59.64
AdaBoost	58.97
Naive Bayes	58.77
Extra Tree Classifier	57.46
Ensemble Subspace Discriminant	57.02
QDA	54.4
Bagging Classifier	45.48
Decision Tree	44.8

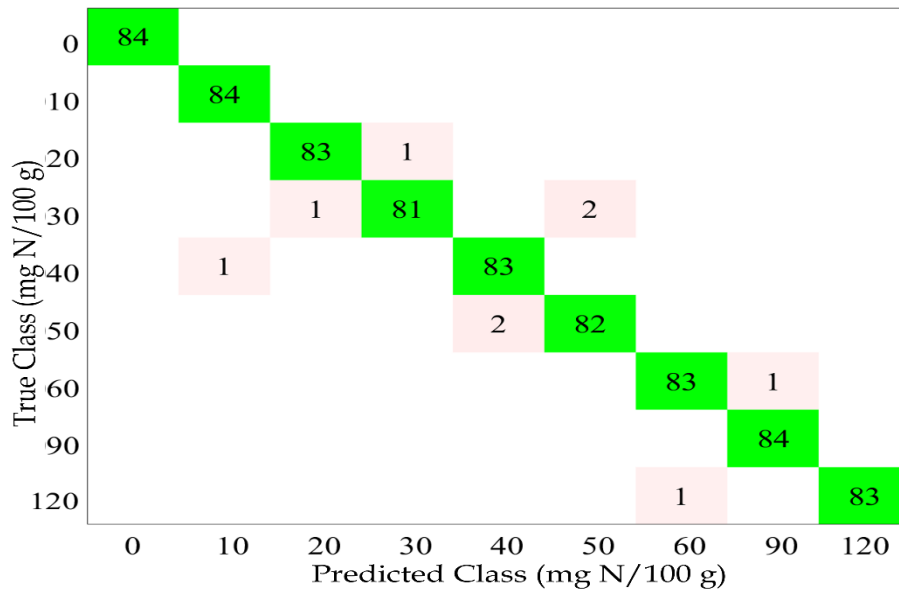
In addition, the proposed system was tested on a real sample to demonstrate its robustness and performance. In that sense, the fish (horse mackerel) sample was monitored and captured with smartphone cameras under seven lighting conditions to create a dataset specific to fish spoilage. After feature extraction and selection were employed, the RF was trained with a fish-feature set and showed 99.6% test accuracy.

Table 5.4: Evaluation of the RF for colorimetric food spoilage detection in terms of Precision, Recall, F1-score, Accuracy, ROC Area, and MCC.

	<i>Precision</i>	<i>Recall</i>	<i>F1 score</i>	<i>Accuracy</i>	<i>ROC</i>	<i>MCC</i>	<i>Class</i>
	1.000	1.000	1.000	1.000	1.000	1.000	0
	1.000	0.988	0.994	1.000	0.994	0.994	10
	0.988	0.988	0.988	0.988	0.993	0.987	20
	0.964	0.988	0.976	0.964	0.992	0.973	30
	0.988	0.976	0.982	0.988	0.987	0.980	40
	0.976	0.976	0.976	0.976	0.987	0.973	50
	0.988	0.988	0.988	0.988	0.993	0.987	60
	1.000	0.988	0.994	1.000	0.994	0.993	90
	0.988	1.000	0.994	0.988	0.999	0.993	120
Weighted Average	0.988	0.988	0.988	0.988	0.993	0.987	

The demonstration with an embedded RF classifier to SmartFood++ was given in Figure 5.4, where the two different selected images were processed and classified in the application after cropping with the adjustable crop box (Figure 5.4c-d-g-h). After classifying the concentration levels, the results were displayed in SmartFood++ as in Figure 5.4(f) and (j), where the fish samples were correctly classified as 10 mg N/100 g and 120 mg N/100 g. The comparison results in Figure 5.4(f) and (j) proved that processing times (149 ms - 68 ms) were significantly reduced, providing real-time colorimetric analysis for fish samples. Moreover, our application informs the user with various stickers based on the test result. If the food is

consumable, the “Bon Appetit” text under a happy-face sticker is displayed on the screen (Figure 5.4(f)). Otherwise, it shows a no-food sticker with “Inconsumable” text (Figure 5.4(j)).



(a)

Figure 5.5: Confusion matrix of RF in different concentrations.

Finally, in our study, ML and colorimetric analysis are integrated for the first time under an Android application for food spoilage. Similar studies [104, 177] reported ML-based colorimetric analysis. However, the proposed study differentiates itself from them by embedding the ML model into Android applications, reducing the response time to about 0.01 sec. Unlike existing studies that require more than minutes for colorimetric analysis due to internet-based cloud and server operations, this study does not require online connections, which reduces the cost and enables real-time video processing. Multiple frames from the video can provide more information than a single image, resulting in improved food monitoring.

Chapter 6

Conclusions and Future Research

Here, on-site colorimetric analysis based on AI-embedded Android smartphone assistants has been investigated. This chapter presents a summary of the critical contributions of this thesis. Furthermore, based on the discussion on the limitations of our work, potential directions for future research are also suggested.

6.1 Conclusions

This thesis discusses AI approaches and smartphone-based on-site colorimetric analyses in three subjects: hydrogen peroxide detection, lactate detection in sweat, and food spoilage detection. We have presented the following three key findings in Chapters 3, 4, and 5, respectively: (1) to the best of our knowledge, this is the first study that links an ML-based smartphone app with chromogenic agents in μ PADs, enabling non-enzymatic quantitative analysis of H_2O_2 for rapid and portable on-site surveillance, (2) to the best of our knowledge, this is the first study to link DL with quantitative and qualitative colorimetric analysis of chemical species, and (3) to the best of our knowledge, this is the first study that embeds an ML classifier into a smartphone application for food spoilage monitoring. These contributions will be elaborated on in more detail in the following subsections.

6.1.1 Non-enzymatic colorimetric detection of hydrogen peroxide using a μ PAD coupled with a machine learning-based smartphone app

Here, an iodide-mediated TMB-H₂O₂ (TMB+KI) reaction system was applied for compassionate, selective, and accurate non-enzymatic colorimetric determination of H₂O₂ in transparent liquids such as water using a μ PAD coupled with an ML-based smartphone app. The results were analyzed by comparison with those of KI. This paper introduced a non-enzymatic H₂O₂ detection system using a smartphone app based on colorimetric analysis with ML. The reaction of H₂O₂ and chromogenic agents (TMB + KI or KI) in μ PADs led to a concentration-dependent color change without requiring any enzymes or catalytic nanoparticles. To the best of our knowledge, this is the first study that links an ML-based smartphone app with chromogenic agents in μ PADs, enabling non-enzymatic quantitative analysis of H₂O₂ for rapid and portable on-site surveillance. To ensure the system works independently of camera optics and ambient light conditions, the dataset was created with four smartphones in seven different illumination conditions to train ML classifiers. Based on the performance comparison of various ML classifiers, TMB+KI gave the highest classification accuracy (97.8%) in the 0 to 5 mM concentration range, whereas KI performed its best between 0.2 and 50 mM with 92.3% accuracy. These results indicated that in the quantitative analysis of H₂O₂, KI performs better in the high concentration range, while TMB+KI is more efficient in the low range.

6.1.2 Smartphone embedded deep learning approach for highly accurate and automated colorimetric lactate analysis in sweat

This study reports a highly accurate and rapid classification of lactate in sweat by a DL model-embedded smartphone app, DeepLactate, offering the advantage of offline analysis. To improve the robustness against illumination variation and ensure inter-phone repeatability, the DL models were trained with the images of μ PAD captured in seven illumination conditions using four smartphones of different brands. The top-performing model, Inception-v3, was embedded in a smartphone app, allowing rapid analysis in a resource-limited setting as no data sharing is required for the server via cloud systems. The proposed system can

detect lactate in sweat with 99.9% accuracy in less than 1 sec, demonstrating its great practical potential in colorimetric analysis. The system was also tested on volunteers, in which the classification results of the app showed an increase in sweat lactate after jogging. To the best of our knowledge, this is the first study to link DL with quantitative and qualitative colorimetric analysis of chemical species.

6.1.3 On-site food spoilage monitoring with smartphone embedded machine learning and colorimetric gelatin films

Herein, we demonstrated a new implementation of ML classifiers that has the potential for on-site real-time monitoring of food spoilage by incorporating FG films with embedded RF into the SmartFood++ application. These FG films can change color in response to the accumulation of ammonia released from spoiled food. The colorimetric response was captured with four smartphones in seven different illumination conditions and three exposure angles to create a comprehensive dataset for the training ML classifiers, leading to improved robustness against the illumination variance and camera optics. Among the tested classifiers, the highest classification accuracy (98.8%) was achieved with RF, demonstrating that the proposed system has great potential in colorimetric food spoilage monitoring. The system was also trained and tested with real fish samples, resulting in 99.6% accuracy. In addition, the RF classifier was embedded in SmartFood++, allowing analysis in about 0.1 sec without internet access. To the best of our knowledge, this is the first study that embeds an ML classifier into a smartphone application for food spoilage monitoring.

6.2 Future Research

There are some possible critical extensions to the work discussed in this thesis based on the problems and limitations of the proposed methods. In this section, we highlight the limitations and drawbacks of the developed techniques and

propose some directions for further improvements. An outline of the possible directions for future research is sketched below.

- In non-enzymatic colorimetric detection of hydrogen peroxide, the system could be further extended by enlarging the dataset for closer concentration levels and employing more sophisticated methodologies such as DL and transfer learning to improve classification accuracy and sensitivity. Overall, the proposed system offers portability, rapid response, easy operation, and high selectivity, which can be applied in point-of-care sensing, healthcare, and environmental monitoring in resource-limited settings.
- In automated colorimetric lactate analysis in sweat, it should be noted that the classification sensitivity of the proposed system can also be improved by training the system with closer concentration levels. The proposed system could be easily used for clinical and environmental monitoring in remote and resource-limited settings by extending colorimetric analysis for multi-analyte detection in real samples such as water, urine, and blood.
- Unlike conventional measurements in on-site food spoilage monitoring with smartphone-embedded ML, our system offers real-time, robust, and easy operation for non-expert users, which can contribute to developing new tools with advanced functions for smart packaging.
- While classifying in colorimetric analysis using AI algorithms, the system rounds up to whichever concentration level the result is close to. This problem can be solved by performing regression analysis.
- We used only Android as the operating system in smartphone applications. In future studies, it can be used on phones with different operating systems (iOS).
- Experimental design will be developed with modeling and optimization studies.

References

- [1] Y. Fan, J. Li, Y. Guo, L. Xie, and G. Zhang, Digital image colorimetry on smartphone for chemical analysis: A review, *Measurement*, vol. 171, p. 108829, 2021.
- [2] G. M. Fernandes, W. R. Silva, D. N. Barreto, R. S. Lamarca, P. C. F. L. Gomes et al., Novel approaches for colorimetric measurements in analytical chemistry—A review, *Analytica Chimica Acta*, vol. 1135, pp. 187-203, 2020.
- [3] R. Ghaffari, J. Choi, M. S. Raj, S. Chen, S. P. Lee et al., Soft wearable systems for colorimetric and electrochemical analysis of biofluids, *Advanced Functional Materials*, vol. 30, no. 37, p. 1907269, 2020.
- [4] B. Liu, J. Zhuang, and G. Wei, Recent advances in the design of colorimetric sensors for environmental monitoring, *Environmental Science: Nano*, vol. 7, no. 8, pp. 2195-2213, 2020.
- [5] H. Xiao-wei, Z. Xiao-bo, S. Ji-yong, L. Zhi-hua, and Z. Jie-wen, Colorimetric sensor arrays based on chemo-responsive dyes for food odor visualization, *Trends in Food Science Technology*, vol. 81, pp. 90-107, 2018.
- [6] S. Qian, Y. Cui, Z. Cai, and L. Li, Applications of smartphone-based colorimetric biosensors, *Biosensors Bioelectronics: X*, vol. 11, p. 100173, 2022.
- [7] M. Wen, J. Li, W. Zhong, J. Xu, S. Qu et al., High-Throughput Colorimetric Analysis of Nanoparticle–Protein Interactions Based on the Enzyme-Mimic Properties of Nanoparticles, *Analytical Chemistry*, vol. 94, no. 24, pp. 8783-8791, 2022.
- [8] Y. Park, B. Ryu, S. J. Ki, B. McCracken, A. Pennington et al., Few-layer MoS₂ photodetector arrays for ultrasensitive on-chip enzymatic colorimetric analysis, *ACS nano*, vol. 15, no. 4, pp. 7722-7734, 2021.

- [9] C. Lin, Y. Du, S. Wang, L. Wang, and Y. Song, Glucose oxidase@ Cu-hemin metal-organic framework for colorimetric analysis of glucose, *Materials Science Engineering: C*, vol. 118, p. 111511, 2021.
- [10] E. Priyadarshini and N. Pradhan, Gold nanoparticles as efficient sensors in colorimetric detection of toxic metal ions: a review, *Sensors Actuators B: Chemical*, vol. 238, pp. 888-902, 2017.
- [11] A. Azzouz, K. Vikrant, K.-H. Kim, E. Ballesteros, T. Rhadfi et al., Advances in colorimetric and optical sensing for gaseous volatile organic compounds, *TrAC Trends in Analytical Chemistry*, vol. 118, pp. 502-516, 2019.
- [12] K. Chaisiwamongkhol, S. Labaidae, S. Pon-in, S. Pinsrithong, T. Bunchuay et al., Smartphone-based colorimetric detection using gold nanoparticles of sibutramine in suspected food supplement products, *Microchemical Journal*, vol. 158, p. 105273, 2020.
- [13] M. Dysinger, G. Marusov, and S. Fraser, Quantitative analysis of four protein biomarkers: An automated microfluidic cartridge-based method and its comparison to colorimetric ELISA, *Journal of immunological methods*, vol. 451, pp. 1-10, 2017.
- [14] H. Moulahoum, F. Ghorbanizamani, and S. J. M. A. Timur, based lateral flow assay using rhodamine B-loaded polymersomes for the colorimetric determination of synthetic cannabinoids in saliva, *Microchimica Acta*, vol. 188, pp. 1-12, 2021.
- [15] W. Tan, L. Zhang, P. Jarujamrus, J. C. Doery, and W. J. M. J. Shen, Improvement strategies on colorimetric performance and practical applications of Paper-based analytical devices, *Microchemical Journal*, p. 107562, 2022.
- [16] V. Doğan, E. Yüzer, V. Kılıç, and M. Şen, Non-enzymatic colorimetric detection of hydrogen peroxide using a μ PAD coupled with a machine learning-based smartphone app, *Analyst*, vol. 146, no. 23, pp. 7336-7344, 2021.

- [17] E. Yüzer, V. Doğan, V. Kılıç, M. J. S. Şen, and A. B. Chemical, Smartphone embedded deep learning approach for highly accurate and automated colorimetric lactate analysis in sweat, *Sensors Actuators B: Chemical*, vol. 371, p. 132489, 2022.
- [18] H. Sharifi, J. Tashkhourian, and B. J. A. C. A. Hemmateenejad, A 3D origami paper-based analytical device combined with PVC membrane for colorimetric assay of heavy metal ions: Application to determination of Cu (II) in water samples, *Analytica Chimica Acta*, vol. 1126, pp. 114-123, 2020.
- [19] M. M. Bordbar, T. A. Nguyen, F. Arduini, and H. Bagheri, A paper-based colorimetric sensor array for discrimination and simultaneous determination of organophosphate and carbamate pesticides in tap water, apple juice, and rice, *Microchimica Acta*, vol. 187, pp. 1-13, 2020.
- [20] A. Choodum, W. Sriprom, and W. Wongniramaikul, Portable and selective colorimetric film and digital image colorimetry for detection of iron, *Spectrochimica Acta Part A: Molecular Biomolecular Spectroscopy*, vol. 208, pp. 40-47, 2019.
- [21] M. Weston, A. D. Tjandra, and R. J. P. C. Chandrawati, Tuning chromatic response, sensitivity, and specificity of polydiacetylene-based sensors, *Polymer Chemistry*, vol. 11, no. 2, pp. 166-183, 2020.
- [22] K. Wang, Y. Liu, D. Li, A. Zhang, P. Mo et al., Electrodeposited Alginate-Based Green Synthesis of CuS Nanoparticles and Nanocomposite Films for Electrochemical and Colorimetric Detection, *Macromolecular Materials Engineering*, vol. 307, no. 8, p. 2200090, 2022.
- [23] B. Kilic, V. Dogan, V. Kilic, and L. N. J. I. J. o. B. M. Kahyaoglu, Colorimetric food spoilage monitoring with carbon dot and UV light reinforced fish gelatin films using a smartphone application, *International Journal of Biological Macromolecules*, vol. 209, pp. 1562-1572, 2022.

- [24] M. A. Akl, C. P. C. Sim, M. E. Nunn, L. L. Zeng, T. A. Hamza et al., Validation of two clinical color measuring instruments for use in dental research, *Journal of Dentistry*, vol. 125, p. 104223, 2022.
- [25] G. de Carvalho Oliveira, C. C. S. Machado, D. K. Inácio, J. F. da Silveira Petrucci, and S. G. Silva, RGB color sensor for colorimetric determinations: Evaluation and quantitative analysis of colored liquid samples, *Talanta*, vol. 241, p. 123244, 2022.
- [26] F. Badar, L. T. Dean, J. Loy, M. Redmond, L.-J. Vandi et al., Preliminary color characterization of HP Multi Jet Fusion additive manufacturing with different orientations and surface finish, *Rapid Prototyping Journal*, vol. 29, no. 3, pp. 582-593, 2023.
- [27] M. Peer and R. J. F. S. I. Sarig, Color change in teeth due to burning: Spectrophotometric analysis, *Forensic Science International*, vol. 345, p. 111608, 2023.
- [28] R. Yang, W. Cheng, X. Chen, Q. Qian, Q. Zhang et al., Color space transformation-based smartphone algorithm for colorimetric urinalysis, *ACS omega*, vol. 3, no. 9, pp. 12141-12146, 2018.
- [29] S. A. Klasner, A. K. Price, K. W. Hoeman, R. S. Wilson, K. J. Bell et al., based microfluidic devices for analysis of clinically relevant analytes present in urine and saliva, *Analytical bioanalytical chemistry*, vol. 397, pp. 1821-1829, 2010.
- [30] E. J. A. B. Rogatsky, Pandora box of BCA assay. Investigation of the accuracy and linearity of the microplate bicinchoninic protein assay: Analytical challenges and method modifications to minimize systematic errors, *Analytical Biochemistry*, vol. 631, p. 114321, 2021.
- [31] Y. Zhang, T. Zhang, and H. J. S. A. P. B. A. S. Li, Application of laser-induced breakdown spectroscopy (LIBS) in environmental monitoring, *Spectrochimica Acta Part B: Atomic Spectroscopy*, vol. 181, p. 106218, 2021.

- [32] V. Cerdà, P. Phansi, and S. Ferreira, From mono-to multicomponent methods in UV-VIS spectrophotometric and fluorimetric quantitative analysis—A review, *TrAC Trends in Analytical Chemistry*, p. 116772, 2022.
- [33] H. P. Jarvie, J. Withers, and C. Neal, Review of robust measurement of phosphorus in river water: sampling, storage, fractionation and sensitivity, *Hydrology Earth System Sciences*, vol. 6, no. 1, pp. 113-131, 2002.
- [34] M. Şen, E. Yüzer, V. Doğan, İ. Avcı, K. Ensarioğlu et al., Colorimetric detection of H₂O₂ with Fe₃O₄@ Chi nanozyme modified µPADs using artificial intelligence, *Microchimica Acta*, vol. 189, no. 10, p. 373, 2022.
- [35] L. B. Ayres, F. J. Gomez, J. R. Linton, M. F. Silva, and C. D. Garcia, Taking the leap between analytical chemistry and artificial intelligence: A tutorial review, *Analytica Chimica Acta*, vol. 1161, p. 338403, 2021.
- [36] E. Sonwani, U. Bansal, R. Alroobaea, A. M. Baqasah, and M. J. F. i. P. H. Hedabou, An Artificial Intelligence Approach Toward Food Spoilage Detection and Analysis, *Frontiers in Public Health*, vol. 9, p. 2254, 2022.
- [37] S. Kaur, J. Singla, L. Nkenyereye, S. Jha, D. Prashar et al., Medical diagnostic systems using artificial intelligence (ai) algorithms: Principles and perspectives, *IEEE Access*, vol. 8, pp. 228049-228069, 2020.
- [38] Y. Himeur, B. Rimal, A. Tiwary, and A. Amira, Using artificial intelligence and data fusion for environmental monitoring: A review and future perspectives, *Information Fusion*, 2022.
- [39] W. Sha, Y. Guo, Q. Yuan, S. Tang, X. Zhang et al., Artificial intelligence to power the future of materials science and engineering, *Advanced Intelligent Systems*, vol. 2, no. 4, p. 1900143, 2020.
- [40] Ö. B. Mercan, V. Kılıç, M. J. S. Şen, and A. B. Chemical, Machine learning-based colorimetric determination of glucose in artificial saliva with different reagents using a smartphone coupled µPAD, *Sensors Actuators B: Chemical*, vol. 329, p. 129037, 2021.

- [41] V. Doğan, T. Isık, V. Kılıç, and N. Horzum, A field-deployable water quality monitoring with machine learning-based smartphone colorimetry, *Analytical Methods*, vol. 14, no. 35, pp. 3458-3466, 2022.
- [42] H. Yang, C. Meng, and C. J. I. A. Wang, Data-driven feature extraction for analog circuit fault diagnosis using 1-D convolutional neural network, *IEEE Access*, vol. 8, pp. 18305-18315, 2020.
- [43] K. Chu and G.-H. Liu, Image retrieval based on a multi-integration features model, *Mathematical problems in engineering*, vol. 2020, pp. 1-10, 2020.
- [44] S. K. Abdulateef and A. N. Hasoon, Comparison of the Components of Different Colour Spaces to Enhanced Image Representation, *Journal of Image Processing Intelligent Remote Sensing*, vol. 3, no. 01, pp. 11-17, 2023.
- [45] C. Li, S. Anwar, J. Hou, R. Cong, C. Guo et al., Underwater image enhancement via medium transmission-guided multi-color space embedding, *IEEE Transactions on Image Processing*, vol. 30, pp. 4985-5000, 2021.
- [46] A. Taheri-Garavand, S. Fatahi, M. Omid, and Y. J. M. s. Makino, Meat quality evaluation based on computer vision technique: A review, *Meat science*, vol. 156, pp. 183-195, 2019.
- [47] S. Y. Kahu, R. B. Raut, K. M. J. C. R. Bhurchandi, and Application, Review and evaluation of color spaces for image/video compression, *Color Research Application*, vol. 44, no. 1, pp. 8-33, 2019.
- [48] F. G. Waldamichael, T. G. Debelee, and Y. M. J. I. J. o. I. S. Ayano, Coffee disease detection using a robust HSV color-based segmentation and transfer learning for use on smartphones, *International Journal of Intelligent Systems*, vol. 37, no. 8, pp. 4967-4993, 2022.
- [49] Z. Wu, S. Jiang, X. Zhou, Y. Wang, Y. Zuo et al., Application of image retrieval based on convolutional neural networks and Hu invariant moment algorithm in computer telecommunications, *Computer Communications*, vol. 150, pp. 729-738, 2020.

- [50] P. Mishra, C. M. Pandey, U. Singh, A. Gupta, C. Sahu et al., Descriptive statistics and normality tests for statistical data, *Annals of cardiac anaesthesia*, vol. 22, no. 1, p. 67, 2019.
- [51] R. J. S. r. Takagi, Skew informations from an operational view via resource theory of asymmetry, *Scientific reports*, vol. 9, no. 1, p. 14562, 2019.
- [52] R. Bono, J. Arnau, R. Alarcón, and M. J. Blanca, Bias, precision, and accuracy of skewness and kurtosis estimators for frequently used continuous distributions, *Symmetry*, vol. 12, no. 1, p. 19, 2019.
- [53] N. J. M. T. Varish and Applications, A modified similarity measurement for image retrieval scheme using fusion of color, texture and shape moments, *Multimedia Tools Applications*, vol. 81, no. 15, pp. 20373-20405, 2022.
- [54] L. J. C. de Mendonça, R. J. Ferrari, and A. s. D. N. Initiative, Alzheimer's disease classification based on graph kernel SVMs constructed with 3D texture features extracted from MR images, *Expert Systems with Applications*, vol. 211, p. 118633, 2023.
- [55] A. A. Alnuaim, M. Zakariah, C. Shashidhar, W. A. Hatamleh, H. Tarazi et al., Speaker gender recognition based on deep neural networks and ResNet50, *Wireless Communications Mobile Computing*, vol. 2022, pp. 1-13, 2022.
- [56] L. Zhu, F. Dang, Y. Xue, W. Ding, L. J. C. Zhang et al., Analysis of micro-structural damage evolution of concrete through coupled X-ray computed tomography and gray-level co-occurrence matrices method, *Construction Building Materials*, vol. 224, pp. 534-550, 2019.
- [57] Y. Park and J.-M. J. E. I. Guldmann, Measuring continuous landscape patterns with Gray-Level Co-Occurrence Matrix (GLCM) indices: An alternative to patch metrics?, *Ecological Indicators*, vol. 109, p. 105802, 2020.
- [58] S. Aouat, I. Ait-hammi, and I. Hamouchene, A new approach for texture segmentation based on the Gray Level Co-occurrence Matrix, *Multimedia Tools Applications*

vol. 80, pp. 24027-24052, 2021.

- [59] X. Yang, S. Tridandapani, J. J. Beitler, D. S. Yu, E. J. Yoshida et al., Ultrasound GLCM texture analysis of radiation-induced parotid-gland injury in head-and-neck cancer radiotherapy: An in vivo study of late toxicity, *Medical physics*, vol. 39, no. 9, pp. 5732-5739, 2012.
- [60] B. Thiyaneswaran, K. Anguraj, S. Kumarganesh, K. J. I. J. o. I. S. Thangaraj, and Technology, Early detection of melanoma images using gray level co-occurrence matrix features and machine learning techniques for effective clinical diagnosis, *International Journal of Imaging Systems Technology*, vol. 31, no. 2, pp. 682-694, 2021.
- [61] R. Zebari, A. Abdulazeez, D. Zeebaree, D. Zebari, J. J. J. o. A. S. Saeed et al., A comprehensive review of dimensionality reduction techniques for feature selection and feature extraction, *Journal of Applied Science Technology Trends*, vol. 1, no. 2, pp. 56-70, 2020.
- [62] G. Chandrashekar and F. Sahin, A survey on feature selection methods, *Computers Electrical Engineering*, vol. 40, no. 1, pp. 16-28, 2014.
- [63] B. H. Nguyen, B. Xue, M. J. S. Zhang, and E. Computation, A survey on swarm intelligence approaches to feature selection in data mining, *Swarm Evolutionary Computation*, vol. 54, p. 100663, 2020.
- [64] G. Kou, P. Yang, Y. Peng, F. Xiao, Y. Chen et al., Evaluation of feature selection methods for text classification with small datasets using multiple criteria decision-making methods, *Applied Soft Computing*, vol. 86, p. 105836, 2020.
- [65] S. Beyaz, A brief history of artificial intelligence and robotic surgery in orthopedics & traumatology and future expectations, *Joint Diseases Related Surgery*, vol. 31, no. 3, p. 653, 2020.
- [66] F. Gargiulo, S. Fontaine, M. Dubois, and P. Tubaro, A meso-scale cartography of the AI ecosystem, *arXiv preprint arXiv:2206.12263*, 2022.

- [67] S. O. Abioye, L. O. Oyedele, L. Akanbi, A. Ajayi, J. M. D. Delgado et al., Artificial intelligence in the construction industry: A review of present status, opportunities and future challenges, *Journal of Building Engineering*, vol. 44, p. 103299, 2021.
- [68] S. S. Gill, M. Xu, C. Ottaviani, P. Patros, R. Bahsoon et al., AI for next generation computing: Emerging trends and future directions, *Internet of Things*, vol. 19, p. 100514, 2022.
- [69] A. Le Glaz, Y. Haralambous, D.-H. Kim-Dufor, P. Lenca, R. Billot et al., Machine learning and natural language processing in mental health: systematic review, *Journal of Medical Internet Research*, vol. 23, no. 5, p. e15708, 2021.
- [70] R. Ptucha, F. P. Such, S. Pillai, F. Brockler, V. Singh et al., Intelligent character recognition using fully convolutional neural networks, *Pattern recognition*, vol. 88, pp. 604-613, 2019.
- [71] A. Serban, E. Poll, and J. J. A. C. S. Visser, Adversarial examples on object recognition: A comprehensive survey, *ACM Computing Surveys*, vol. 53, no. 3, pp. 1-38, 2020.
- [72] P. Gopal, A. Gesta, and A. Mohebbi, A systematic study on electromyography-based hand gesture recognition for assistive robots using deep learning and machine learning models, *Sensors*, vol. 22, no. 10, p. 3650, 2022.
- [73] H. S. R. Rajula, G. Verlato, M. Manchia, N. Antonucci, and V. J. M. Fanos, Comparison of conventional statistical methods with machine learning in medicine: diagnosis, drug development, and treatment, *Medicina*, vol. 56, no. 9, p. 455, 2020.
- [74] J. Yan and X. J. T. P. J. Wang, Unsupervised and semi-supervised learning: the next frontier in machine learning for plant systems biology, *The Plant Journal*, vol. 111, no. 6, pp. 1527-1538, 2022.
- [75] M. Alloghani, D. Al-Jumeily, J. Mustafina, A. Hussain, and A. J. Aljaaf, A systematic review on supervised and unsupervised machine learning algorithms for data science, *Supervised unsupervised learning for data science*

pp. 3-21, 2020.

- [76] R. Sarikhani and F. J. I. C. L. Keynia, Cooperative spectrum sensing meets machine learning: Deep reinforcement learning approach, *IEEE Communications Letters*, vol. 24, no. 7, pp. 1459-1462, 2020.
- [77] J. Pearce and S. J. E. m. Ferrier, Evaluating the predictive performance of habitat models developed using logistic regression, *Ecological modelling*, vol. 133, no. 3, pp. 225-245, 2000.
- [78] L. Cai, J. Gu, J. Ma, and Z. Jin, Probabilistic wind power forecasting approach via instance-based transfer learning embedded gradient boosting decision trees, *Energies*, vol. 12, no. 1, p. 159, 2019.
- [79] C.-C. Chern, Y.-J. Chen, and B. Hsiao, Decision tree-based classifier in providing telehealth service, *BMC medical informatics decision making*, vol. 19, pp. 1-15, 2019.
- [80] C. Prianka, B. Kavida, M. J. E. Bibin, and S. I. Journal, Cervical cancer cell prediction using machine learning classification algorithms, *Engineering Scientific International Journal*, vol. 8, no. 1, pp. 25-29, 2021.
- [81] M. T. García-Ordás, H. Alaiz-Moretón, J.-L. Casteleiro-Roca, E. Jove, J. A. Benítez-Andrades et al., Clustering techniques selection for a hybrid regression model: a case study based on a solar thermal system, *Cybernetics Systems*, vol. 54, no. 3, pp. 286-305, 2023.
- [82] R. Chowdhury, M. Mahdy, T. N. Alam, G. D. Al Quaderi, and M. A. Rahman, Predicting the stock price of frontier markets using machine learning and modified Black-Scholes Option pricing model, *Physica A: Statistical Mechanics its Applications*, vol. 555, p. 124444, 2020.
- [83] M. Alkhayrat, M. Aljnidi, and K. Aljoumaa, A comparative dimensionality reduction study in telecom customer segmentation using deep learning and PCA, *Journal of Big Data*, vol. 7, pp. 1-23, 2020.

- [84] O. Eluyode and D. T. Akomolafe, Comparative study of biological and artificial neural networks, *European Journal of Applied Engineering Scientific Research*, vol. 2, no. 1, pp. 36-46, 2013.
- [85] K. D. Julian, M. J. Kochenderfer, and M. P. Owen, Deep neural network compression for aircraft collision avoidance systems, *Journal of Guidance, Control, Dynamics*, vol. 42, no. 3, pp. 598-608, 2019.
- [86] C. Moler and J. J. P. o. t. A. o. P. L. Little, A history of MATLAB, *Proceedings of the ACM on Programming Languages*, vol. 4, no. HOPL, pp. 1-67, 2020.
- [87] B. H. Toby and R. B. J. J. o. A. C. Von Dreele, GSAS-II: the genesis of a modern open-source all purpose crystallography software package, *Journal of Applied Crystallography*, vol. 46, no. 2, pp. 544-549, 2013.
- [88] R. Garud, S. Jain, and A. Kumaraswamy, Institutional entrepreneurship in the sponsorship of common technological standards: The case of Sun Microsystems and Java, *Academy of management journal*, vol. 45, no. 1, pp. 196-214, 2002.
- [89] D. Parsons, D. J. F. J. K. E. Parsons, and P. Programming, *The Java Story, Foundational Java: Key Elements Practical Programming*, pp. 1-10, 2020.
- [90] R. R. Bouckaert, E. Frank, M. A. Hall, G. Holmes, B. Pfahringer et al., WEKA--Experiences with a Java Open-Source Project, *The Journal of Machine Learning Research*, vol. 11, pp. 2533-2541, 2010.
- [91] T. Leino, *Collecting Usage Data with Google Analytics for Firebase*, 2021.
- [92] O. M. Ahmed and A. B. Sallow, Android security: a review, *Academic Journal of Nawroz University*, vol. 6, no. 3, pp. 135-140, 2017.
- [93] D. Chicco and G. Jurman, The advantages of the Matthews correlation coefficient (MCC) over F1 score and accuracy in binary classification evaluation, *BMC genomics*, vol. 21, pp. 1-13, 2020.
- [94] S. G. J. S. Rhee, H₂O₂, a necessary evil for cell signaling, *Science*, vol. 312, no. 5782, pp. 1882-1883, 2006.

- [95] S. Bocanegra-Rodríguez, N. Jornet-Martínez, C. Molins-Legua, and P. Campíns-Falcó, New reusable solid biosensor with covalent immobilization of the horseradish peroxidase enzyme: in situ liberation studies of hydrogen peroxide by portable chemiluminescent determination, *ACS omega*, vol. 5, no. 5, pp. 2419-2427, 2020.
- [96] J. E. Giaretta, F. Oveissi, F. Dehghani, and S. Naficy, Paper-Based, Chemiresistive Sensor for Hydrogen Peroxide Detection, *Advanced Materials Technologies*, vol. 6, no. 4, p. 2001148, 2021.
- [97] Q. Wang, R. Xue, H. Guo, Y. Wei, and W. J. J. o. E. C. Yang, A facile horseradish peroxidase electrochemical biosensor with surface molecular imprinting based on polyaniline nanotubes, *Journal of Electroanalytical Chemistry*, vol. 817, pp. 184-194, 2018.
- [98] K. Ragavan, S. R. Ahmed, X. Weng, S. J. S. Neethirajan, and A. B. Chemical, Chitosan as a peroxidase mimic: Paper based sensor for the detection of hydrogen peroxide, *Sensors Actuators B: Chemical*, vol. 272, pp. 8-13, 2018.
- [99] X. Xiong, C. You, X. Cao, L. Pang, R. Kong et al., Ni₂P nanosheets array as a novel electrochemical catalyst electrode for non-enzymatic H₂O₂ sensing, *Electrochimica Acta*, vol. 253, pp. 517-521, 2017.
- [100] N. Jiang, N. D. Tansukawat, L. Gonzalez-Macia, H. C. Ates, C. Dincer et al., Low-cost optical assays for point-of-care diagnosis in resource-limited settings, *ACS sensors*, vol. 6, no. 6, pp. 2108-2124, 2021.
- [101] A. W. Martinez, S. T. Phillips, M. J. Butte, and G. M. J. A. C. Whitesides, Patterned paper as a platform for inexpensive, low-volume, portable bioassays, *Angewandte Chemie*, vol. 119, no. 8, pp. 1340-1342, 2007.
- [102] Ö. B. Mercan and V. Kılıç, Fuzzy classifier based colorimetric quantification using a smartphone, in *Intelligent and Fuzzy Techniques: Smart and Innovative Solutions: Proceedings of the INFUS 2020 Conference, Istanbul, Turkey, July 21-23, 2020*, 2021, pp. 1276-1283: Springer.

- [103] T. Gölcez, V. Kilic, and M. Şen, A portable smartphone-based platform with an offline image-processing tool for the rapid paper-based colorimetric detection of glucose in artificial saliva, *Analytical Sciences*, vol. 37, no. 4, pp. 561-567, 2021.
- [104] H. Kim, O. Awofeso, S. Choi, Y. Jung, and E. J. A. O. Bae, Colorimetric analysis of saliva–alcohol test strips by smartphone-based instruments using machine-learning algorithms, *Applied optics*, vol. 56, no. 1, pp. 84-92, 2017.
- [105] M. E. Solmaz, A. Y. Mutlu, G. Alankus, V. Kılıç, A. Bayram et al., Quantifying colorimetric tests using a smartphone app based on machine learning classifiers, *Sensors Actuators B: Chemical*, vol. 255, pp. 1967-1973, 2018.
- [106] L. L. Mølgaard, O. T. Buus, J. Larsen, H. Babamoradi, I. L. Thygesen et al., Improved detection of chemical substances from colorimetric sensor data using probabilistic machine learning, in *Chemical, Biological, Radiological, Nuclear, and Explosives (CBRNE) Sensing XVIII*, 2017, vol. 10183, pp. 38-45: SPIE.
- [107] B. R. Sun, A. G. Zhou, X. Li, and H.-Z. J. A. s. Yu, Development and application of mobile apps for molecular sensing: a review, *ACS sensors*, vol. 6, no. 5, pp. 1731-1744, 2021.
- [108] Ö. B. Mercan, V. Doğan, and V. Kılıç, Time Series Analysis based Machine Learning Classification for Blood Sugar Levels, in *2020 Medical Technologies Congress (TIPTEKNO)*, 2020, pp. 1-4: IEEE.
- [109] M. Nixon and A. Aguado, *Feature extraction and image processing for computer vision*. Academic press, 2019.
- [110] D. J. I. J. o. M. Ping Tian and U. Engineering, A review on image feature extraction and representation techniques, *International Journal of Multimedia Ubiquitous Engineering*, vol. 8, no. 4, pp. 385-396, 2013.
- [111] A. Y. Mutlu and V. Kılıç, Machine learning based smartphone spectrometer for harmful dyes detection in water, in *2018 26th Signal Processing and Communications Applications Conference (SIU)*, 2018, pp. 1-4: IEEE.

- [112] Z. Fan, Y. Xu, and D. Zhang, Local linear discriminant analysis framework using sample neighbors, *IEEE Transactions on Neural Networks*, vol. 22, no. 7, pp. 1119-1132, 2011.
- [113] S. Sreng, N. Maneerat, K. Hamamoto, and R. J. A. S. Panjaphongse, Automated diabetic retinopathy screening system using hybrid simulated annealing and ensemble bagging classifier, *Applied Sciences*, vol. 8, no. 7, p. 1198, 2018.
- [114] R. Bandi, M. Alle, C.-W. Park, S.-Y. Han, G.-J. Kwon et al., Cellulose nanofibrils/carbon dots composite nanopapers for the smartphone-based colorimetric detection of hydrogen peroxide and glucose, *Sensors Actuators B: Chemical*, vol. 330, p. 129330, 2021.
- [115] Y. Cheng, L. Liang, F. Ye, and S. Zhao, Ce-MOF with intrinsic haloperoxidase-like activity for ratiometric colorimetric detection of hydrogen peroxide, *Biosensors*, vol. 11, no. 7, p. 204, 2021.
- [116] M. Parrilla, M. Cuartero, and G. A. J. T. T. i. A. C. Crespo, Wearable potentiometric ion sensors, *TrAC Trends in Analytical Chemistry*, vol. 110, pp. 303-320, 2019.
- [117] N. V. Zaryanov, V. N. Nikitina, E. V. Karpova, E. E. Karyakina, and A. A. J. A. c. Karyakin, Nonenzymatic sensor for lactate detection in human sweat, *Analytical Chemistry*, vol. 89, no. 21, pp. 11198-11202, 2017.
- [118] M. A. Komkova, A. A. Eliseev, A. A. Poyarkov, E. V. Daboss, P. V. Evdokimov et al., Simultaneous monitoring of sweat lactate content and sweat secretion rate by wearable remote biosensors, *Biosensors Bioelectronics*, vol. 202, p. 113970, 2022.
- [119] P. J. Derbyshire, H. Barr, F. Davis, and S. P. Higson, Lactate in human sweat: a critical review of research to the present day, *The journal of physiological sciences*, vol. 62, no. 6, pp. 429-440, 2012.
- [120] N. Promphet, P. Rattanawaleedirojn, K. Siralertmukul, N. Soatthiyanon, P. Potiyaraj et al., Non-invasive textile based colorimetric sensor for the

- simultaneous detection of sweat pH and lactate, *Talanta*, vol. 192, pp. 424-430, 2019.
- [121] E. V. Karpova, A. I. Laptev, E. A. Andreev, E. E. Karyakina, and A. A. J. C. Karyakin, Relationship between sweat and blood lactate levels during exhaustive physical exercise, *ChemElectroChem*, vol. 7, no. 1, pp. 191-194, 2020.
- [122] Y. Seki, D. Nakashima, Y. Shiraishi, T. Ryuzaki, H. Ikura et al., A novel device for detecting anaerobic threshold using sweat lactate during exercise, *Scientific reports*, vol. 11, no. 1, p. 4929, 2021.
- [123] K. Rathee, V. Dhull, R. Dhull, S. J. B. Singh, and b. reports, Biosensors based on electrochemical lactate detection: A comprehensive review, *Biochemistry biophysics reports*, vol. 5, pp. 35-54, 2016.
- [124] W. Jia, A. J. Bhandodkar, G. Valdés-Ramírez, J. R. Windmiller, Z. Yang et al., Electrochemical tattoo biosensors for real-time noninvasive lactate monitoring in human perspiration, *Analytical Chemistry*, vol. 85, no. 14, pp. 6553-6560, 2013.
- [125] G. Rattu, N. Khansili, V. K. Maurya, and P. M. J. E. C. L. Krishna, Lactate detection sensors for food, clinical and biological applications: A review, *Environmental Chemistry Letters*, vol. 19, pp. 1135-1152, 2021.
- [126] T. Saha, J. Fang, S. Mukherjee, C. T. Knisely, M. D. Dickey et al., Osmotically enabled wearable patch for sweat harvesting and lactate quantification, *Micromachines*, vol. 12, no. 12, p. 1513, 2021.
- [127] A. Khan, M. Winder, G. J. B. Hossain, and B. X, Modified graphene-based nanocomposite material for smart textile biosensor to detect lactate from human sweat, *Biosensors Bioelectronics: X*, vol. 10, p. 100103, 2022.
- [128] V. Kılıç, Ö. B. Mercan, M. Tetik, Ö. Kap, and N. J. A. S. Horzum, Non-enzymatic colorimetric glucose detection based on Au/Ag nanoparticles using smartphone and machine learning, *Analytical Sciences*, vol. 38, no. 2, pp. 347-358, 2022.

- [129] F. Wu, Y. Huang, C. J. B. Huang, and Bioelectronics, Chemiluminescence biosensor system for lactic acid using natural animal tissue as recognition element, *Biosensors Bioelectronics*, vol. 21, no. 3, pp. 518-522, 2005.
- [130] Ö. Kap, V. Kılıç, J. G. Hardy, and N. J. A. Horzum, Smartphone-based colorimetric detection systems for glucose monitoring in the diagnosis and management of diabetes, *Analyst*, vol. 146, no. 9, pp. 2784-2806, 2021.
- [131] M. Liang, K. Fan, Y. Pan, H. Jiang, F. Wang et al., Fe₃O₄ magnetic nanoparticle peroxidase mimetic-based colorimetric assay for the rapid detection of organophosphorus pesticide and nerve agent, *Analytical Chemistry*, vol. 85, no. 1, pp. 308-312, 2013.
- [132] S. Wu, D. Li, J. Wang, Y. Zhao, S. Dong et al., Gold nanoparticles dissolution based colorimetric method for highly sensitive detection of organophosphate pesticides, *Sensors Actuators B: Chemical*, vol. 238, pp. 427-433, 2017.
- [133] G. Klambauer, T. Unterthiner, A. Mayr, and S. J. A. i. n. i. p. s. Hochreiter, Self-normalizing neural networks, *Advances in neural information processing systems*, vol. 30, 2017.
- [134] A. G. Howard, M. Zhu, B. Chen, D. Kalenichenko, W. Wang et al., Mobilenets: Efficient convolutional neural networks for mobile vision applications, *arXiv preprint arXiv:1704.04861*, 2017.
- [135] F. Chollet, Xception: Deep learning with depthwise separable convolutions, in *Proceedings of the IEEE conference on computer vision and pattern recognition*, 2017, pp. 1251-1258.
- [136] S. Dodge and L. Karam, Understanding how image quality affects deep neural networks, in *2016 eighth international conference on quality of multimedia experience (QoMEX)*, 2016, pp. 1-6: IEEE.
- [137] J. Johnson, A. Alahi, and L. Fei-Fei, Perceptual losses for real-time style transfer and super-resolution, in *Computer Vision—ECCV 2016: 14th European Conference, Amsterdam, The Netherlands, October 11-14, 2016, Proceedings, Part II 14*, 2016, pp. 694-711: Springer.

- [138] Y. Tai, J. Yang, and X. Liu, Image super-resolution via deep recursive residual network, in Proceedings of the IEEE conference on computer vision and pattern recognition, 2017, pp. 3147-3155.
- [139] C. Szegedy, V. Vanhoucke, S. Ioffe, J. Shlens, and Z. Wojna, Rethinking the inception architecture for computer vision, in Proceedings of the IEEE conference on computer vision and pattern recognition, 2016, pp. 2818-2826.
- [140] Ö. B. Mercan and V. Kılıç, Deep Learning based Colorimetric Classification of Glucose with Au-Ag nanoparticles using Smartphone, in 2020 Medical Technologies Congress (TIPTEKNO), 2020, pp. 1-4: IEEE.
- [141] Z. Palaz, V. Doğan, and V. J. A. B. v. T. D. KILIÇ, Smartphone-based Multi-parametric Glucose Prediction using Recurrent Neural Networks, Avrupa Bilim ve Teknoloji Dergisi, no. 32, pp. 1168-1174, 2021.
- [142] B. Palsson, J. R. Sveinsson, M. O. J. I. J. o. S. T. i. A. E. O. Ulfarsson, and R. Sensing, Blind hyperspectral unmixing using autoencoders: A critical comparison, IEEE Journal of Selected Topics in Applied Earth Observations Remote Sensing, vol. 15, pp. 1340-1372, 2022.
- [143] J. Tian, Y. Liu, W. Zheng, and L. J. U. C. Yin, Smog prediction based on the deep belief-BP neural network model (DBN-BP), Urban Climate, vol. 41, p. 101078, 2022.
- [144] K. Moses, A. Miglani, P. K. J. C. Kankar, and E. i. Agriculture, Deep CNN-based damage classification of milled rice grains using a high-magnification image dataset, Computers Electronics in Agriculture, vol. 195, p. 106811, 2022.
- [145] J. Chang, Y. Lu, P. Xue, Y. Xu, and Z. Wei, Automatic channel pruning via clustering and swarm intelligence optimization for CNN, Applied Intelligence, pp. 1-21, 2022.
- [146] N. Wang, Y. Wang, and M. J. J. C. E. P. Er, Review on deep learning techniques for marine object recognition: Architectures and algorithms, Control Engineering Practice, vol. 118, p. 104458, 2022.

- [147] P. S. Pakchin, H. Ghanbari, R. Saber, Y. J. B. Omid, and Bioelectronics, Electrochemical immunosensor based on chitosan-gold nanoparticle/carbon nanotube as a platform and lactate oxidase as a label for detection of CA125 oncomarker, *Biosensors Bioelectronics*, vol. 122, pp. 68-74, 2018.
- [148] Y. Munesue, T. Masui, T. J. E. E. Fushima, and P. Studies, The effects of reducing food losses and food waste on global food insecurity, natural resources, and greenhouse gas emissions, *Environmental Economics Policy Studies*, vol. 17, pp. 43-77, 2015.
- [149] E. Poyatos-Racionero, J. V. Ros-Lis, J.-L. Vivancos, and R. J. J. o. c. p. Martinez-Manez, Recent advances on intelligent packaging as tools to reduce food waste, *Journal of cleaner production*, vol. 172, pp. 3398-3409, 2018.
- [150] A. Paschalidou, M. Tsatiris, K. Kitikidou, C. Papadopoulou, A. Paschalidou et al., Global Nutritional Need—The Energy Problem, Using Energy Crops for Biofuels or Food: The Choice, pp. 1-9, 2018.
- [151] B. J. J. J. o. a. e. Revell, One Man's Meat... 2050? Ruminations on future meat demand in the context of global warming, *Journal of agricultural economics*, vol. 66, no. 3, pp. 573-614, 2015.
- [152] C. M. Fernandez, J. Alves, P. D. Gaspar, T. M. Lima, and P. D. Silva, Innovative processes in smart packaging. A systematic review, *Journal of the Science of Food Agriculture*, vol. 103, no. 3, pp. 986-1003, 2023.
- [153] J. Brockgreitens and A. Abbas, Responsive food packaging: Recent progress and technological prospects, *Comprehensive Reviews in Food Science Food Safety*, vol. 15, no. 1, pp. 3-15, 2016.
- [154] D. Neves, P. B. Andrade, R. A. Videira, V. de Freitas, and L. J. F. H. Cruz, Berry anthocyanin-based films in smart food packaging: A mini-review, *Food Hydrocolloids*, p. 107885, 2022.
- [155] H. Yong, J. J. F. P. Liu, and S. Life, Recent advances in the preparation, physical and functional properties, and applications of anthocyanins-based

active and intelligent packaging films, *Food Packaging Shelf Life*, vol. 26, p. 100550, 2020.

- [156] M. Ghorbani, E. Divsalar, R. Molaei, P. Ezati, M. Moradi et al., A halochromic indicator based on polylactic acid and anthocyanins for visual freshness monitoring of minced meat, chicken fillet, shrimp, and fish roe, *Innovative Food Science Emerging Technologies*, vol. 74, p. 102864, 2021.
- [157] N. Phuangsaibai, J. Jakmunee, S. J. J. o. A. S. Kittiwachana, and Technology, Investigation into the predictive performance of colorimetric sensor strips using RGB, CMYK, HSV, and CIELAB coupled with various data preprocessing methods: A case study on an analysis of water quality parameters, *Journal of Analytical Science Technology*, vol. 12, no. 1, pp. 1-16, 2021.
- [158] K. Pounds, H. Bao, Y. Luo, J. De, K. Schneider et al., Real-Time and Rapid Food Quality Monitoring Using Smart Sensory Films with Image Analysis and Machine Learning, *ACS Food Science Technology*, vol. 2, no. 7, pp. 1123-1134, 2022.
- [159] Y. Jung, J. Kim, O. Awofeso, H. Kim, F. Regnier et al., Smartphone-based colorimetric analysis for detection of saliva alcohol concentration, *Applied optics*, vol. 54, no. 31, pp. 9183-9189, 2015.
- [160] N. Lopez-Ruiz, V. F. Curto, M. M. Erenas, F. Benito-Lopez, D. Diamond et al., Smartphone-based simultaneous pH and nitrite colorimetric determination for paper microfluidic devices, *Analytical Chemistry*, vol. 86, no. 19, pp. 9554-9562, 2014.
- [161] J. Chandrasekhar, M. Madhusudhan, and K. Raghavarao, Extraction of anthocyanins from red cabbage and purification using adsorption, *Food bioproducts processing*, vol. 90, no. 4, pp. 615-623, 2012.
- [162] S. Fang, Z. Guan, C. Su, W. Zhang, J. Zhu et al., Accurate fish-freshness prediction label based on red cabbage anthocyanins, *Food Control*, vol. 138, p. 109018, 2022.

- [163] N. Dhenadhayalan, K.-C. Lin, R. Suresh, and P. Ramamurthy, Unravelling the multiple emissive states in citric-acid-derived carbon dots, *The Journal of Physical Chemistry C*, vol. 120, no. 2, pp. 1252-1261, 2016.
- [164] J. Cai, J. Luo, S. Wang, and S. Yang, Feature selection in machine learning: A new perspective, *Neurocomputing*, vol. 300, pp. 70-79, 2018.
- [165] E. H. Houssein, D. Oliva, E. Çelik, M. M. Emam, and R. M. Ghoniem, Boosted sooty tern optimization algorithm for global optimization and feature selection, *Expert Systems with Applications*, vol. 213, p. 119015, 2023.
- [166] X. Cui, Y. Li, J. Fan, and T. Wang, A novel filter feature selection algorithm based on relief, *Applied Intelligence*, vol. 52, no. 5, pp. 5063-5081, 2022.
- [167] H. Zhou, X. Wang, and R. J. A. I. Zhu, Feature selection based on mutual information with correlation coefficient, *Applied Intelligence*, pp. 1-18, 2022.
- [168] A. Sharma and P. K. J. I. J. o. I. T. Mishra, Performance analysis of machine learning based optimized feature selection approaches for breast cancer diagnosis, *International Journal of Information Technology*, pp. 1-12, 2021.
- [169] M. Alweshah, S. Alkhalaileh, M. A. Al-Betar, and A. A. Bakar, Coronavirus herd immunity optimizer with greedy crossover for feature selection in medical diagnosis, *Knowledge-Based Systems*, vol. 235, p. 107629, 2022.
- [170] L. Yuan, G. Yang, Q. Xu, and T. J. P. R. Lu, Discriminative feature selection with directional outliers correcting for data classification, *Pattern recognition*, vol. 126, p. 108541, 2022.
- [171] Z. Jiao, S. Chen, H. Shi, and J. Xu, Multi-modal feature selection with feature correlation and feature structure fusion for MCI and AD classification, *Brain Sciences*, vol. 12, no. 1, p. 80, 2022.
- [172] L. Breiman, Random forests, *Machine learning*, vol. 45, pp. 5-32, 2001.
- [173] Y. J. P. i. M. B. Xia and T. Science, Correlation and association analyses in microbiome study integrating multiomics in health and disease, *Progress in Molecular Biology Translational Science*, vol. 171, pp. 309-491, 2020.

- [174] M. Alizadeh-Sani, M. Tavassoli, D. J. McClements, and H. Hamishehkar, Multifunctional halochromic packaging materials: Saffron petal anthocyanin loaded-chitosan nanofiber/methyl cellulose matrices, *Food Hydrocolloids*, vol. 111, p. 106237, 2021.
- [175] P. Ezati and J.-W. Rhim, pH-responsive chitosan-based film incorporated with alizarin for intelligent packaging applications, *Food Hydrocolloids*, vol. 102, p. 105629, 2020.
- [176] J. Zhang, X. Zou, X. Zhai, X. Huang, C. Jiang et al., Preparation of an intelligent pH film based on biodegradable polymers and roselle anthocyanins for monitoring pork freshness, *Food Chemistry*, vol. 272, pp. 306-312, 2019.
- [177] W. Gong, H.-B. Yao, T. Chen, Y. Xu, Y. Fang et al., Smartphone platform based on gelatin methacryloyl (GelMA) combined with deep learning models for real-time monitoring of food freshness, *Talanta*, vol. 253, p. 124057, 2023.

Appendices

Appendix A

Analysis of precision, recall and F1 score for LDA and EBC classification algorithms in the classification of H₂O₂ concentration at t=30 s and t=10 minutes of KI and TMB+KI mixtures:

Table A.1: Evaluation of the LDA for KI at t=30 s in terms of precision, recall and F1 score.

	precision	recall	F1 score
0 mM	0.79	0.71	0.73
0.01 mM	0.78	0.82	0.72
0.05 mM	0.59	0.61	0.62
0.1 mM	0.64	0.67	0.65
0.2 mM	0.88	0.82	0.78
0.5 mM	0.9	0.88	1
1 mM	0.83	0.71	0.77
5 mM	0.97	1	1
10 mM	0.9	0.84	0.91
25 mM	0.88	1	1
50 mM	1	1	1
Average	0.83	0.82	0.84

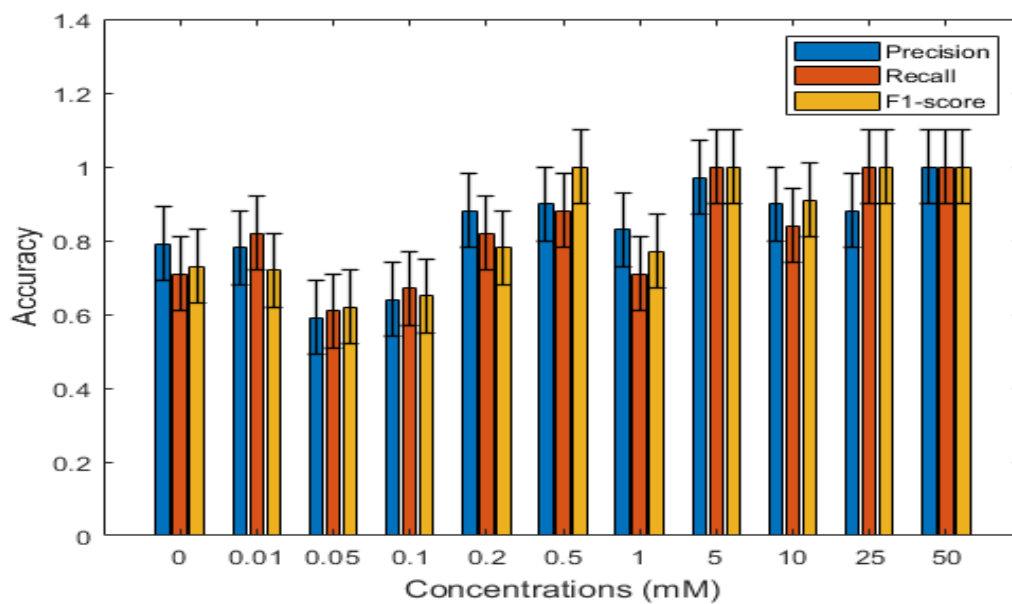


Figure A.1: Evaluation of LDA with error bars in terms of precision, recall, and F1 score at $t=30$ s for TMB+KI.

Table A.2: Evaluation of the LDA for KI at $t=30$ s in terms of precision, recall and F1 score.

	precision	recall	F1 score
0 mM	0.92	0.79	0.85
0.01 mM	0.87	0.9	0.9
0.5 mM	0.93	1	0.88
1 mM	0.97	0.92	0.91
5 mM	0.94	1	1
10 mM	0.9	0.91	0.98
25 mM	1	1	1
50 mM	0.92	0.96	0.98
Average	0.93	0.94	0.94

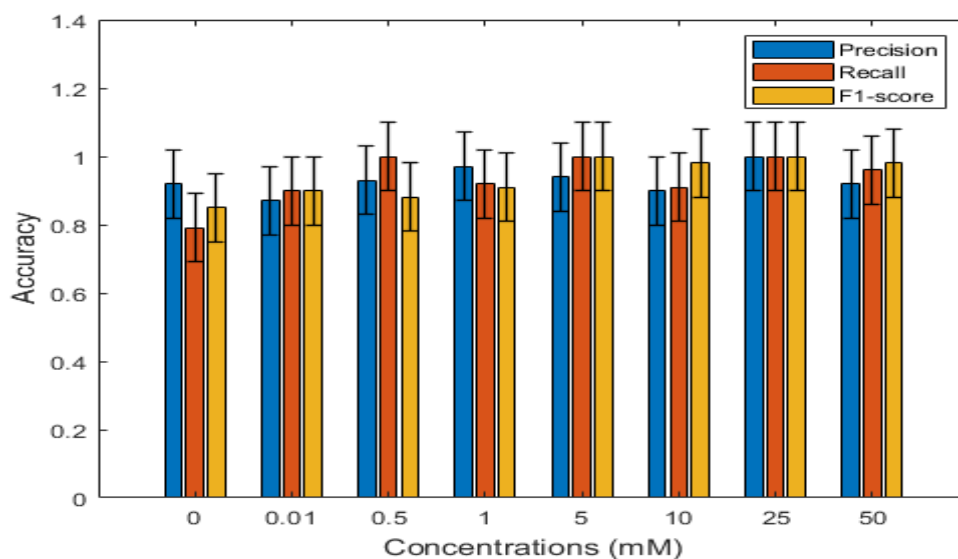


Figure A.2: Evaluation of LDA with error bars in terms of precision, recall, and F1 score at $t=30$ s for TMB+KI.

Table A.3: Evaluation of the LDA for KI at $t=10$ min in terms of precision, recall and F1 score.

	precision	recall	F1 score
0 mM	0.83	0.68	0.73
0.01 mM	0.86	0.86	0.86
0.05 mM	0.77	0.86	0.81
0.1 mM	0.81	0.79	0.8
0.2 mM	0.88	0.93	0.88
0.5 mM	0.9	0.96	0.95
1 mM	0.96	0.93	0.95
5 mM	1	0.89	0.94
10 mM	0.81	0.89	0.85
25 mM	0.96	0.93	0.95
50 mM	0.9	0.93	0.91
Average	0.88	0.88	0.88

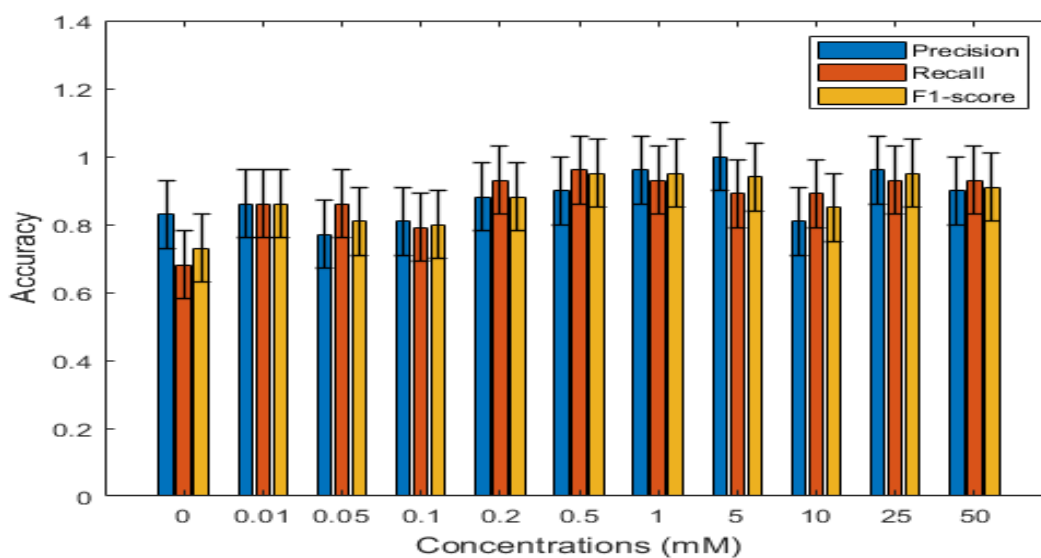


Figure A.3: Evaluation of LDA with error bars in terms of precision, recall, and F1 score at t=10 min for TMB+KI.

Table A.4: Evaluation of the LDA for KI at t=10 min in terms of precision, recall and F1 score.

	precision	recall	F1 score
0 mM	0.96	0.82	0.88
0.01 mM	0.9	0.93	0.91
0.5 mM	0.93	0.96	0.95
1 mM	0.93	0.93	0.93
5 mM	1	1	1
10 mM	0.9	0.89	0.89
25 mM	0.93	0.93	0.93
50 mM	0.84	0.96	0.9
Average	0.92	0.93	0.92

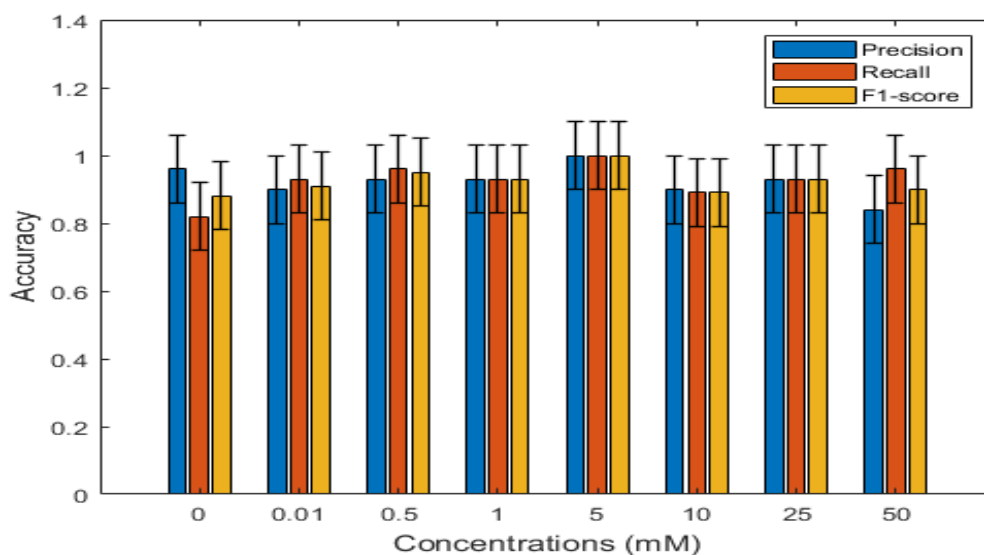


Figure A.4: Evaluation of LDA with error bars in terms of precision, recall, and F1 score at $t=10$ min for TMB+KI.

Table A.5: Evaluation of the EBC for TMB+KI at $t=30$ s in terms of precision, recall and F1 score.

	precision	recall	F1 score
0 mM	0.96	0.96	0.96
0.01 mM	0.9	0.93	0.91
0.05 mM	0.96	0.93	0.95
0.1 mM	0.97	1	0.98
0.2 mM	0.96	0.96	0.96
0.5 mM	1	1	1
1 mM	0.96	0.93	0.95
5 mM	0.88	0.86	0.81
10 mM	0.85	0.92	0.86
25 mM	0.88	0.84	0.8
50 mM	0.81	0.72	0.77
Average	0.92	0.92	0.91

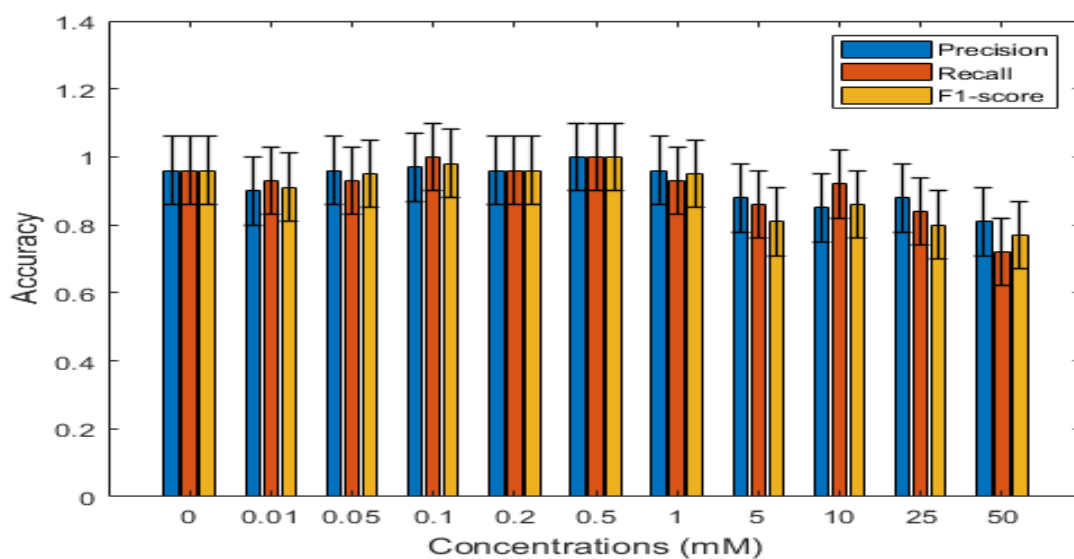


Figure A.5: Evaluation of EBC with error bars in terms of precision, recall, and F1 score at $t=30$ s for TMB+KI.

Table A.6: Evaluation of the EBC for TMB+KI at $t=30$ s in terms of precision, recall and F1 score.

	precision	recall	F1 score
0 mM	0.96	0.96	0.96
0.01 mM	0.81	0.93	0.87
0.05 mM	0.96	0.82	0.88
0.1 mM	1	1	1
0.2 mM	1	1	1
0.5 mM	1	1	1
1 mM	1	1	1
5 mM	1	1	1
Average	0.97	0.96	0.96

Table A.7: Evaluation of the EBC for TMB+KI at t=10 min in terms of precision, recall and F1 score.

	precision	recall	F1 score
0 mM	0.96	0.98	0.96
0.01 mM	0.86	0.86	0.86
0.05 mM	0.96	0.86	0.81
0.1 mM	0.96	0.96	0.96
0.2 mM	0.96	0.93	0.88
0.5 mM	0.96	0.96	0.95
1 mM	1	1	1
5 mM	0.7	0.74	0.78
10 mM	0.9	0.89	0.85
25 mM	0.45	0.52	0.58
50 mM	0.68	0.72	0.65
Average	0.85	0.86	0.84

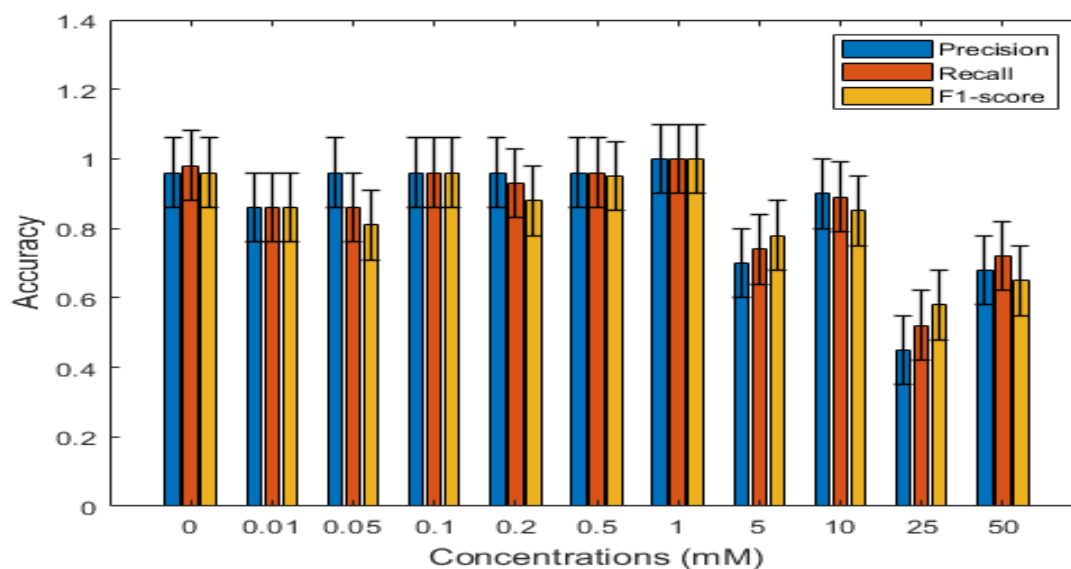


Figure A.6: Evaluation of EBC with error bars in terms of precision, recall, and F1 score at t=10 min for TMB+KI.

Table A.8: Evaluation of the EBC for TMB+KI at t=10 min in terms of precision, recall and F1 score.

	precision	recall	F1 score
0 mM	0.98	0.96	0.96
0.01 mM	0.92	0.93	0.91
0.05 mM	0.92	0.89	0.91
0.1 mM	0.98	0.96	0.96
0.2 mM	0.98	0.98	0.98
0.5 mM	1	1	1
1 mM	0.94	0.93	0.93
5 mM	1	1	1
Average	0.97	0.96	0.96

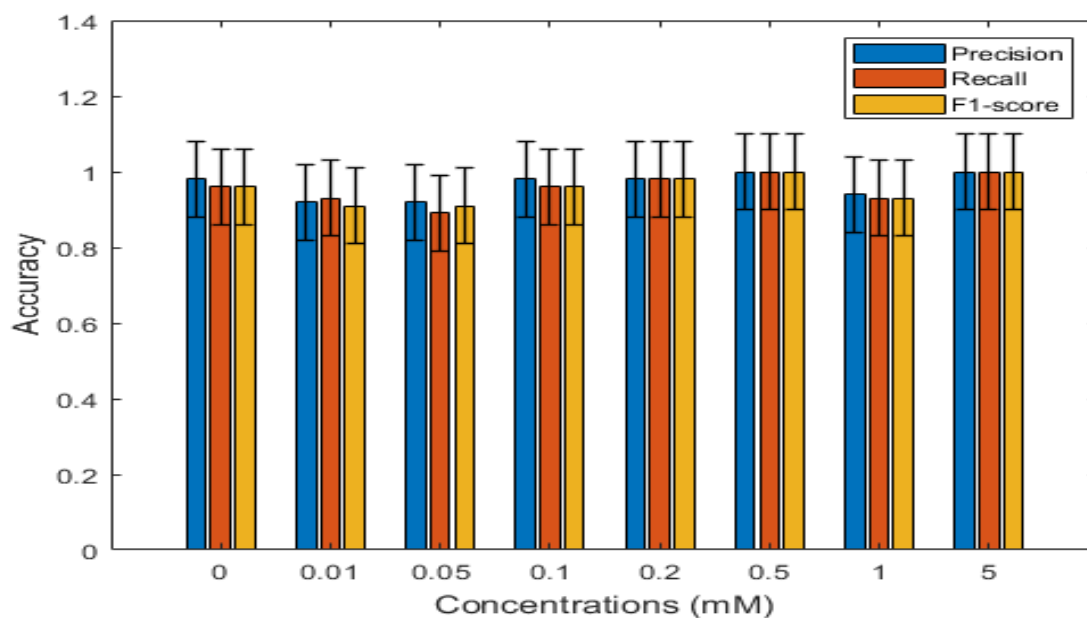


Figure A.7: Evaluation of EBC with error bars in terms of precision, recall, and F1 score at t=10 min for TMB+KI.

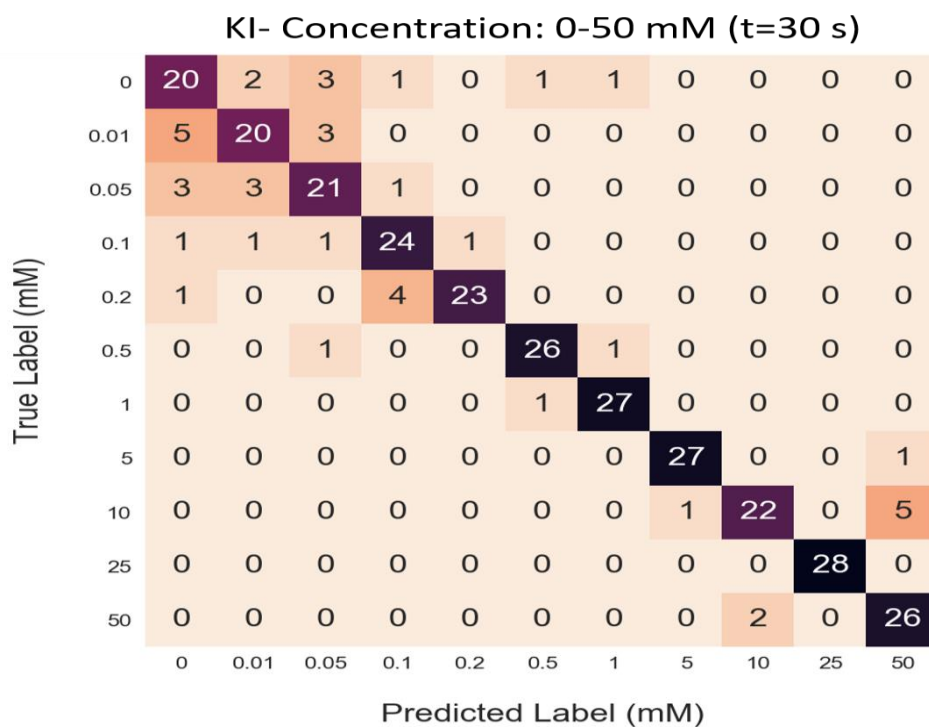


Figure A.8: Confusion matrix of KI at t=30 s for the LDA classifier including 0-50 mM concentration.

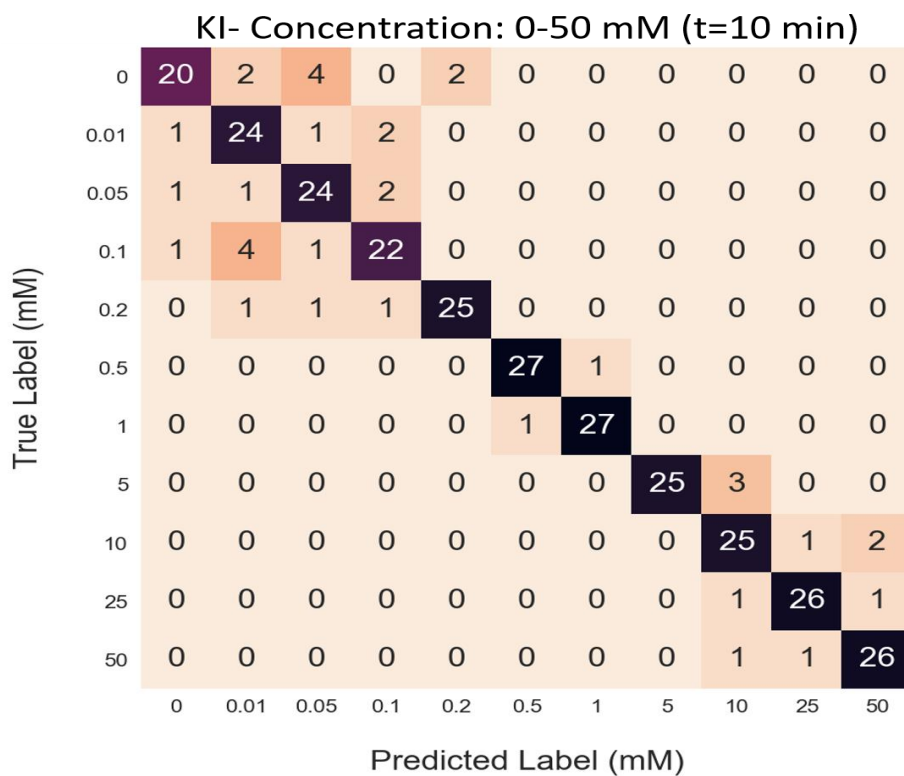


Figure A.9: Confusion matrix of KI at t=10 min for the LDA classifier including 0-50 mM concentration.

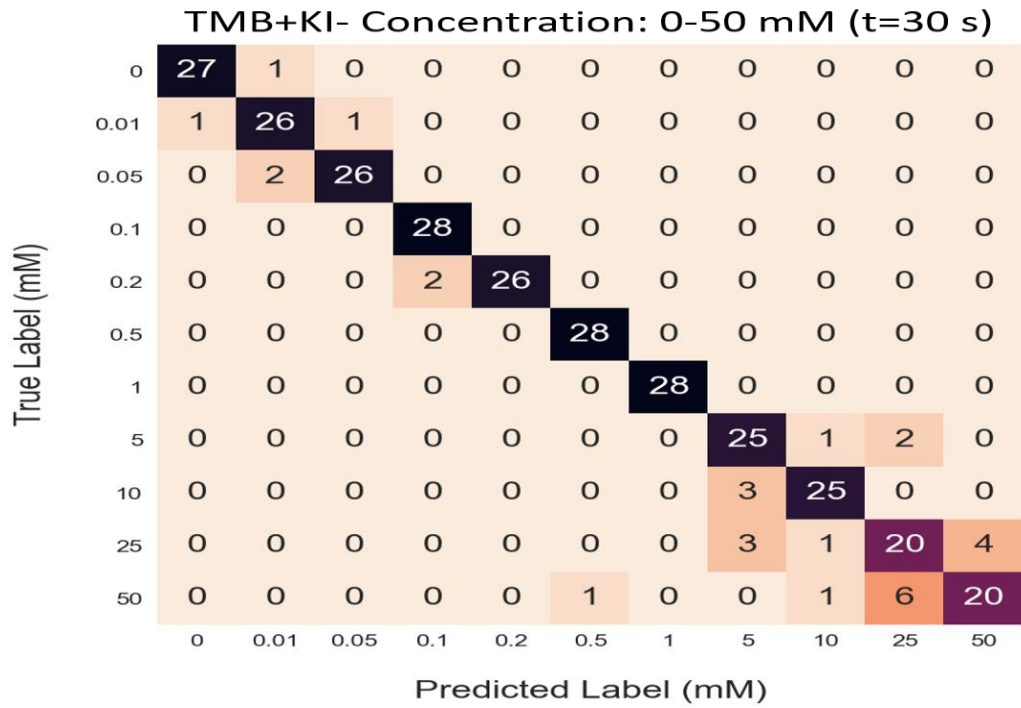


Figure A.10: Confusion matrix of TMB+KI at t=30 s for the EBC classifier including 0-50 mM concentration.

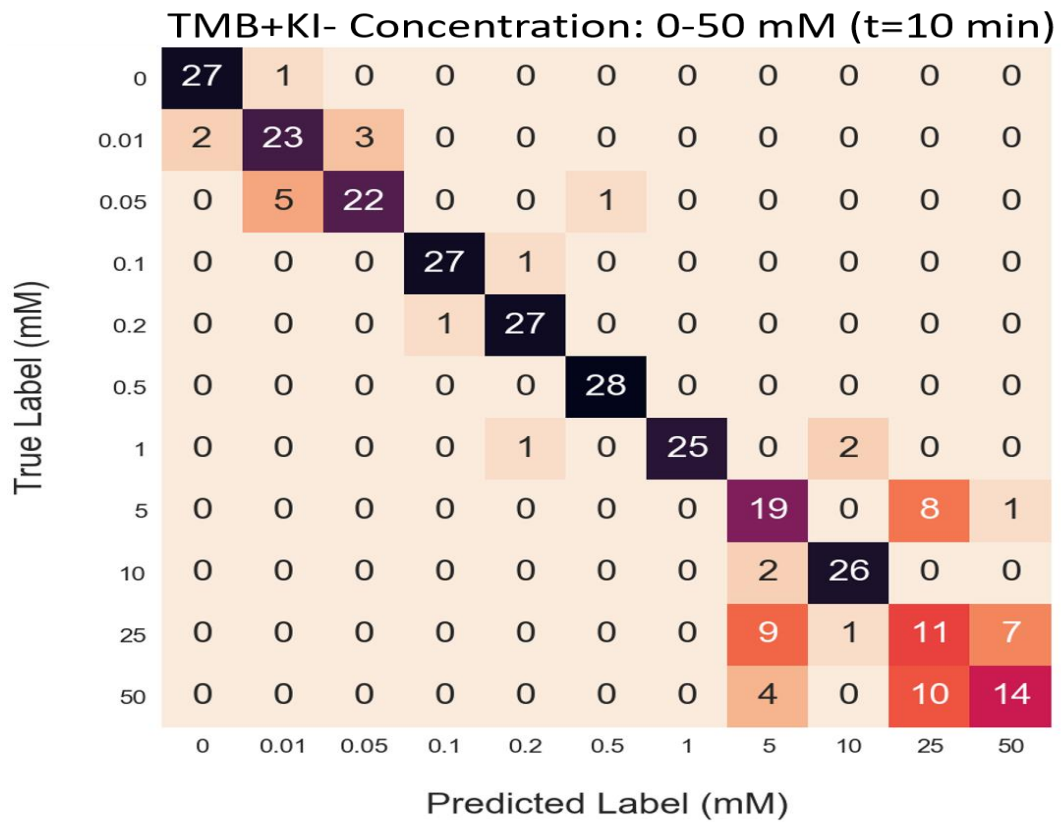


Figure A.11: Confusion matrix of TMB+KI at t=10 min for the EBC classifier including 0-50 mM concentration.

Appendix B

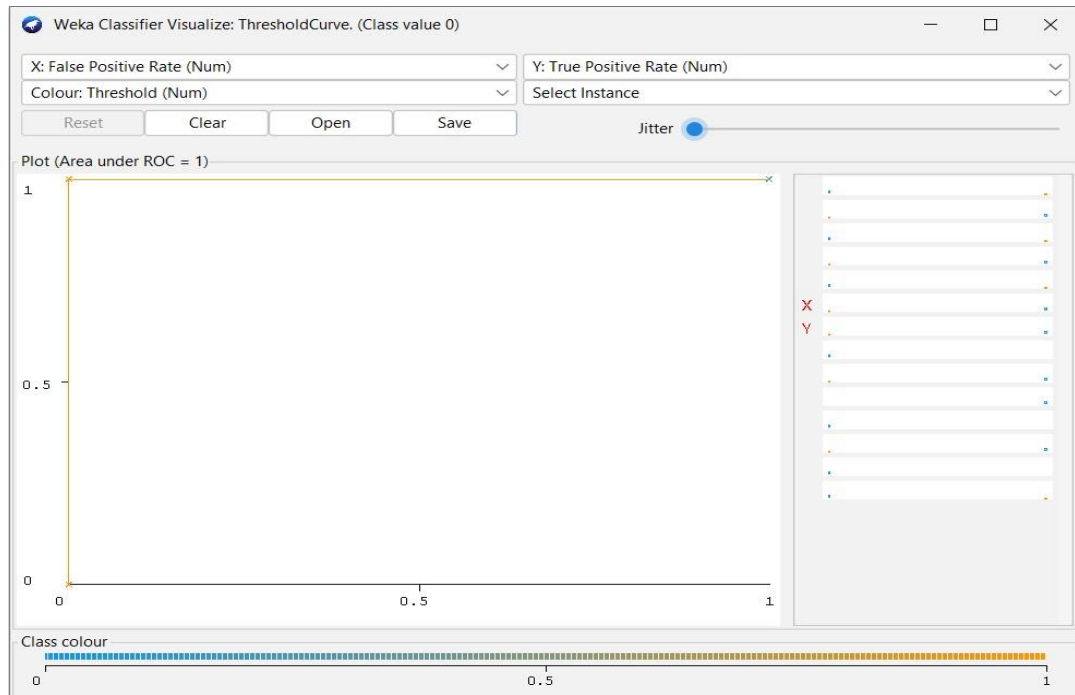


Figure B.1: ROC curve of 0 mg N/100 g concentration with the RF.

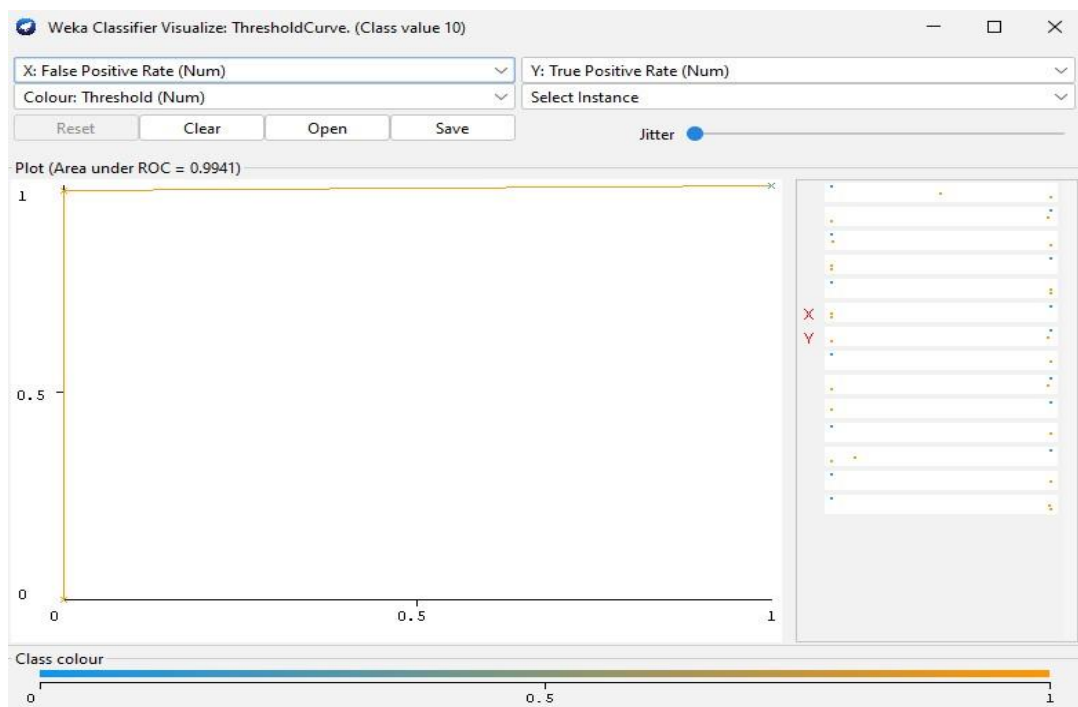


Figure B.2: ROC curve of 10 mg N/100 g concentration with the RF.

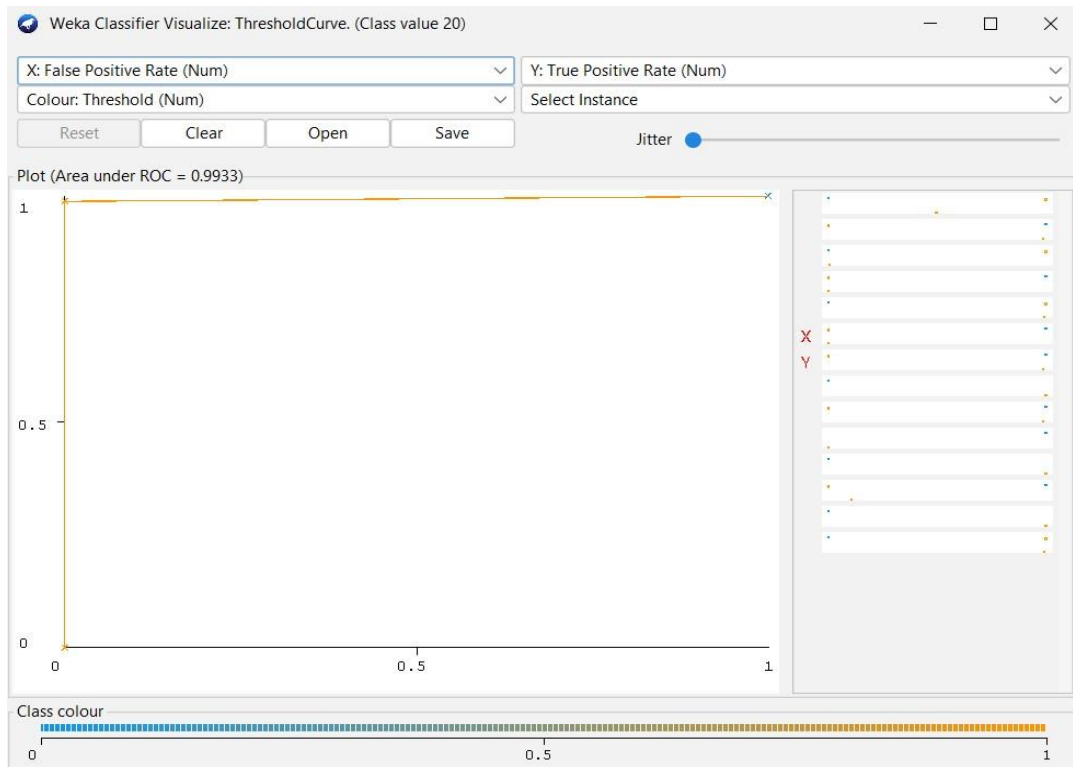


Figure B.3: ROC curve of 20 mg N/100 g concentration with the RF.

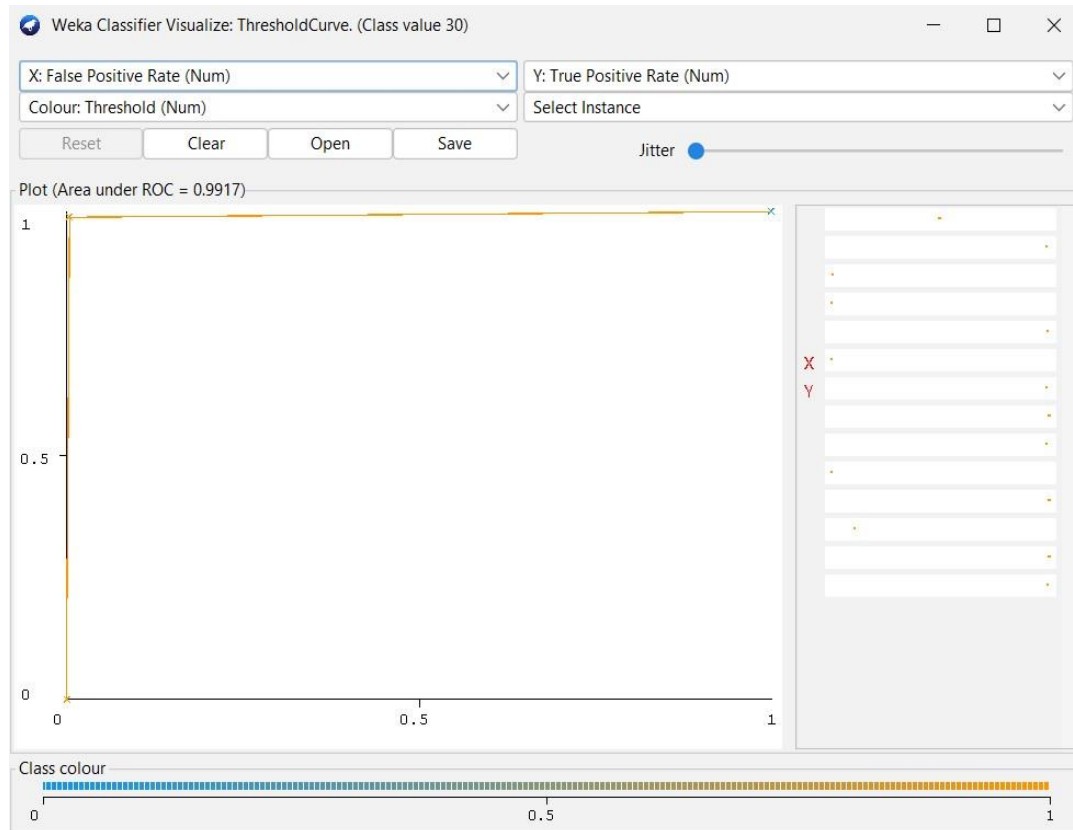


Figure B.4: ROC curve of 30 mg N/100 g concentration with the RF.

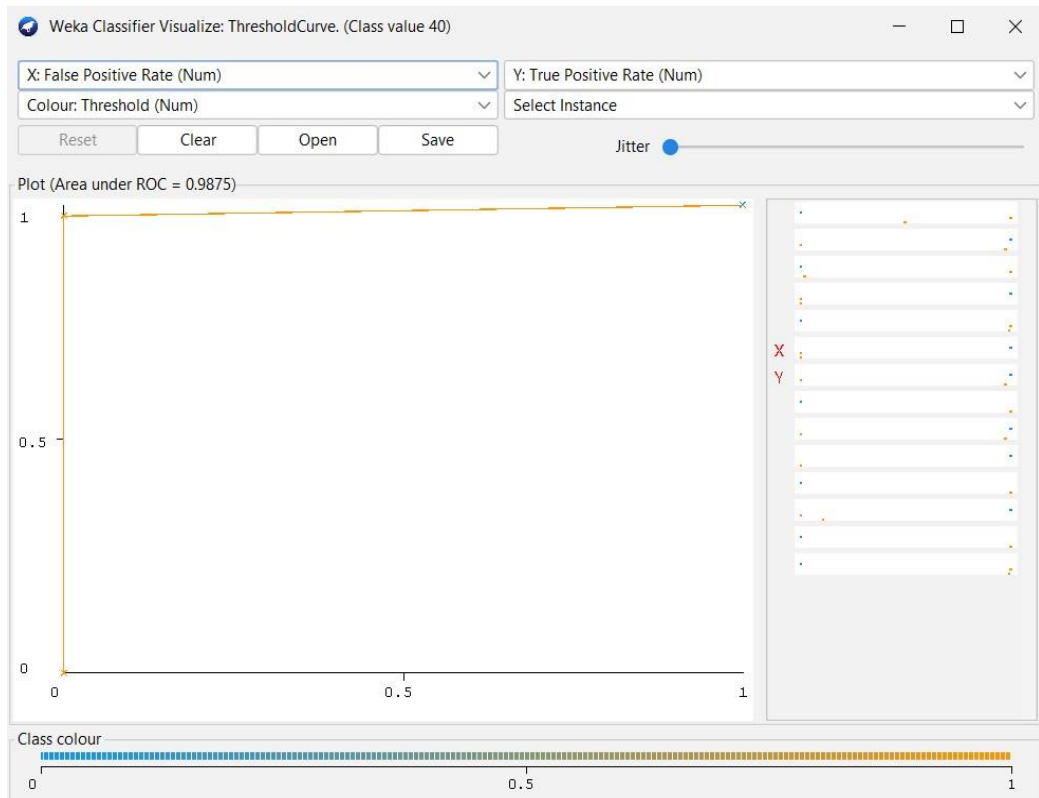


Figure B.5: ROC curve of 40 mg N/100 g concentration with the RF.

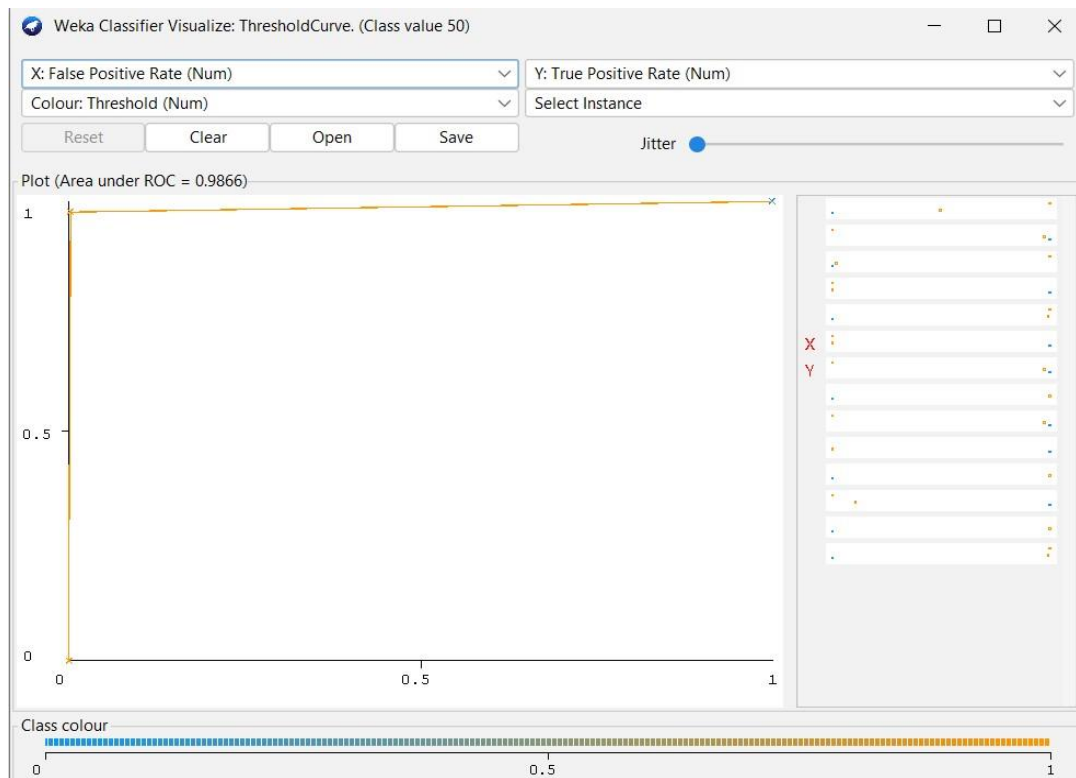


Figure B.6: ROC curve of 50 mg N/100 g concentration with the RF.

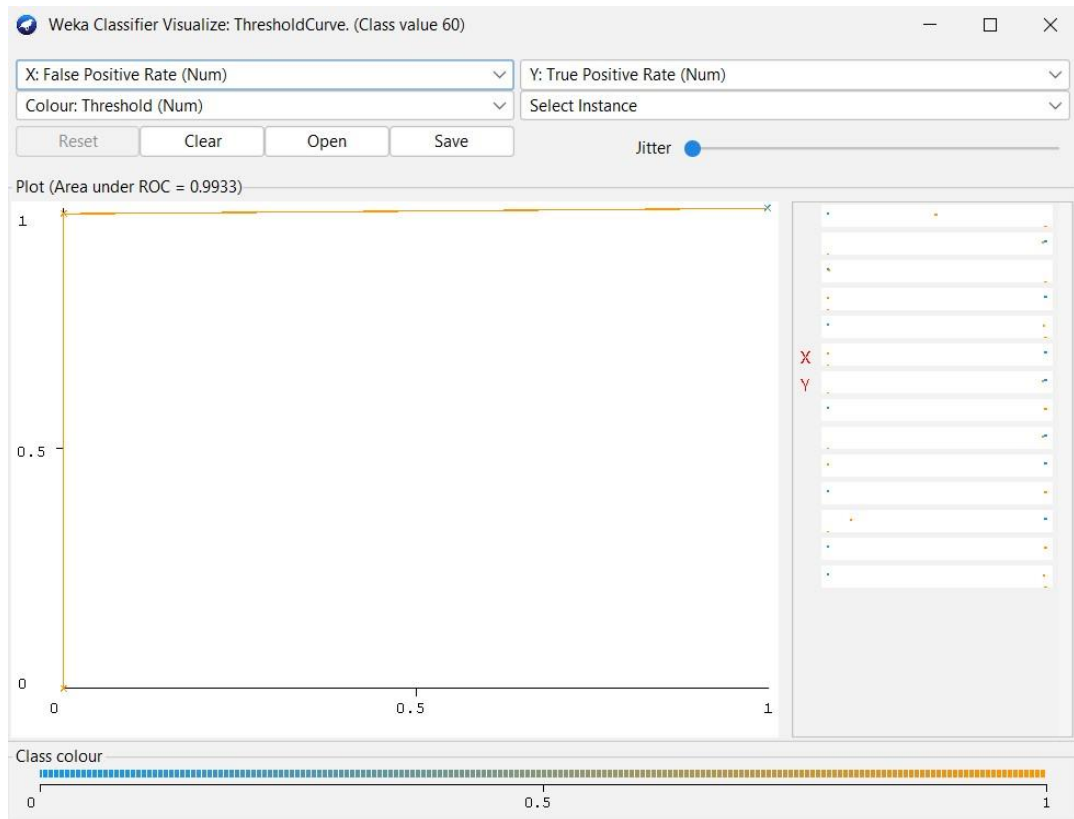


Figure B.7: ROC curve of 60 mg N/100 g concentration with the RF.

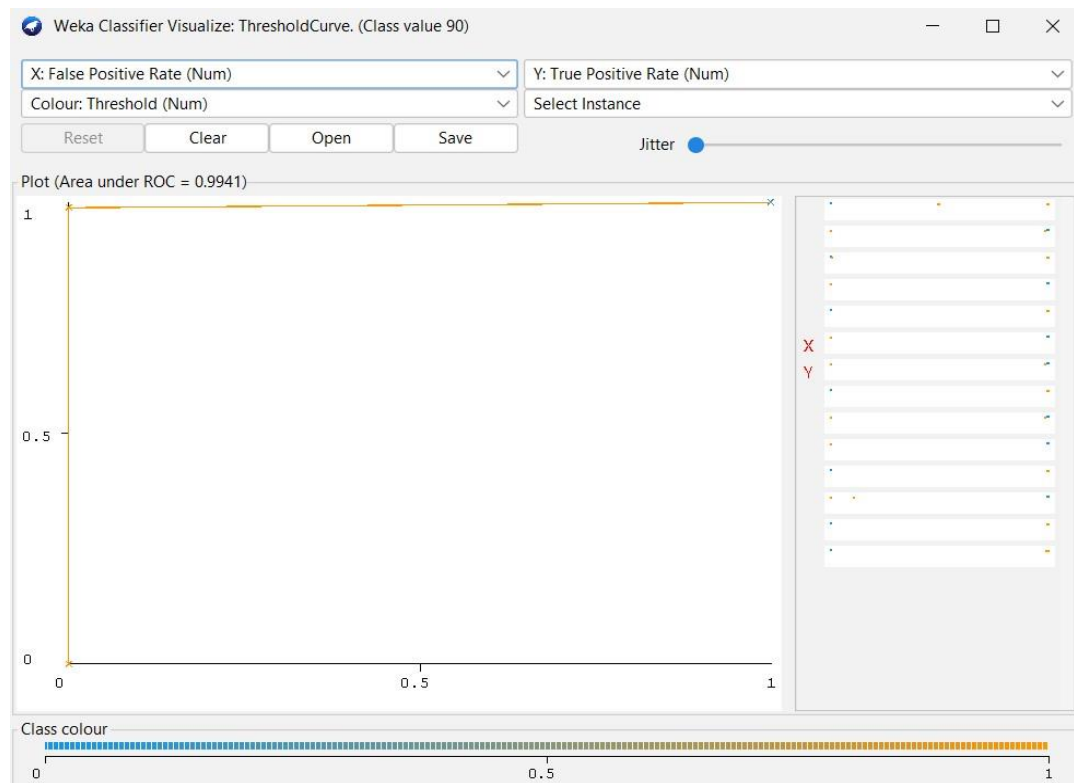


Figure B.8: ROC curve of 90 mg N/100 g concentration with the RF.

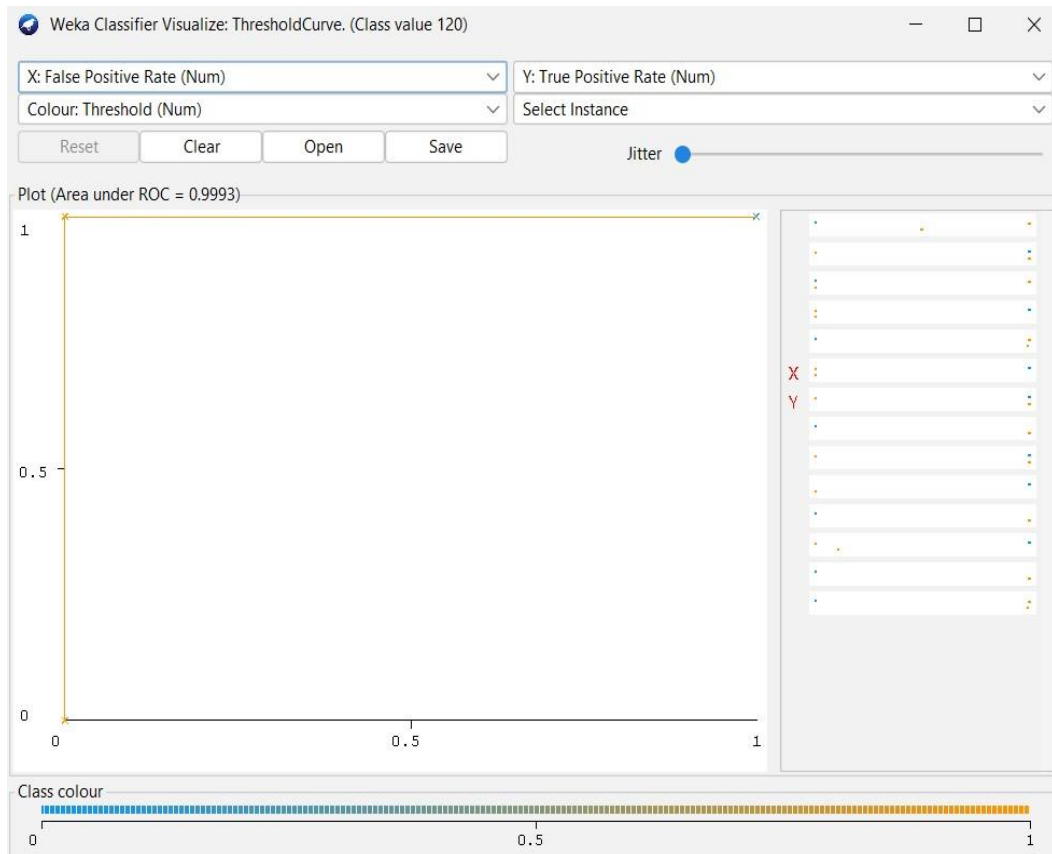


Figure B.9: ROC curve of 120 mg N/100 g concentration with the RF.

Appendix C

Publications from the Thesis

Journal Articles

1. **Doğan, V.**, Yüzer, E., Kılıç, V., & Şen, M. (2021), Non-enzymatic colorimetric detection of hydrogen peroxide using a μ PAD coupled with a machine learning-based smartphone app, *Analyst*, 146(23), 7336-7344.
2. Yüzer, E., **Doğan, V.**, Kılıç, V., & Şen, M. (2022), Smartphone embedded deep learning approach for highly accurate and automated colorimetric lactate analysis in sweat. *Sensors and Actuators B: Chemical*, 371, 132489.
3. **Doğan, V.**, Evliya, M., Kılıç, V., & Kahyaoğlu, L.N. (2023), On-site colorimetric food spoilage monitoring with smartphone embedded machine learning. (Under review in *Talanta*)

Curriculum Vitae

Name Surname : Vakkas DOĞAN

E-mail (1) :

E-mail (2) :

Education:

2015–2020 İzmir Kâtip Çelebi University, Dept. of Electrical-Electronics Eng.

2021–2023 İzmir Kâtip Çelebi University, Dept. of Electrical-Electronics Eng.

Work Experience:

2020-2021: NEW SENSES SPACE TECHNOLOGIES AND HEALTH RESEARCH
A.Ş. (INTERN)

2021-2023: İKÇÜ-SCIENTIFIC RESEARCH PROJECTS COORDINATOR
(TUBITAK ID=TBTK-0069-2766, NEWTON PROJECT NO:120N995)

Publications:

1. Mercan, Öykü Berfin, **Vakkas Doğan**, and Volkan Kılıç. Time Series Analysis based Machine Learning Classification for Blood Sugar Levels. Medical Technologies Congress (TIPTEKNO). IEEE, 2020.
2. **Doğan, Vakkas**, Öykü Berfin Mercan, and Volkan Kılıç. Smartphone Based Blood Glucose Prediction with Recurrent Neural Network. 2nd International Eurasian Conference on Science, Engineering and Technology (EurasianSciEnTech 2020).
3. **Doğan, Vakkas**, Öykü Berfin Mercan, and Volkan Kılıç. Classification of Blood Glucose Levels with Multiple Machine Learning Classifiers in Diabetes Patients. 2nd International Eurasian Conference on Science, Engineering and Technology (EurasianSciEnTech 2020).

4. Yüzer, E., **Doğan, V.**, Kılıç, V., & Şen, M. (2022), Smartphone embedded deep learning approach for highly accurate and automated colorimetric lactate analysis in sweat. *Sensors and Actuators B: Chemical*, 371, 132489.
5. Kilic, B., **Dogan, V.**, Kilic, V., & Kahyaoglu, L. N. (2022), Colorimetric food spoilage monitoring with carbon dot and UV light reinforced fish gelatin films using a smartphone application, *International Journal of Biological Macromolecules*, 209, 1562-1572.
6. **Doğan, V.**, Yüzer, E., Kılıç, V., & Şen, M. (2021), Non-enzymatic colorimetric detection of hydrogen peroxide using a μ PAD coupled with a machine learning-based smartphone app, *Analyst*, 146(23), 7336-7344.
7. Şen, M., Yüzer, E., **Doğan, V.**, Avcı, İ., Ensarioğlu, K., Aykaç, A., ... & Kılıç, V. (2022), Colorimetric detection of H₂O₂ with Fe₃O₄@ Chi nanozyme modified μ PADs using artificial intelligence, *Microchimica Acta*, 189(10), 1-11.
8. **Doğan, V.**, Isık, T., Kılıç, V., & Horzum, N. (2022), A field-deployable water quality monitoring with machine learning-based smartphone colorimetry, *Analytical Methods*.
9. **Doğan, V.**, & Kılıç, V. (2021), Artificial Intelligence Based Pharyngitis Detection Using Smartphone, *Journal of Artificial Intelligence in Health Sciences* ISSN: 2757-9646, 1(2), 14-19.
10. Palaz, Z., **Doğan, V.**, & KILIÇ, V. (2021), Smartphone-based Multi-parametric Glucose Prediction using Recurrent Neural Networks, *Avrupa Bilim ve Teknoloji Dergisi*, (32), 1168-1174.
11. **Doğan, V.**, Evliya, M., Kılıc., V., & Kahyaoglu, L.N. (2023), On-site colorimetric food spoilage monitoring with smartphone embedded machine learning (Under review in *Talanta*).

**DOĞAN Artificial Intelligence Based Android Assistant for Colorimetric Detection
MASTER' S THESIS 2023**